SILICON-SENSITIZED ERBIUM EXCITATION IN SILICON-RICH SILICA FOR INTEGRATED PHOTONICS

by

OLEKSANDR SAVCHYN
M.S., Lviv Ivan Franko National University (Ukraine), 2002
M.S., University of Central Florida, 2007

A dissertation submitted in partial fulfillment of the requirements
for the degree of Doctor of Philosophy
in CREOL, the College of Optics and Photonics
at the University of Central Florida
Orlando, Florida

Summer Term
2010

Major Professor: Pieter G. Kik

ABSTRACT

It is widely accepted that the continued increase of processor performance requires at least partial replacement of electronic interconnects with their photonic counterparts. The implementation of optical interconnects requires the realization of a silicon-based light source, which is challenging task due to the low emission efficiency of silicon. One of the main approaches to address this challenge is the use of doping of silicon based matrices with optical centers, including erbium ions. Erbium ions incorporated in various hosts assume the trivalent state (Er^{3+}) and demonstrate a transition at 1.54 μm, coinciding with optical transmission windows in both silicon and silica. Due to the low absorption cross-section and discrete energy levels of the Er^{3+} ion, indirect excitation is necessary. In late 90s it was demonstrated that the incorporation of excess silicon in erbium-doped silica results in strong erbium sensitization, leading to an increase of the effective absorption cross-section by orders of magnitude. The sensitization was considered to occur via silicon nanocrystals that formed at high annealing temperatures. While a large increase of the absorption cross-section was demonstrated, the incorporation of Si nanocrystals was found to result in a low concentration of excited erbium, as well as silicon related free-carrier absorption.

The focus of this dissertation is the investigation of the nature of the sensitization mechanism of erbium in silicon-rich silica. The results presented in the dissertation demonstrate that erbium in silicon-rich silica is predominantly excited by silicon-excess-related luminescence centers, as opposed to the commonly considered silicon nanocrystals. This is a remarkable conclusion that changes the view on the exact origin of erbium sensitization, and that resolves several technical challenges that exist for nanocrystal-based sensitization. The work shows that the density of indirectly excited erbium ions is significantly larger in samples without silicon

nanocrystals (annealed at $T < 1000°C$) as opposed to samples with silicon nanocrystals (annealed at $T > 1000°C$). The density of indirectly excited erbium ions, defining the maximum achievable gain, was demonstrated to be approximately excitation wavelength independent, while the effective erbium absorption cross-section was shown to significantly depend on the excitation wavelength. The excitation mechanism of erbium by luminescence centers was shown to be fast (< 30 ns) and capable of erbium sensitization to different energy levels. This multilevel nature of erbium excitation was demonstrated to result in two different mechanisms of the excitation of the first excited state of erbium: fast (< 30 ns) direct excitation by the luminescence centers, and slow (> 2.3 μs) excitation due to the relaxation of erbium ions excited into higher energy levels to the first excited state. Based on photoluminescence studies conducted in the temperature range 15 - 300K it was shown that the relaxation efficiency of erbium from the second excited state to the first excited state (responsible for the slow excitation mechanism) is temperature independent and approaches unity. The relative stability of the optical properties demonstrated in the temperature range 20 - 200°C, implies that relatively stable optical gain can be achieved under realistic on-chip operating conditions. The optimum Si excess concentration corresponding to the highest density of sensitized Er^{3+} ions is shown to be relatively insensitive to the presence of Si nanocrystals and is ~ 14.5 at.% and ~ 11.5 at.% for samples without and with Si nanocrystals respectively.

The presented results and conclusions have significant implications for silicon photonics and the industrial application of Er doped SiO_2. The work shows that in order to sensitize erbium ions in silicon-rich silica there is no need for the presence of silicon nanocrystals, and consequently lower fabrication temperatures can be used. More importantly, the results strongly

suggest that higher gain values can be acquired in samples annealed at lower temperature (without silicon nanocrystals) as compared to samples annealed at high temperatures (with silicon nanocrystals). In addition, the maximum gain is predicted to be relatively independent of excitation wavelength, significantly relaxing the requirements on the pump source. Based on the experimental results it is predicted that relatively stable performance of erbium-doped silicon-rich silica is possible up to typical processor operating temperatures of ~ 80 - 90°C making it a viable material for on-chip devices. The results suggest that low temperature annealed erbium-doped silicon-rich silica is a preferable material for on-chip photonic devices as compared with its high temperature annealed counterpart.

To my father, my mother and my brother

ACKNOWLEDGEMENTS

I joined CREOL in 2004 and since then had a chance to meet many interesting and knowledgeable people who directly or indirectly helped me complete this dissertation. In this section I would like to briefly acknowledge all of them. First and most of all I would like to acknowledge my advisor Dr. Pieter Kik. It was a real pleasure to work with such a knowledgeable, professional and positive person throughout all these years. I'm grateful to Dr. Kik for inspiring and supporting me in my scientific endeavors, for the generosity with his time in helping me succeed, his valuable scientific discussions, his positive outlook, his advising and scientific input in this dissertation. Working for Dr. Kik I had a chance and luck to face many interesting challenges which endowed me with technical, scientific and life experience indispensible in my career. Besides my adviser, I would also like to acknowledge Dr. Kevin Coffey for trusting me and letting me use his state of the art magnetron sputtering system, for being extremely helpful with his advice regarding troubleshooting the sputtering and Rutherford backscattering spectroscopy systems and for his very thorough scientific thoughts and suggestions regarding the materials science involved, which highly increased the quality of this dissertation and corresponding publications. Dr. Michael Bass for his willingness to answer my scientific questions, his valuable suggestions regarding improving this dissertation and his generosity in lending us equipment without which writing this dissertation would be impossible. Dr. Winston Schoenfeld for the generosity with his time, his important advice in improving this project and for trusting me and letting me use some of his equipment crucial for completing this dissertation. Dr. Robert Peale for lending us a Nd:YAG laser without which this project would not be completed. Dr. George Stegeman for providing us with an annealing furnace that was

used for sample preparation throughout the entire project. Forrest Ruhge for his contribution to setting up the lab. Ravi Todi and Edward Dein for teaching me the tricks of operating the magnetron sputtering system. Kirk Scammon for his help with Rutherford backscattering system. Grady Webb-Wood for his support in my scientific endeavors and for a number of very valuable science and life related pieces of advice I was very lucky to get. Dana Kohlgraf-Owens for being very supportive during my studies and for teaching me Matlab tricks and chemicals handling. Amitabh Ghoshal for valuable discussions of scientific challenges. Dr. Beatriz Roldán Cuenya and Luis Ono for doing the X-ray photoelectron spectroscopy measurements. Dr. Helge Heinrich and Haritha Nukala for doing transmission electron microscopy measurements. Dr. Glenn Boreman, Guy Zummo, Brian Slovick and Samuel Wadsworth for doing ellipsometry measurements. Dr. Patrick LiKamWa and Yat-Ming "Tony" Ho for teaching me how to use metalizer. Ivan Divliansky, Nathan Bickel, Jeremy Mares and Hubert Seigneur for teaching me equipment use in the cleanroom. The faculty of CREOL for the courses they taught and for their willingness to answer the questions related both to classes and to my research field. The CREOL staff for taking on all the chores and freeing me up for doing research (special thanks to Rachel Franzetta, Richard Zotti, Denise Whiteside, Amy Perry, Gail Drabczuk, Michael Torrance). My family for letting me pursue my dreams. And also I would like to acknowledge all the other people I had an honor to work with but might have forgotten to mention.

TABLE OF CONTENTS

LIST OF FIGURES x
LIST OF TABLES xv
CHAPTER 1. INTRODUCTION 1
1.1 Silicon Photonics 1
1.2 Silicon Photonics and Erbium 2
1.3 Dissertation Overview 10
1.4 References 15
CHAPTER 2. LUMINESCENCE CENTER MEDIATED EXCITATION AS THE DOMINANT Er SENSITIZATION MECHANISM IN Er-DOPED Si-RICH SiO_2 FILMS 20
2.1 Introduction 21
2.2 Experimental Techniques 24
2.3 Results and Discussion 26
2.3.1 Composition and Microstructure 26
2.3.2 Photoluminescence Spectra 29
2.3.3 Evidence for Luminescence Center Mediated Excitation 32
2.3.4 Evidence for Nanocrystal Mediated Excitation 39
2.3.5 Discussion 44
2.4 Conclusions 49
2.5 References 50
CHAPTER 3. EFFECT OF HYDROGEN PASSIVATION ON LUMINESCENCE-CENTER-MEDIATED Er EXCITATION IN Si-RICH SiO_2 WITH AND WITHOUT Si NANOCRYSTALS 54
3.1 Introduction 55
3.2 Experimental Techniques 58
3.3 Results and Discussion 59
3.3.1 Experimental Results 59
3.3.2 Discussion 70
3.4 Conclusions 86
3.5 References 87
CHAPTER 4. MULTI-LEVEL SENSITIZATION OF Er^{3+} IN LOW-TEMPERATURE-ANNEALED Si-RICH SiO_2 91
4.1 Introduction 91
4.2 Experimental Techniques 92
4.3 Results and Discussion 93
4.4 Conclusions 99
4.5 References 100
CHAPTER 5. OBSERVATION OF TEMPERATURE-INDEPENDENT INTERNAL Er^{3+} RELAXATION EFFICIENCY IN Si-RICH SiO_2 FILMS 102
5.1 Introduction 102
5.2 Experimental Techniques 103
5.3 Results and Discussion 104

5.4 Conclusions 111
5.5 References 112
CHAPTER 6. EXCITATION WAVELENGTH-INDEPENDENT SENSITIZED Er^{3+} CONCENTRATION IN AS-DEPOSITED AND LOW TEMPERATURE ANNEALED Si-RICH SiO_2 FILMS 114
6.1 Introduction 114
6.2 Experimental Techniques 115
6.3 Results and Discussion 116
6.4 Conclusions 122
6.5 References 123
CHAPTER 7. HIGH TEMPERATURE OPTICAL PROPERTIES OF SENSITIZED Er^{3+} IN Si-RICH SiO_2 – IMPLICATIONS FOR GAIN PERFORMANCE 125
7.1 Introduction 126
7.2 Experimental Techniques 128
7.3 Results and Discussion 130
7.4 Conclusions 137
7.5 References 138
CHAPTER 8. DETERMINTATION OF OPTIMUM Si-EXCESS CONCENTRATION IN Er-DOPED Si-RICH SiO_2 FOR OPTICAL APMLIFICATION AT 1.54 μm 142
8.1 Introduction 142
8.2 Experimental Techniques 144
8.3 Results and Discussion 145
8.4 Conclusions 150
8.5 References 151
CHAPTER 9. SUMMARY 152
APPENDIX: LIST OF PUBLICATIONS 157

LIST OF FIGURES

Figure 1.1. Energy levels of Er^{3+} in its free ionic state (a) and in silicate glass (b), showing excitation at 800 nm followed by non-radiative relaxation and emission at 1.53 μm.[39] 3

Figure 2.1 Experimental RBS spectrum of the XSE sample (black line) and the corresponding simulated spectrum (red line)... 26

Figure 2.2. High-resolution bright field TEM images of Er-doped Si rich SiO_2 samples (a) as-deposited, (b) annealed at 600°C, (d) annealed at 1000°C, (e) annealed at 1200°C, and electron diffraction patterns for the samples annealed at 600°C (c) and the sample annealed at 1200°C (f). The insets show a magnified view of the area indicated by the dashed squares. 28

Figure 2.3. (Color) Photoluminescence spectra of passivated Si-rich SiO_2 films with (XSE) and without (XSO) erbium, annealed at temperatures in the range 600 – 1200°C. The inferred spectral dependence of the transfer efficiency is included for annealing temperatures of 600°C and 1100°C. 29

Figure 2.4. (Color) Near-infrared photoluminescence spectra of passivated Er-doped Si-rich SiO_2 samples annealed at temperatures in the range 600 – 1200°C. Inset: the Er^{3+}-related peak emission intensity at 981 nm and 1535 nm as a function of pump power. The dashed line indicates a linear dependence.. 31

Figure 2.5. (Color) Photoluminescence excitation spectra of passivated Si rich SiO_2 films with (XSE) and without (XSO) erbium for an as-deposited sample as well as samples annealed at 600°C and at 1100°C, measured at emission wavelengths predominantly corresponding to luminescence center emission (650 nm), Si nanocrystal emission (875 nm), and Er^{3+} emission (1535 nm)... 33

Figure 2.6. Measured and deduced photoluminescence (PL) parameters of passivated Si-rich SiO_2 films with (XSE) and without (XSO) erbium as a function of annealing temperature, showing (a) the Er PL peak intensity (I_{Er}) and the decay time (τ_{Er}) at 1535 nm in XSE samples. (b) the PL intensities at 650 nm (I_{LC}^{XSE}) and 900 nm (I_{NC}^{XSE}) in XSE samples, the derived Er^{3+} excitation density in XSE samples (I_{Er}/τ_{Er}), the relative concentration of Er^{3+} ions coupled to sensitizers ($N_{Er,c}$), and the transfer efficiency at 650 nm derived from the spectral measurements ($\eta_{tr,PL}$). (c) The decay rate of the emission at 900 nm in XSO and XSE samples ($R_{dec,\mathrm{NC}}^{XSO}$ and $R_{dec,\mathrm{NC}}^{XSE}$ respectively), the derived transfer rate at 900 nm (R_{tr}), the excitation rate of the nanocrystals measured at 900 nm in XSO samples ($R_{\mathrm{exc,NC}}^{XSO}$), the Er^{3+} excitation rate measured in XSE samples ($R_{exc,Er}$), the transfer efficiency at 900 nm derived from the lifetime measurements ($\eta_{tr,LT}$), and the transfer efficiency at 900 nm derived from spectral measurements ($\eta_{tr,PL,NC}$)..... 35

Figure 2.7. (Color) Schematic representation of the Er^{3+} excitation processes in Er-doped Si rich SiO_2 samples (a) at low annealing temperatures, showing a high concentration of excess-Si-related luminescence centers (LCs) indicated by crosses, as well as Er^{3+} ions, indicated by open circles, and (b) the corresponding schematic band diagram, indicating the SiO_2 valence band and conduction band, LC-related electronic levels in the band gap indicated by the horizontal lines, as well as the Er^{3+} energy levels. LC-mediated excitation is indicated by the vertical arrows; (c) at intermediate annealing temperatures, showing a reduced concentration of LCs. (d) at high annealing temperatures, showing the formation of Si nanocrystals (dark circles), and (e) the corresponding band diagram indicating the presence of Si nanocrystals with a quantum confined bandgap. A weak exciton-mediated contribution to the Er^{3+} excitation is indicated by the light vertical arrow. 45

Figure 3.1. (Color) Photoluminescence spectra in the visible-near-infrared region of LTA samples passivated in the temperature range 300 - 600ºC. The PL spectrum of an unpassivated sample is included as a reference. Inset: PL intensity of the luminescence center emission of LTA samples at 750 nm as a function of passivation temperature. 60

Figure 3.2. (Color) Photoluminescence spectra in the near-infra-red region of LTA samples passivated in the temperature range 300 - 600ºC. The PL spectrum of an unpassivated sample is included as a reference. Inset: PL intensity of the Er^{3+}-related emission of LTA samples at 1535 nm as a function of passivation temperature 61

Figure 3.3. (Color) Photoluminescence spectra in the visible-near-infrared region of HTA samples passivated in the temperature range 300 - 800ºC. The PL spectrum of an unpassivated sample is included as a reference. Inset: PL intensity of nanocrystal-related emission of HTA samples at 900 nm as a function of passivation temperature. 62

Figure 3.4. (Color) Photoluminescence spectra in the near-infrared region of HTA samples passivated in the temperature range 300 - 800ºC. The PL spectrum of an unpassivated sample is included as a reference. Inset: PL intensity of Er^{3+}-related emission of HTA samples at 1535 nm as a function of passivation temperature. 64

Figure 3.5. Measured and deduced photoluminescence parameters of LTA (solid symbols) and HTA samples (open symbols) as a function of passivation temperature: (a) Er^{3+} PL decay times at 1535 nm of LTA and HTA samples ($\tau_{dec,Er}^{LTA}$ and $\tau_{dec,Er}^{HTA}$ respectively), silicon nanocrystal PL decay times at 800 nm and 900 nm in HTA samples ($\tau_{dec,NC}^{HTA}$), (b) the effective absorption cross-section of the Er^{3+} PL at 1535nm in the LTA and HTA samples ($\sigma_{abs,Er}^{LTA}$ and $\sigma_{abs,Er}^{HTA}$ respectively), and of the silicon nanocrystal PL at 900 nm in the HTA samples ($\sigma_{abs,NC}^{HTA}$), (c) luminescence center PL intensity at 750 nm in LTA samples ($I_{PL,LC}^{LTA}$), the relative density of the sensitized optically active Er^{3+} ions in LTA and HTA samples (N_{Er}^{LTA} and N_{Er}^{HTA} respectively), the relative density of the optically active silicon nanocrystals contributing to the emission at 900 nm

(N_{NC}^{HTA}). The arbitrary units of the relative density of the sensitized optically active Er^{3+} ions and optically active silicon nanocrystals are not related 65

Figure 3.6. (Color) Proposed model of the effect of hydrogen passivation on the Si nanocrystal and Er^{3+} emission at three different passivation temperatures: (a) 300°C, (b) 500°C, and (c) 600°C. The large dark and bright solid circles represent Si nanocrystals with low and high emission efficiency respectively. The crosses represent dangling bonds, the dashed circles schematically indicate the interaction range of a dangling bond, and the letter H represents a hydrogen terminated dangling bond. The small solid and open circles represent Er^{3+} ions that are affected or unaffected by a dangling bond respectively. 76

Figure 3.7. (Color) Measured and deduced photoluminescence parameters of the silicon-nanocrystal-related emission in HTA samples as a function of passivation temperature: silicon nanocrystal PL decay times of the HTA samples at 900 nm ($\tau_{dec,NC}^{HTA}$), silicon nanocrystal PL decay time dispersion factor of HTA samples at 900 nm ($\beta_{dec,NC}^{HAT}$), the ratio of the silicon nanocrystal PL intensity at 900 nm to that of 850 nm ($I_{PL,900nm}^{HTA} / I_{PL,850nm}^{HTA}$). Insets: measured silicon nanocrystal emission spectrum (thick solid line) for an unpassivated (left) and passivated at 700ºC (right) HTA samples, normalized at a wavelength of 900 nm. The Gaussian curves underneath the PL spectrum schematically depict the individual PL contributions of silicon nanocrystals with different sizes. 82

Figure 4.1. (Color) Photoluminescence spectrum of low-temperature-annealed Er-doped Si-rich SiO_2 measured at 15K. Emission from luminescence centers and Er^{3+} ions is indicated schematically on energy diagrams. 94

Figure 4.2. (Color) Time-dependent photoluminescence intensity at 981 nm under pulsed excitation (I_{PL}, solid line) with the corresponding fit (I_3, dashed line). The Er^{3+} level diagram indicates possible excitation pathways and typical multi-phonon relaxation times. Inset: Er^{3+} emission at 981 nm (I_{PL}, solid line), the LC emission at 750 nm (I_{PL}, dotted line) and the pump pulse (I_{pulse}, open circles) scaled to the same maximum value. 95

Figure 4.3. (Color) Time-dependent photoluminescence intensity at 1535 nm under pulsed excitation (I_{PL}, solid line) with the corresponding fit (N_2^{tot}, dashed line), including the individual time-dependent contributions due to excitation by the fast (N_2^{fast}) and slow (N_2^{slow}) mechanisms. The Er^{3+} level diagram indicates possible excitation pathways. The inset shows the same data in the range 0 – 27 μs. 97

Figure 5.1. (Color) Temperature-dependent photoluminescence spectra of Er-doped Si-rich SiO_2 annealed at 600°C (LTA) (a) and at 1100°C (HTA) (b). The corresponding optical transitions are schematically indicated. 105

Figure 5.2. Temperature dependence of (a) the Er^{3+} first excited state excitation rate in LTA (R_{exc}^{LTA}) and HTA (R_{exc}^{HTA}) samples, (b) the Er^{3+} second excited state relaxation rate (W_3) found from the time-dependent intensities at 981 nm (I_3) and 1535 nm (I_2), the first excited state relaxation rate (W_2), and the dispersion factors corresponding to the relaxation from the first (β_2) and second (β_3) excited states, (c) the relative fractions of the first excited state excitation events due to the fast (f_{fast}) and slow (f_{slow}) excitation processes.. 106

Figure 5.3. (Color) Time-dependent Er^{3+} PL intensity at 981 nm [(a) and (b)] and at 1535 nm [(c) and (d)] under pulsed excitation at 355 nm (solid lines) with the corresponding fits (dashed lines). All intensities are shown on the same relative scale. Contributing excitation channels are schematically indicated by the horizontal and dashed vertical arrows. The relevant optical transitions are indicated by the solid vertical arrows... 107

Figure 6.1. (Color) PL spectra of Er-doped SRSO of as-deposited, LTA and HTA samples under cw excitation at 351 nm.. 116

Figure 6.2. (Color) Excitation spectra of Er^{3+} emission at 1535 nm (as-deposited, LTA and HTA samples), LC emission at 850 nm (LTA sample) and Si NCs emission at 850 nm (HTA sample). The corresponding scaling factors are included. Inset: XPS spectra of as-deposited and annealed (600°C and 1100°C) Er-doped SRSO, a Si (100) substrate and a sputtered $Er:SiO_2$ film.. 117

Figure 6.3. (Color) The dependence of the relative density of excited Er^{3+} ions N_{Er}* in LTA (squares) and as-deposited (circles) Er-doped SRSO on pump flux under (a) 355 nm and (b) 532 nm pulsed excitation. The solid lines represent fits to the data....................................... 119

Figure 7.1. (Color) Photoluminescence spectra of Er-doped Si-rich SiO_2 annealed at 600°C (LTA) measured in the temperature range 20 – 200°C. Inset: normalized emission from the first excited state of Er^{3+} ($^4I_{13/2}$)... 130

Figure 7.2. (Color) Photoluminescence spectra of Er-doped Si rich SiO_2 annealed at 1060°C (HTA) measured in the temperature range 20 – 200°C. The values of the PL intensity may be compared to the intensities in Fig. 1. Inset: normalized emission from the first excited state of Er^{3+} ($^4I_{13/2}$)... 131

Figure 7.3. Temperature dependence of (a) integrated photoluminescence intensity I_{Er} corresponding to the $^4I_{13/2} \rightarrow {}^4I_{15/2}$ transition of Er^{3+} and (b) decay time τ_{dec} of the first excited state of Er^{3+} ($^4I_{13/2}$) in samples annealed at low (LTA) and high (HTA) temperature.............. 132

Figure 7.4. Temperature dependence of the (a) effective absorption cross-section of the first excited state of Er^{3+} (σ_{eff}) and (b) the density of optically active sensitized Er^{3+} ions in samples annealed at low (LTA) and high (HTA) temperature.. 133

Figure 7.5. (Color) Calculated pump flux dependence of the Er^{3+} related optical gain at 1535 nm under excitation at 351 nm for different sample temperatures, in samples annealed at (a) low (LTA) and (b) high (HTA) temperature.. 135

Figure 8.1. (Color) PL spectra of LTA (a) and HTA (b) samples with different silicon excess concentrations. 145

Figure 8.2 (a) PL intensity of Er^{3+} transition $^4I_{13/2} \rightarrow {}^4I_{15/2}$ integrated in the region 1350 – 1700 nm I and the decay time of Er^{3+} PL at 1535 nm τ_{dec}, (b) excitation cross-section of the first excited state of Er^{3+} σ_{Er}, and (c) density of sensitized Er^{3+} ions N_{Er} of LTA and HTA samples as a function of Si excess concentration.. 147

LIST OF TABLES

Table 6.1. Values of σ_{Er} and N_{Er} under pulsed 355 nm and 532 nm excitation for as-deposited and LTA samples... 120

CHAPTER 1. INTRODUCTION

1.1 Silicon Photonics

The continued increase of computer performance requires a larger number of transistors to be incorporated on a single chip operating at clock speeds exceeding several GHz. These advances necessitate an increase of the on-chip data transfer bandwidth and a reduction in the size of the copper interconnects. It is known that copper interconnects become bandwidth limited at switching speeds exceeding ~ 10 GHz mainly due to the frequency dependent wire resistance and impedance mismatches.[1] In addition the increase of the number of transistors and the decrease of chip sizes results in a tighter packing of the electrical interconnects and consequently in higher parasitic capacitance. As a result the copper interconnects become the limiting factor in the improvement of computer performance. To keep up with Moore's Law a new approach to the realization of inter- and intra-chip interconnects is necessary.

It is currently widely accepted that the most viable solution to the interconnect problem is the substitution of at least a subset of the electronic interconnects with optical interconnects.[2-5] Photonic interconnects demonstrate a number of advantages over their electronic counterparts: they exhibit immunity to electromagnetic noise, low latency, low power dissipation, large bandwidth, bit rate transparency, and low crosstalk. Moreover photonic interconnects remove the need for signal repetition and regeneration that is required in their electronic counterparts.

The realization of photonic interconnects requires the development of new efficient and reliable on-chip optical device elements, including light sources, modulators, amplifiers, buffers, switches and detectors. The transition from electronic to photonic interconnects will be cost-effective only if it is performed within mature CMOS technology. This requires silicon

compatibility of all the integrated optical components. A significant amount of work has already been done and different approaches to the realization of each of the mentioned components have been attempted: microdetectors based on III-V structures evanescently coupled to the silicon waveguide,[6] Ge-on-Si[7-10] and ion-implanted silicon[11] have been demonstrated; modulators based on the free carrier plasma dispersion effect[12-14] and electro-absorption effect[15] have been realized; hybrid evanescent amplifiers,[16] optical buffers[17] and switches[18] have been shown.

Of all the necessary components the realization of a silicon-based light source is considered to be one of the most challenging tasks. Due to the indirect nature of the silicon bandgap the emission efficiency of silicon is low and even at liquid helium temperatures does not exceed ~ 10^{-4} %.[19] Consequently alternative ways of realizing a CMOS compatible light source are to be used. Approaches that are currently considered include silicon Raman lasers,[20] hybrid evanescent lasers,[21] devices based on germanium-on-silicon,[22] silicon nanocrystal doped SiO_2, [23-28] silicon nanocrystal doped silicon nitride,[29] erbium-doped Si-rich silicon nitride,[30] and erbium-doped silicon-rich SiO_2. [31-38]

1.2 Silicon Photonics and Erbium

One of the possible solutions to the realization of silicon based light source is to use the emission not from silicon itself but rather from optical centers incorporated into silicon based matrices. The use of erbium ions incorporated in a silicon based host material is one of the possible approaches. Erbium is a rare earth metal belonging to the lanthanide series. The electronic structure of metallic erbium can be described as [Xe] $4f^{12}$ $6s^2$. Upon the incorporation of erbium into a host, Er assumes its trivalent state (Er^{3+}) with the electronic configuration [Xe] $4f^{11}$. The

incompletely filled 4f shell of the Er^{3+} ion is shielded by closed 5s and 5p shells. The spin-spin and spin-orbit interaction of the electrons in the 4f shell results in the formation of several allowed electronic configurations with relatively high energy differences (Figure 1.1).

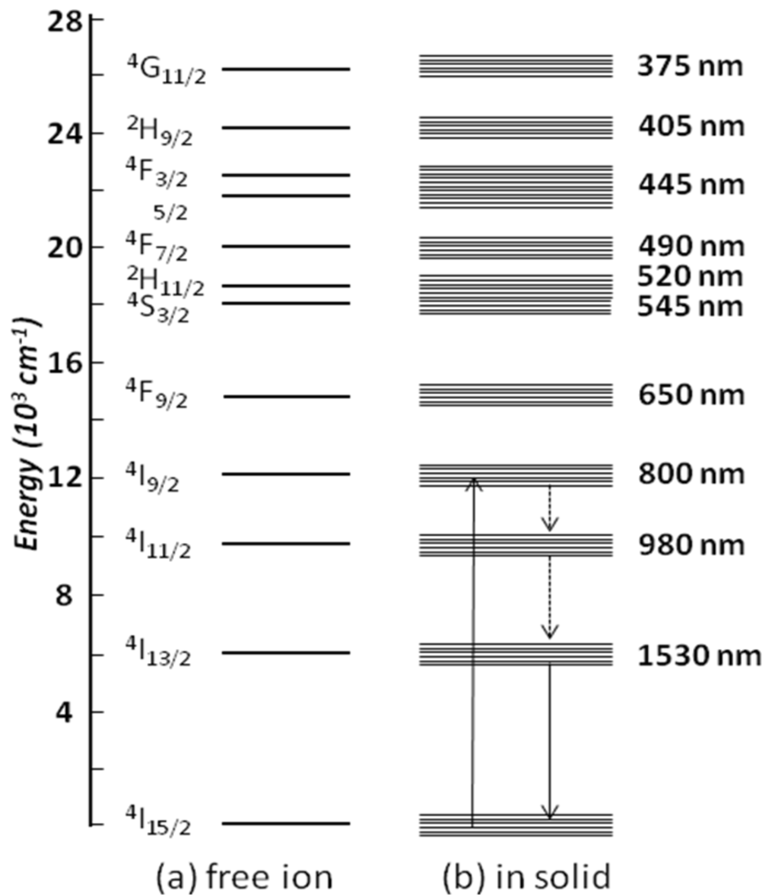

Figure 1.1. Energy levels of Er^{3+} in its free ionic state (a) and in silicate glass (b), showing excitation at 800 nm followed by non-radiative relaxation and emission at 1.53 μm.[39]

For free Er^{3+} ions the magnetic-dipole and electric-quadrupole transitions are allowed while electric-dipole transitions within the 4f shell are parity forbidden.[40] However, the incorporation of Er^{3+} into a host can perturb the erbium electron wave functions and thus

introduce higher energy states of opposite parity (5d) into the 4f configuration, making the electric-dipole transitions weakly allowed. In addition to perturbations modifying the parity of the wavefunctions, the local field introduced by the host material introduces Stark splitting of the Er^{3+} levels and consequently the broadening of the erbium emission and absorption spectra. Due to the shielding by the closed 5s and 5p shells the energies of the levels within the 4f shell remain relatively constant in different matrices, thus making the location of the emission and absorption maxima of Er^{3+} ions approximately independent of the host material, while the exact absorption and emission line shapes and their cross-sections are host dependent.

Denotation of the Er^{3+} energy levels shown in Fig. 1.1 is done using the Russell-Saunders notation scheme of the form $^{2S+1}L_J$ where S is the total unpaired spin of all 4f electrons, L is the total orbital angular momentum (labeled S, P, D, F, G, H, I, ..) and J = L + S is the total angular momentum. The transition of Er^{3+} ion from its first excited ($^4I_{13/2}$) to the ground state ($^4I_{15/2}$) corresponds to an emission wavelength λ = 1.53 μm and has been extensively used in telecommunication technology due to the overlap of this wavelength with the maximum transmission window of silica-based fibers.[41] The long decay times (typically ~ 1 – 15 ms) of the $^4I_{13/2}$ level combined with the fast non-radiative phonon-assisted relaxation from level $^4I_{11/2}$ to level $^4I_{13/2}$ enable the realization of population inversion between the $^4I_{13/2}$ and $^4I_{15/2}$ level . This has enabled the use of Er-doped glasses for optical amplification of signals at 1.53 μm. The absorption spectrum of Er^{3+} incorporated in silica matrices is characterized by a number of relatively narrow absorption lines with low absorption cross-sections (e.g. $\sigma_{abs} \sim 10^{-20} - 10^{-21}$ cm^2 for the $^4I_{15/2} \rightarrow {}^4I_{13/2}$ transition).[42] The combination of these two factors results in the necessity of resonant high-power excitation in order to achieve population inversion and gain.

The power and wavelength demands on the pump source can be significantly relaxed by the incorporation of Er in a silicon matrix. Contrary to the case of the Er-doped SiO_2 where the excitation of Er^{3+} takes place by the direct resonant absorption of photons, Er^{3+} in bulk silicon is excited by electrons and holes generated in the semiconductor host. The intensity of Er^{3+} excited in this way has been found to be strongly dependent on temperature with a significant decrease of the photoluminescence intensity at temperatures exceeding 100K.[43] The decrease of the intensity has been explained by two independent processes.[44] exciton dissociation and energy backtransfer from the Er^{3+} first excited state to an Er^{3+} related exciton trap level. These processes make bulk silicon unviable for efficient Er^{3+} excitation and emission at room temperature.

An alternative concept of Er^{3+} excitation that can facilitate the realization of a silicon-based light source is the use of a host material that includes sensitizers with a large absorption cross-section, a broad absorption band, and a high transfer efficiency to the erbium ions. Different types of sensitizers have been realized, including semiconductor nanocrystals,[31, 38, 45-48] metal ions,[49] and organic complexes.[50]

The possibility of indirect excitation of Er^{3+} by silicon nanostructures was successfully demonstrated in the mid-1990s by a number of scientific groups.[31, 45, 51, 52] The incorporation of silicon nanocrystals in Er-doped SiO_2 has been shown to result in a significant[31, 53] increase of the Er^{3+} photoluminescence intensity as compared to that of Er^{3+} in pure SiO_2. In addition these studies showed that incorporation of Er^{3+} into Si-rich SiO_2 results in the Er-concentration-dependent suppression of nanocrystal emission as well as in the appearance of continuous semiconductor-like excitation spectra of the Er^{3+} emission.[31] The anticorrelation of the Er^{3+}- and nanocrystal-related emission together with the broad excitation spectra not representative of

directly excited Er^{3+} ions pointed to the presence of indirect excitation of the Er^{3+} ions by silicon nanocrystals incorporated in the SiO_2 host. Additionally amorphous silicon clusters which form at annealing temperatures below those needed for silicon crystallization (T < 1000°C) were also considered as possible sensitizers of Er^{3+} ions.[54-57]

The possibility of Er^{3+} sensitization brings a number of important advantages to the optical properties of Er^{3+} in SiO_2. Sensitization results in a dramatic increase of the Er^{3+} effective absorption cross-section by 3 – 6 orders of magnitude depending on the excitation wavelength used: from ~10^{-20} - 10^{-21} cm^2 [Ref. 42] in the case of resonant excitation of Er^{3+} incorporated in pure-silica to ~10^{-15} - 10^{-17} cm^2 [Refs. 46, 47, 58] in the case of indirect Er^{3+} excitation in a Si-rich silica host, making it comparable in value to the absorption cross-section of the nanocrystals. Additionally silicon-based sensitizers possess inherently broad absorption bands, thus significantly reducing the wavelength requirements on the excitation source. Incorporation of excess silicon also results in a local increase of the effective refractive index of SiO_2 thus enabling the realization of waveguides using an Er-doped Si-sensitized SiO_2 core with a SiO_2 based cladding.[59] The excitation of Er^{3+} ions in Si-nanocrystal-doped SiO_2 is considered to occur through excitons formed within the nanocrystals upon the absorption of photons. The exciton can recombine either radiatively by emitting a photon, or nonradiatively, losing its energy to a defect serving as an exciton trap or transferring its energy to a nearby Er^{3+} ion. An Er^{3+} ion excited by the latter process can emit a photon at 1.54 μm upon radiative relaxation to the ground state.

Several studies have focused on determining the physical location of the sesitized Er^{3+} ions in the matrix. It was found that upon the formation of silicon nanocrystals in Er-doped Si-rich SiO_2 the Er^{3+} ions are mostly situated in the SiO_2 matrix[60, 61] or on the surface of

nanocrystals[62] rather than inside the nanocrystals. This likely results from the higher solubility of Er^{3+} in SiO_2 as compared to that in silicon.[60, 61] The characteristic interaction distance between the silicon nanoclusters and Er^{3+} ions appears to depend on the crystallinity of the clusters and is reported to be in the range ~ 0.4 - 0.5 nm in the case of amorphous silicon layers,[63] and clusters[55] and ~ 2.5 – 2.6 nm in the case of crystalline silicon clusters.[55, 64]

In time resolved studies the nanocrystal-erbium energy transfer was found to be characterized by two different transfer processes occurring on different time scales: a fast process (transfer time τ_{tr} < 100 ns) and a slow process (τ_{tr} ~ 2 – 70 μs)[65] with the former dominating over the latter. The exact nature and origin of the two processes was not known, however it was suggested that the transfer time can be dependent on the distance between the nanocrystals and Er^{3+} ions.[66] The transfer time of the slow process is strongly dependent on the nanocrystal size and has been shown to increase from ~ 10 μs to ~ 115 μs with increasing nanocrystal size from 2.7 nm to 5.5 nm.[65, 67, 68]

Based on the fact that the ionic radius of Er^{3+} is ~ 0.1 nm while typical radii of Si nanocrystals are ~ 2 - 6 nm, at high Er^{3+} concentrations a large number of Er^{3+} ions can be situated around a single nanocrystal within the characteristic interaction distance. However the number of Er^{3+} ions which can couple to a nanocrystal is limited. Currently there is no agreement on the actual number of Er^{3+} ions capable of coupling to a single silicon nanocrystal. Two main experimental observations exist: the first one strongly suggests that a single nanocrystals cannot excite more than 1 – 2 Er^{3+} ions[48, 68] while the other suggests that as many as ~ 20 – 40 Er^{3+} ions[38, 60] can be excited by a single silicon nanocrystal. The former claim is based on the observation of a similar excitation rate of the Si nanocrystals and Er^{3+} ions within the same

sample, as well as the saturation of the Er^{3+} excitation rate with the increase of the Er^{3+} concentration[48] while the latter claim is based on the difference in the saturation level of the Er^{3+} photoluminescence intensity under continuous wave and pulsed pumping.[38]

In addition to the number of Er^{3+} ions that can be excited by a single nanocrystal, an important factor to consider for applications is the fraction of indirectly excitable Er^{3+} ions. This parameter becomes important when gain is considered as it is related to the background loss introduced by Er^{3+} ions that are optically active but not coupled to sensitizers. In Er-doped SiO_2 prepared under optimum conditions almost 100% of the Er^{3+} ions are optically active.[69] However recent studies showed that the concentration of indirectly excitable Er^{3+} ions in Si-rich SiO_2 films typically does not exceed ~ 0.01 - 0.04 at.%.[48, 70-72]

In order to investigate the interaction between Si nanocrystals and Er^{3+} ions, the emission properties of Si nanocrystals must be considered. The photoluminescence of Si nanocrystals with diameters ~ 3 – 6 nm is characterized by an emission band peaking in the range of ~ 1.4 – 1.8 eV attributed to the radiative recombination of quantum confined excitons. This range overlaps with at least two Er^{3+} levels ($^4I_{11/2}$ corresponding to 1.24 eV and $^4I_{9/2}$ corresponding to 1.55 eV). This overlap suggests the possibility of resonant and possibly phonon-mediated excitation of Er^{3+} ions. Consequently one could expect the presence of dips in the nanocrystal emission spectrum at energies corresponding to the Er^{3+} transition energies. Although a decrease in the peak intensity as well as in the integrated intensity of the nanocrystal-related emission band has been observed upon Er incorporation[31, 48] either no or only very minor Er-related dips (at cryogenic temperatures only)[68, 73] have been observed. The absence of such resonance features has been a source of ongoing debate.

To summarize, significant work has been done in the field of Si nanocrystal-Er^{3+} interaction, however a number of important questions still remain. The first unresolved issue is the presence of two different erbium excitation processes occurring on significantly different time scale first observed by Fujii et al.[65] The two processes were tentatively explained in terms of a distance-dependent energy transfer,[66] however no clear experimental evidence of this theory has been provided. A second unresolved issue is related to the exact mechanism of the nanocrystal-Er^{3+} excitation. The observed overall decrease of the nanocrystal emission band upon erbium incorporation without clear evidence of resonant energy transfer[31] suggests a counterintuitive non-resonant energy transfer mechanism which cannot be explained within existing theories. And finally, the observed possibility of the indirect excitation of Er^{3+} in samples which potentially cannot contain crystalline silicon aggregates[54, 74] brings into question the importance of Si nanocrystals in the Er^{3+} sensitization model.

In the current dissertation experimental results are presented that resolve the issues listed above. It is shown that not Si nanocrystals but rather silicon-excess-related luminescence centers are the dominant source of Er^{3+} excitation in Er-doped Si-rich SiO_2 films. The excitation by luminescence centers can explain not only the observations made in the studies presented in this thesis but also the seemingly contradictory observations presented in independent studies by other scientific groups. The discovery of luminescence center mediated sensitization of Er^{3+} in Si-rich SiO_2 presented in this dissertation also has significant implications for the realization of devices based on silicon sensitized gain media. The observed presence of indirect excitation of Er^{3+} in samples without silicon nanocrystals suggests that silicon nanocrystal related detrimental processes such as confined carrier absorption[75, 76] and scattering[77] which are known to introduce

losses can potentially be avoided in low temperature annealed Er-doped Si-rich SiO_2 by avoiding the formation of silicon nanocrystals. This dissertation also shows that Er-doped Si-rich SiO_2 without silicon nanocrystals can provide an up to two orders of magnitude higher density of sensitized Er^{3+} ions as compared with the corresponding material containing silicon nanocrystals. These considerations clearly suggest that higher gain values can be achieved in devices based on low temperature processed Er-doped Si-rich SiO_2. Additionally, as presented in this dissertation Er-doped Si-rich SiO_2 without silicon nanocrystals enables a simplified fabrication process as compared with the material containing silicon nanocrystals. All these considerations suggest that Er-doped Si-rich SiO_2 without silicon nanocrystals is the preferred material for the realization of on-chip devices as compared with the material containing silicon nanocrystals.

1.3 Dissertation Overview

The dissertation is organized as follows:

Chapter 2 presents clear experimental evidence that silicon-excess related luminescence centers rather than silicon nanocrystals are the dominant source of Er^{3+} excitation in Er-doped Si-rich SiO_2. Since the inception of the field of indirect excitation of Er^{3+} in Si-rich SiO_2 and the development of the theory of nanocrystal mediated sensitization of Er^{3+}, a number of discrepancies between the actual experimental results and theoretically predicted results were observed. It is essential to understand the reason behind these discrepancies, both from a scientific and technological standpoint. In this chapter it is demonstrated that indirect excitation of Er^{3+} occurs in sputter deposited Si-rich SiO_2 for all annealing temperatures in the range 600-1200°C, including temperatures below 1000°C for which no silicon nanocrystals are

observed. A new theory considering luminescence center mediated excitation with high transfer efficiency as the dominant excitation mechanism independent of the presence of silicon nanocrystals is developed. It is demonstrated that increasing the annealing temperature up to the temperatures necessary for nanocrystal formation results in the significant drop in the density of optically active sensitized Er^{3+} ions. These results provide an alternative explanation for several seemingly contradictory observations existing in the literature.

Chapter 3 presents studies of the influence of hydrogen passivation on luminescence-center-mediated excitation of Er^{3+} in samples without (annealed at 600°C) and with (annealed at 1100°C) silicon nanocrystals. For the industrial implementation of devices based on Er-doped Si-rich SiO_2 it is necessary to find the fabrication conditions that produce optimal optical properties of the considered material. It is known that passivation has a significant positive effect on the optical properties of the silicon nanocrystals. Consequently, it is important to understand the effect of passivation on the optical properties of Er^{3+} in samples with and without silicon nanocrystals. In this chapter it is demonstrated that passivation has little effect on the Er^{3+} emission in samples without silicon nanocrystals while a significant increase of the Er^{3+} emission is observed upon passivation of samples containing silicon nanocrystals. This latter observation is attributed to two interrelated effects, namely (a) an increase in the density of fully passivated optically active nanocrystals due to the passivation-induced removal of silicon dangling bonds, and (b) a concurrent reduction of nonradiative Er^{3+} relaxation from levels above the $^4I_{13/2}$ level attributed to a direct interaction of excited Er^{3+} ions with silicon dangling bonds. The additional observation of a counterintuitive gradual increase of the nanocrystal photoluminescence decay time upon passivation is successfully explained using a new approach that takes into account the

inhomogeneous nature of the nanocrystal-related emission band. The combination of luminescence-center-mediated Er^{3+} excitation and silicon dangling bond induced Er^{3+} de-excitation is shown to explain at least fourteen experimental observations reported in literature.

Chapter 4 presents studies of the Er^{3+} sensitization mechanism in low-temperature-annealed Si-rich SiO_2. Detailed knowledge of the sensitization characteristics is essential for modeling of actual gain media based on this material. To study the excitation dynamics, decay traces of the Er^{3+} emission from the first and second excited state recorded under pulsed excitation were analyzed. It is demonstrated that the sensitization of Er^{3+} by luminescence centers is fast (transfer time $\tau_{tr} < 27$ ns) and appears to occur not only into higher energy states of Er^{3+} but also directly into first excited state ($^4I_{13/2}$). The multi-level nature of the Er^{3+} sensitization is shown to result in two types of excitation of the $^4I_{13/2}$ state: a fast excitation process ($\tau_{tr} < 27$ ns) directly into the $^4I_{13/2}$ level and a slow excitation process due to fast excitation into Er^{3+} levels above the $^4I_{13/2}$ level, followed by internal Er^{3+} relaxation with a time constant $\tau_{32} > 2.3$ μs. The fast and slow excitation of the $^4I_{13/2}$ level are shown to account for an approximately equal fraction of the excitation events: 45 – 50 % and 50 – 55 % respectively.

Chapter 5 presents temperature dependent studies of the erbium emission dynamics of the second ($^4I_{11/2}$) and first ($^4I_{13/2}$) excited state upon luminescence-center-mediated excitation in low-temperature-annealed Er-doped Si-rich SiO_2 at sample temperatures in the range 15 – 300K. While Chapter 4 demonstrated that 50 – 55 % of the $^4I_{13/2}$ excitation events occurred via the $^4I_{11/2}$ level, the data left open the possibility that a large fraction of $^4I_{11/2}$ excitations were followed by direct relaxation to the ground state, which would correspond to a low $^4I_{13/2}$ excitation efficiency. The presented temperature dependent study of the emission dynamics in Chapter 5 provides

information on the efficiency of the $^4I_{11/2} \rightarrow {}^4I_{13/2}$ relaxation process through consideration of phonon assisted relaxation. It is known that the relaxation from the second excited state to the first excited state of Er^{3+} in common SiO_2 based host materials is predominantly phonon assisted, resulting in a strongly temperature dependent relaxation rate. In this chapter it is demonstrated that contrary to the case of Er^{3+} in stoichiometric SiO_2, in Si-rich SiO_2 the Er^{3+} relaxation efficiency from the second to the first excited state is approximately temperature-independent. The presented data indicate that the relaxation efficiency from the second to the first excited state is near-unity. Internal relaxation is shown to account for 50 - 55% of the $^4I_{13/2}$ excitation events in the considered temperature range. The presented conclusions suggest high pump efficiency and stable operation of devices based on this material at different temperatures is possible.

Chapter 6 presents studies of the pump wavelength dependence of the density of sensitized Er^{3+} ions in as-deposited Si-rich SiO_2. The demonstration of indirect excitation of Er^{3+} in samples annealed at 600°C provided a strong indication that Si nanocrystals could not be the main source of the observed sensitization. The data presented in this chapter further strengthen this conclusion through the demonstration of indirect excitation of Er^{3+} in as-deposited (not annealed) Er-doped Si-rich SiO_2. The presented data definitively rule out the involvement of Si nanocrystals in the Er^{3+} excitation in these samples. Furthermore, the Er^{3+} absorption cross-section, and consequently the sensitization mechanism, is shown to be similar in as-deposited samples to that in samples annealed at 600°C and at 1100°C. A second issue addressed in this chapter involves the spectral dependence of the sensitization process. To select the optimal pump wavelength for use in an actual device based on Er-doped Si-rich SiO_2 it is essential to

know whether the density of sensitized Er^{3+} ions – and therefore the maximum achievable gain – is dependent on the excitation wavelength. In this chapter the results of excitation spectroscopy measurements as well as photoluminescence saturation measurements under pulsed excitation at 355 nm and 532 nm are presented. The density of excitable Er^{3+} ions is found to be approximately excitation wavelength independent, while the shape of the Er^{3+} excitation spectra is shown to be governed by a wavelength-dependent Er^{3+} absorption cross-section. These results suggest that similar gain values can be acquired using a broad range of excitation wavelengths.

Chapter 7 studies the effect of high sample temperature on the optical properties of Er-doped Si-rich SiO_2 in the range 20 – 200°C. To implement Er-doped Si-rich SiO_2 in actual on-chip devices it is important to investigate the optical properties of this material up to realistic processor case temperatures, which can approach ~ 90°C. The optical properties of Er-doped Si-rich SiO_2 with and without silicon nanocrystals are shown to exhibit a similar temperature dependence. Based on the presented experimental results an increase of the sample temperature from 20°C to 200°C is predicted to result in a decrease of the maximum optical gain at 1535 nm by a factor of ~ 1.8 and ~ 1.6 for samples with and without nanocrystals respectively. It is predicted that a temperature increase from room temperature to 90°C leads to a maximum optical gain reduction of ~ 1.3 for both materials. In addition, the predicted erbium related optical gain at significant inversion levels in samples processed at low temperature (600°C) is a factor ~ 9 higher than for samples processed at high temperature (1060°C). These results suggest that relatively stable gain performance can be achieved in this material under typical processor operating temperatures.

Chapter 8 investigates the effect of the Si excess concentration on the Er^{3+} sensitization for samples annealed at low temperature and at high temperature. It is found that a Si excess concentration of ~ 14.5 at.% is optimum for achieving the highest density of sensitized Er^{3+} ions in low-temperature annealed Si-rich SiO_2 (without Si nanocrystals). A similar optimum concentration of Si excess of ~ 11.5 at.% is found for samples annealed at high temperature (with Si nanocrystals).

Chapter 9 summarizes the results presented in this dissertation and discusses the implications of these results for the realization of actual devices based on Er-doped Si-rich SiO_2. A short overview of possible future research directions in the field of Er^{3+} sensitization in Si-rich SiO_2 is given.

1.4 References

[1] D. A. B. Miller, Proc. IEEE **88**, 728 (2000).

[2] N. Daldosso and L. Pavesi, Laser Phot. Rev. **3**, 508 (2009).

[3] R. Soref, IEEE J. Sel. Top. Quantum Electron **12**, 1678 (2006).

[4] B. Jalali and S. Fathpour, J. Light. Tech. **24**, 4600 (2006).

[5] A. Shacham, K. Bergman, and L. P. Carloni, IEEE Trans. Computing **57**, 1246 (2006).

[6] H. Park, A. W. Fang, R. Jones, O. Cohen, O. Raday, M. N. Sysak, M. J. Paniccia, and J. E. Bowers, Opt. Express **15**, 6044 (2007).

[7] J. Liu, D. D. Cannon, K. Wada, Y. Ishikawa, S. Jongthammanurak, D. T. Danielson, J. Michel, and L. C. Kimerling, Appl. Phys. Lett. **87**, 011110 (2005).

[8] Y. Kang, et al., Nat. Photon. **3**, 59 (2008).

[9] T. Yin, R. Cohen, M. M. Morse, G. Sarid, Y. Chetrit, D. Rubin, and M. J. Paniccia, Opt. Express **15**, 13965 (2007).

[10] D. Ahn, C. Hong, J. Liu, W. Giziewicz, M. Beals, L. C. Kimerling, J. Michel, J. Chen, and F. X. Kärtner, Opt. Express **15**, 3916 (2007).

[11] A. P. Knights, J. D. B. Bradley, S. H. Gou, and P. E. Jessop, J. Vac. Sci. Technol. A **24(3)**, 783 (2006).

[12] A. Liu, R. Jones, L. Liao, D. Samara-Rubio, D. Rubin, O. Cohen, R. Nicolaescu, and M. Paniccia, Nature **427**, 615 (2004).

[13] A. Liu, L. Liao, D. Rubin, H. Nguyen, B. Ciftcioglu, Y. Chetrit, N. Izhaky, and M. Paniccia, Opt. Express **15**, 660 (2007).

[14] Q. Xu, B. Schmidt, S. Pradhan, and M. Lipson, Nature **435**, 325 (2005).

[15] J. Liu, M. Beals, A. Pomerene, S. Bernardis, R. Sun, J. Cheng, L. C. Kimerling, and J. Michel, Nat. Photon. **2**, 433 (2008).

[16] H. Park, A. W. Fang, O. Cohen, R. Jones, M. J. Paniccia, and J. E. Bowers, IEEE Photon. Technol. Lett. **19**, 230 (2007).

[17] F. Xia, L. Sekaric, and Y. Vlasov, Nat. Photon. **1**, 65 (2006).

[18] Y. Vlasov, W. M. J. Green, and F. Xia, Nat. Photon. **2**, 242 (2008).

[19] D. Kovalev, H. Heckler, G. Polisski, and F. Koch, Phys. Stat. Sol. (b) **215**, 871 (1999).

[20] H. Rong, A. Liu, R. Jones, O. Cohen, D. Hak, R. Nicolaescu, A. Fang, and M. Paniccia, Nature **433**, 292 (2005).

[21] A. W. Fang, H. Park, O. Cohen, R. Jones, M. J. Paniccia, and J. E. Bowers, Opt. Express **14**, 9203 (2006).

[22] X. Sun, J. Liu, L. C. Kimerling, and J. Michel, Opt. Lett. **34**, 1198 (2009).

[23] L. Pavesi, L. D. Negro, C. Mazzoleni, G. Franzò, and F. Priolo, Nature **408**, 440 (2000).

[24] R. J. Walters, G. I. Bourianoff, and H. A. Atwater, Nat. Mater. **4**, 143 (2005).

[25] I. Sychugov, N. Elfström, A. Hallén, J. Linnros, and M. Qiu, Opt. Lett. **32**, 1878 (2007).

[26] R. J. Zhang, S.-Y. Seo, A. P. Milenin, M. Zacharias, and U. Gösele, Appl. Phys. Lett. **88**, 153120 (2006).

[27] M. L. Brongersma, P. G. Kik, A. Polman, K. S. Min, and H. A. Atwater, Appl. Phys. Lett. **76**, 351 (2000).

[28] J. Ruan, P. M. Fauchet, L. D. Negro, M. Cazzanelli, and L. Pavesi, Appl. Phys. Lett. **83**, 5479 (2003).

[29] K. S. Cho, N.-M. Park, T.-Y. Kim, K.-H. Kim, G. Y. Sung, and J. H. Shin, Appl. Phys. Lett. **86**, 071909 (2005).

[30] S. Yerci, R. Li, S. O. Kucheyev, T. v. Buuren, S. N. Basu, and L. Dal Negro, Appl. Phys. Lett. **95**, 031107 (2009).

[31] M. Fujii, M. Yoshida, Y. Kanzawa, S. Hayashi, and K. Yamamoto, Appl. Phys. Lett. **71**, 1198 (1997).

[32] P. G. Kik, M. L. Brongersma, and A. Polman, Appl. Phys. Lett. **76**, 2325 (2000).

[33] A. J. Kenyon, M. Wojdak, I. Ahmad, W. H. Loh, and C. J. Oton, Phys. Rev. B **77**, 035318 (2008).

[34] H.-S. Han, S.-Y. Seo, and J. H. Shin, Appl. Phys. Lett. **79**, 4568 (2001).

[35] D. Pacifici, G. Franzò, F. Priolo, F. Iacona, and L. D. Negro, Phys. Rev. B **67**, 245301 (2003).

[36] D. Navarro-Urrios, A. Pitanti, N. Daldosso, F. Gourbilleau, R. Rizk, B. Garrido, and L. Pavesi, Phys. Rev. B **79**, 193312 (2009).

[37] K. Hijazi, R. Rizk, J. Cardin, L. Khomenkova, and F. Gourbilleau, J. Appl. Phys. **106**, 024311 (2009).

[38] M. Wojdak, M. Klik, M. Forcales, O. B. Gusev, T. Gregorkiewicz, D. Pacifici, G. Franzò, F. Priolo, and F. Iacona, Phys. Rev. B **69**, 233315 (2004).

[39] W. Miniscalco, in Rare-earth-doped fiber lasers and amplifiers (edited by M. Digonnet, Marcel Dekker, Inc., New York, 2001), p. 63.

[40] W. Miniscalco, in Rare-earth-doped fiber lasers and amplifiers (edited by M. Digonnet, Marcel Dekker, Inc., New York, 2001), p. 26

[41] E. Desurvire, Erbium-Doped Fiber Amplifiers (John Wiley & Sons, Inc, Hoboken, New Jersey, 2002).

[42] W. Miniscalco, J. Light. Tech. **9**, 234 (1991).

[43] P. G. Kik, M. J. A. de Dood, K. Kikoin, and A. Polman, Appl. Phys. Lett. **70**, 1721 (1997).

[44] F. Priolo, G. Franzò, S. Coffa, A. Polman, S. Libertino, R. Barklie, and D. Carey, J. Appl. Phys. **78**, 3874 (1995).

[45] A. J. Kenyon, P. F. Trwoga, M. Federighi, and C. W. Pitt, J. Phys.: Condens. Matter **6**, L319 (1994).

[46] G. Franzò, V. Vinciguerra, and F. Priolo, Appl. Phys. A **69**, 3 (1999).

[47] F. Gourbilleau, M. Levalois, C. Dufour, J. Vicens, and R. Rizk, J. Appl. Phys. **95**, 3717 (2004).

[48] P. G. Kik and A. Polman, J. Appl. Phys. **88**, 1992 (2000).

[49] C. Strohhöfer and A. Polman, Appl. Phys. Lett. **81**, 1414 (2002).

[50] L. H. Slooff, A. Polman, M. P. O. Wolbers, F. C. J. M. v. Veggel, D. Reinhoudt, and J. W. Hofstraat, J. Appl. Phys. **83**, 497 (1998).

[51] T. Kimura, A. Yokoi, H. Horiguchi, R. Saito, T. Ikoma, and A. Sato, Appl. Phys. Lett. **65**, 983 (1994).

[52] G. N. van den Hoven, J. Shin, and A. Polman, J. Appl. Phys. **78**, 2642 (1995).

[53] C. E. Chryssou, A. J. Kenyon, T. S. Iwayama, C. W. Pitt, and D. E. Hole, Appl. Phys. Lett. **75**, 2011 (1999).

[54] G. Franzò, S. Boninelli, D. Pacifici, F. Priolo, F. Iacona, and C. Bongiorno, Appl. Phys. Lett. **82**, 3871 (2003).

[55] F. Gourbilleau, R. Madelon, C. Dufour, and R. Rizk, Opt. Mat. **27**, 868 (2005).

[56] F. Enrichi, G. Mattei, C. Sada, E. Trave, D. Pacifici, G. Franzò, F. Priolo, F. Iacona, M. Prassas, M. Falconieri, and E. Borsella, Opt. Mat. **27**, 904 (2005).

[57] A. Hryciw, C. Blois, A. Meldrum, T. Clement, R. DeCorby, and Q. Li, Opt. Mat. **28**, 873 (2006).

[58] P. G. Kik, Energy transfer in erbium doped optical waveguides based on silicon (PhD dissertation) (2000).

[59] P. G. Kik and A. Polman, J. Appl. Phys. **91**, 534 (2002).

[60] G. Franzò, D. Pacifici, V. Vinciguerra, F. Priolo, and F. Iacona, Appl. Phys. Lett. **76**, 2167 (2000).

[61] G. Franzò, F. Iacona, V. Vinciguerra, and F. Priolo, Mat. Sci. Eng. B, 335 (2000).

[62] X. L. Wu, Y. F. Mei, G. G. Siu, K. L. Wong, K. Moulding, M. J. Stokes, C. L. Fu, and X. M. Bao, Phys. Rev. Lett. **86**, 3000 (2001).

[63] J.-H. Jhe, J. H. Shin, K. J. Kim, and D. W. Moon, Appl. Phys. Lett. **82**, 4489 (2003).

[64] T. Kimura, H. Isshiki, S. Ide, T. Shimizu, T. Ishida, and R. Saito, J. Appl. Phys. **93**, 2595 (2003).

[65] M. Fujii, K. Imakita, K. Watanabe, and S. Hayashi, J. Appl. Phys. **95**, 272 (2004).

[66] K. Imakita, M. Fujii, and S. Hayashi, Eur. Phys. J. D **34**, 161 (2005).

[67] I. N. Yassievich and A. S. Moskalenko, Mater. Sci. Eng. B **105**, 192 (2003).

[68] K. Watanabe, M. Fujii, and S. Hayashi, J. Appl. Phys. **90**, 4761 (2001).

[69] A. Polman, G. N. v. d. Hoven, J. S. Custer, J. H. Shin, R. Serna, and P. F. A. Alkemade, J. Appl. Phys. **77**, 1256 (1995).

[70] B. Garrido, C. García, P. Pellegrino, D. Navarro-Urrios, N. Daldosso, L. Pavesi, F. Gourbilleau, and R. Rizk, Appl. Phys. Lett. **89**, 163103 (2006).

[71] C. J. Oton, W. H. Loh, and A. J. Kenyon, Appl. Phys. Lett. **89**, 031116 (2006).

[72] C. Garcıa, P. Pellegrino, Y. Lebour, B. Garrido, F. Gourbilleau, and R. Rizk, J. Lumin. **121**, 204 (2006).

[73] K. Imakita, M. Fujii, and S. Hayashi, Phys. Rev. B **71**, 193301 (2005).

[74] F. Gourbilleau, R. Madelon, C. Dufour, and R. Rizk, Opt. Mat. **27**, 868 (2005).

[75] D. Navarro-Urrios, A. Pitanti, N. Daldosso, F. Gourbilleau, R. Rizk, G. Pucker, and L. Pavesi, Appl. Phys. Lett. **92**, 051101 (2008).

[76] R. D. Kekatpure and M. L. Brongersma, Nano Lett. **8**, 3787 (2008).

[77] R. D. Kekatpure and M. L. Brongersma, Phys. Rev. A **78**, 023829 (2008).

CHAPTER 2. LUMINESCENCE CENTER MEDIATED EXCITATION AS THE DOMINANT Er SENSITIZATION MECHANISM IN Er-DOPED Si-RICH SiO_2 FILMS

(Based on work published in Physical Review B **76**, 195419 (2007))

The structural and optical properties of erbium-doped silicon-rich silica samples containing 12 atomic % of excess silicon and 0.63 atomic % of erbium are studied as a function of annealing temperature in the range 600 – 1200°C. Indirect excitation of Er^{3+} ions is shown to be present for all annealing temperatures, including annealing temperatures well below 1000°C for which no silicon nanocrystals are observed. Two distinct efficient ($\eta_{tr} > 60\%$) transfer mechanisms responsible for Er^{3+} excitation are identified: a fast transfer process ($\tau_{tr} < 80$ ns) involving isolated luminescence centers (LC), and a slow transfer process ($\tau_{tr} \sim 4 - 100\ \mu s$) involving excitation by quantum confined excitons inside Si nanocrystals. The LC-mediated excitation is shown to be the dominant excitation mechanism for all annealing temperatures. The presence of a LC-mediated excitation process is deduced from the observation of an annealing-temperature-independent Er^{3+} excitation rate, a strong similarity between the LC and Er^{3+} excitation spectra, as well as an excellent correspondence between the observed LC-related emission intensity and the derived Er^{3+} excitation density for annealing temperatures in the range of 600 – 1000ºC. The proposed interpretation provides an alternative explanation for several observations existing in the literature.

2.1 Introduction

In recent years there has been tremendous interest in the use of erbium in silicon based photonics.[1-7] Erbium is a well-known optical dopant that can provide optical gain at 1.54 μm when incorporated into glass hosts. The gain is due to the $^4I_{13/2} \rightarrow ^4I_{15/2}$ transition in the incompletely filled 4f shell of the Er^{3+} ion. The Er^{3+} ion exhibits several sharp absorption lines with a typical absorption cross-section on the order of $\sim 10^{-20} - 10^{-21}$ cm^2 [Ref. 8]. For this reason high power resonant excitation is generally needed in order to reach population inversion and gain. This problem can be overcome by the incorporation of the sensitizers into the host material that exhibit a high absorption cross-section and efficient energy transfer to the Er^{3+} ions.[9] Silicon nanocrystals have been considered as a possible optical sensitizer for Er^{3+} excitation since the first publications on indirect Er^{3+} excitation in several SiO_2 based materials. After the initial observations of indirect Er^{3+} excitation in partly oxidized porous silicon[10] and in oxygen doped silicon,[11] convincing evidence for Er^{3+} excitation via quantum confined excitons in silicon nanocrystals in SiO_2 was found by Fujii et al.[12] In particular, a clear anti-correlation was observed between the intensity of a Si-nanocrystal-related emission band at ~ 800 nm and the Er^{3+} photoluminescence at 1535 nm. Additionally, the Er^{3+} excitation spectrum was found to be continuous, rather than exhibiting the sharp absorption lines associated with Er^{3+} intra-4f transitions. The large absorption cross-section of Si nanocrystals makes this an interesting material system with the potential of providing absorption cross-sections in the range $\sim 10^{-18}$ - 10^{-14} cm^2 for excitation energies between 1.5 eV and 3.5 eV.[13] This represents an increase of the Er^{3+} effective cross-section by 3 – 6 orders of magnitude[14-18] which opens the possibility of using low cost broadband light emitting diodes (LED) rather than diode lasers as

pump sources for achieving gain. Since the initial observations of Si nanocrystal sensitized Er^{3+} excitation, Er^{3+}-related gain has been demonstrated in Er-doped Si-rich SiO_2 both under LED[19] and laser[19-21] excitation.

Despite the extensive amount of research on the topic, several important challenges and questions remain. An important practical challenge is the existence of confined carrier absorption, in which a quantum confined exciton can absorb sub-bandgap radiation with a cross-section far exceeding the emission cross-section of Er^{3+} at 1535 nm.[1, 20, 22, 23] The magnitude of this effect depends on the lifetime of the excitons, and decreases with a decreasing nanocrystal-erbium transfer time. Work by Fujii et al.[24] revealed that while a slow transfer process exists ($\tau_{tr} \sim 1 - 70$ μs), the dominant energy transfer process occurs on a much faster timescale ($\tau_{tr} < 100$ ns). The presence of these two processes is ascribed to energy transfer at different nanocrystal-erbium separations.[25] Further understanding of the origin of the fast transfer process is needed to minimize the effect of confined carrier absorption. A second unresolved issue involves the number of excitable Er^{3+} ions per nanocrystal, which affects the maximum gain that can be achieved in a Si-sensitized gain medium. Conflicting results exist in the literature, with some studies indicating that a Si nanocrystal can excite only 1 – 2 Er^{3+} ions based on lifetime measurements[16, 26] while other studies show that as many as ~20 Er^{3+} ions can be excited by a single nanocrystal by comparing photoluminescence intensities observed under continuous wave and pulsed excitation.[18] A third issue involves the relatively small contribution of resonant Er^{3+} excitation. Resonant excitation would introduce dips in the nanocrystal photoluminescence spectrum due to energy transfer selectively from nanocrystals with an emission energy corresponding to an Er^{3+} transition. However the incorporation of Er in Si-nanocrystal-doped

SiO_2 generally leads to an overall intensity decrease across the entire nanocrystal spectrum, while only very minor dips have been observed at the location of Er^{3+}-related absorption bands at cryogenic temperatures.[27, 28] This indicates that most of the energy transfer occurs non-resonantly. A fourth issue involves the observed independent behavior of the nanocrystal photoluminescence intensity and the Er^{3+} photoluminescence intensity in temperature dependent studies,[26, 29] which has been explained by the existence of fast energy transfer. However subsequent studies revealed that in many samples, the energy transfer to Er^{3+} at room temperature takes place on a time scale of tens of microseconds, posing a challenge to this explanation. A final issue is the relatively recent observation of indirect Er^{3+} excitation in Si-doped SiO_2 annealed at temperatures below the onset of the nanocrystal formation.[30-36]

In the present chapter the structural properties and the room temperature photoluminescence behavior of Er-doped Si-rich SiO_2 were studied as a function of annealing temperature in the range 600 – 1200ºC. On the basis of the experimental results we argue that luminescence centers (LC) associated with excess-silicon-related electronic defects are responsible for most of the indirect Er^{3+} excitation at all annealing temperatures, with small contribution due to nanocrystal-mediated Er^{3+} excitation in samples annealed at $T_{ann} \geq 1000°C$. We show that the coexistence of LC-mediated and nanocrystal-mediated excitation can clarify several observations present in the literature.

2.2 Experimental Techniques

Samples were prepared using a multi-gun magnetron sputter deposition system (AJA International, Inc., ATC 2200-V). Silicon- and erbium-doped SiO_2 films were deposited onto P-doped silicon wafers (100) with a resistivity of 3 – 7 Ωcm by co-sputtering from Si, SiO_2 and SiO_2:Er_2O_3 targets. The Er concentration in the mixed SiO_2:Er_2O_3 target was 1.8 atomic %. Depositions were conducted at room temperature in an Ar background pressure of 4 mTorr. The sample composition and thickness were verified using a Rutherford backscattering spectrometry (RBS) system (General IONEX 1.7 MU Tandetron), and RUMP software[37] was used to fit the recorded RBS spectra. Three types of samples were prepared: samples containing both excess Si (12 atomic %) and Er (0.63 atomic %) labeled 'XSE' ('eXcess Silicon and Erbium') and two types of reference samples: samples containing excess Si (11.5 atomic %) and no Er labeled 'XSO' ('eXcess Silicon Only'), and samples containing Er (0.49 atomic %) and no excess silicon, labeled 'EO' ('Erbium Only'). The film thickness varied from sample to sample and was found to be 92 ± 20 nm. The samples were subsequently annealed for 100 seconds in flowing N_2 (flow rate 3 SLPM) at ambient pressure using a rapid thermal processor (Modular Process Technology Corp., RTP-600S) at temperatures in the range of 600 – 1200°C. The samples were then passivated at a temperature of 500°C for 30 min in flowing forming gas (N_2:H_2 = 95%:5%, flow rate 65 SCCM) in a tube furnace (Lindberg, 58114) and were allowed to cool down to room temperature under continued forming gas flow for 10 min. Mircrostructural characterization of the annealed samples was performed using a transmission electron microscope (FEI Technai F30). Sample cross-sections for transmission electron microscopy measurements were prepared by focused ion-beam (FIB) milling. Room temperature photoluminescence measurements were

taken using the 351 nm emission line of a Kr-ion laser (Spectra-Physics, BeamLok 2060) as the excitation source. The pump power used was 0.66 mW and the spot-size on the sample was ~1 mm^2 unless specified otherwise. The photoluminescence signal was focused into the entrance slits of a single monochromator (Acton, 2300i), and a long pass filter with a cut-off wavelength of 400 nm was placed in front of the entrance slits to block the laser light. Visible photoluminescence spectra were recorded using a thermo-electrically-cooled CCD camera (Andor, DU401-BR-DD). Near-infrared spectra were obtained using a liquid-nitrogen-cooled Ge-detector (Applied Detector Corp., 403S) in combination with standard lock-in techniques. All spectra were corrected for the system response and intensities were corrected for variations in film thickness. For time-dependent photoluminescence measurements the pump beam was modulated using an acousto-optic modulator (NEOS Technologies, 38210-6AS). Photoluminescence traces were obtained using photomultiplier tubes (Hamamatsu R4330-02 for the visible region and Hamamatsu 5509-73 for the near-infrared region) in combination with a multi-channel scaler (Stanford Research Systems, SR430). The spectral resolution in all photoluminescence measurements was ~15 nm. The time resolution in all measurements presented in this study was better than 80 ns. Photoluminescence excitation spectra were taken using multiple Kr-ion emission lines at a pump power of ~1 mW and a spot-size of ~3 mm^2.

2.3 Results and Discussion

2.3.1 Composition and Microstructure

The sample composition was studied using Rutherford Backscattering Spectroscopy (RBS). The samples were continuously randomly tilted during the RBS measurement to avoid channeling. The incident ion energy was 2.219 MeV and scattering angle was 15°. Figure 2.1 shows the acquired RBS spectrum of the XSE sample.

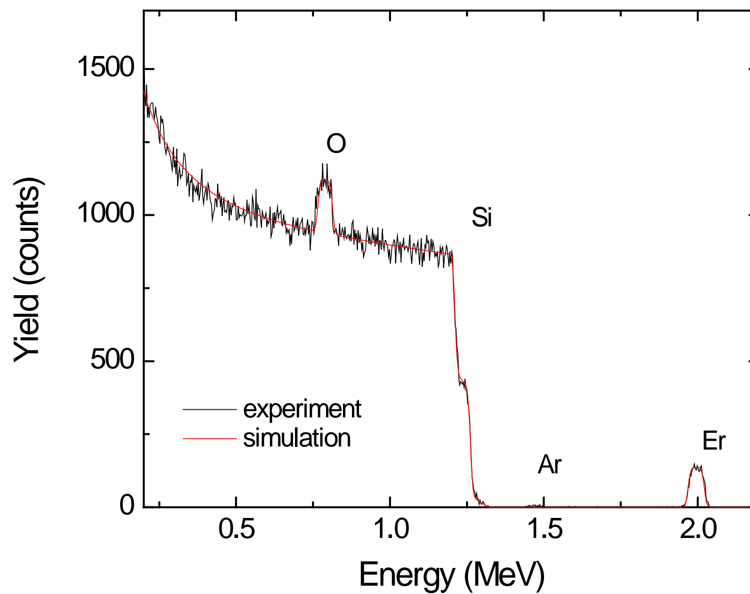

Figure 2.1 Experimental RBS spectrum of the XSE sample (black line) and the corresponding simulated spectrum (red line).

The spectrum exhibits peaks corresponding to oxygen and erbium, as well as a Si edge corresponding to the Si concentration in the deposited film. An additional small peak is observed at an energy of ~1.5 MeV corresponding to Ar. This signal is attributed to a small concentration

(~ 0.4 at.%) of Ar incorporated in the film due to the use of Ar as the sputtering gas. Based on the fit to the experimentally acquired RBS spectrum using RUMP software the concentration of excess Si and Er was found to be 12 at.% and 0.63 at.% respectively. The thickness of the film was found to be 110 nm. A similar analysis of the XSO sample containing no Er yielded a Si excess concentration of 11.5 at.% and the analysis of the reference sample (EO) containing no Si excess yielded an Er concentration of 0.49 at.%.

The microstructure of the samples was studied using cross-sectional transmission electron microscopy (TEM). Figure 2.2 (a) shows the bright field cross-sectional TEM image of an as-deposited XSE sample. The inset shows a magnified view of the area marked by the dashed white square. No clear phase separation is observed, and no lattice fringes could be detected. For the sample annealed at 600°C (Figure 2.2 (b)) a similar sample structure is observed, although a slight intensity contrast appears to be present at length scales on the order of ~10 nm. Again no lattice fringes are observed. The electron diffraction pattern shows bright spots due to the diffraction from the substrate. No diffraction spots related to randomly oriented nanocrystals are observed (Figure 2.2 (c)). For the annealing temperature of 1000°C (Figure 2.2 (d)) clearly separated dark regions with typical diameters in the range 5 – 10 nm are observed, indicating the onset of nanocluster formation. In some of these dark regions lattice fringes are clearly observed, indicating that at least some of the observed clusters are crystalline. Samples annealed at 1200°C (Figure 2.2 (e)) show larger cluster sizes and extended regions with clear lattice fringes, indicating continued nanocrystal growth. Figure 2.2 (f) shows the electron diffraction pattern obtained from a sample annealed at 1200°C. An array of bright diffraction spots is seen due to diffraction from the substrate imaged along [001], and faint rings consisting of individual

diffraction spots are observed. The latter are caused by the diffraction from randomly oriented crystallites in the SiO_2 matrix.

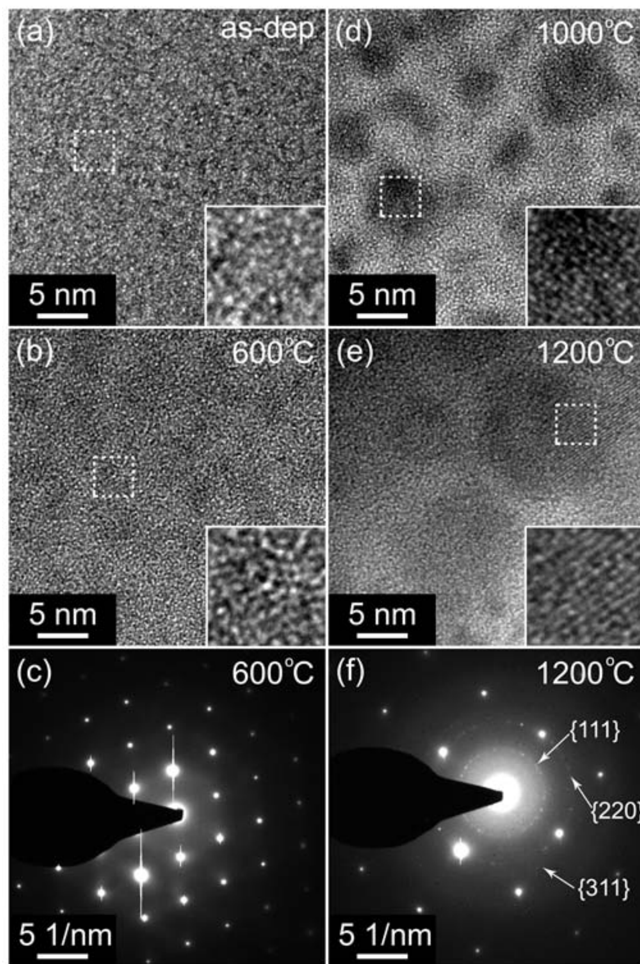

Figure 2.2. High-resolution bright field TEM images of Er-doped Si rich SiO_2 samples (a) as-deposited, (b) annealed at 600°C, (d) annealed at 1000°C, (e) annealed at 1200°C, and electron diffraction patterns for the samples annealed at 600°C (c) and the sample annealed at 1200°C (f). The insets show a magnified view of the area indicated by the dashed squares.

The rings corresponding to the diffraction from {111}, {220}, and {311} lattice planes of Si nanocrystals are clearly seen. Note that one of the diffraction rings crosses a Si substrate diffraction spot, indicating that the crystallites indeed have a lattice spacing corresponding to that of silicon.

2.3.2 Photoluminescence Spectra

Figure 2.3 (top) shows the photoluminescence (PL) spectra obtained from samples containing excess silicon only (labeled XSO) annealed at temperatures in the range of 600 – 1200°C. A broad emission band peaking at wavelengths near 500 nm is observed for all annealing temperatures, and is stronger for the lower annealing temperatures used. Note that this band is observed at annealing temperatures (T_{ann}) well below those required for the onset of silicon nanocrystal nucleation and growth, which has been shown to occur at $T_{ann} > 1000°C$.[38]

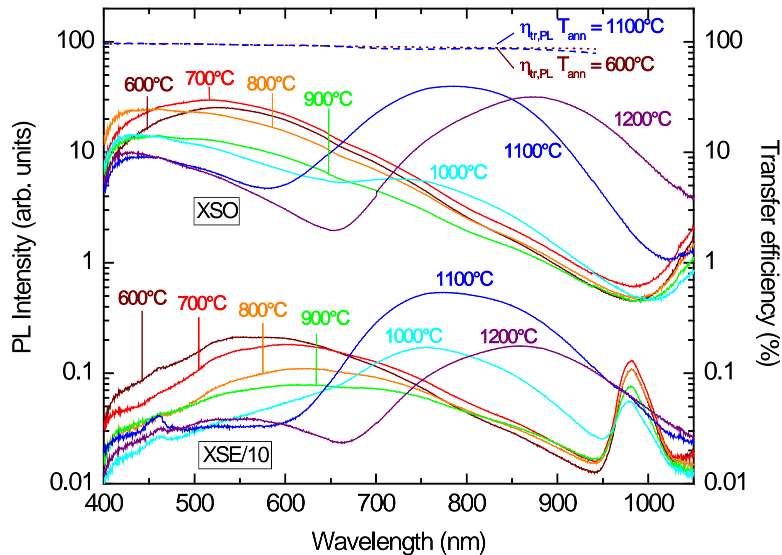

Figure 2.3. (Color) Photoluminescence spectra of passivated Si-rich SiO_2 films with (XSE) and without (XSO) erbium, annealed at temperatures in the range 600 – 1200°C. The inferred spectral dependence of the transfer efficiency is included for annealing temperatures of 600°C and 1100°C.

Photoluminescence decay measurements at an emission wavelength of 500 nm (not shown) reveal a resolution limited decay, indicating that the decay time of this feature is less than 80 ns.

This type of fast short-wavelength emission has been observed in several studies, and is considered to be caused by luminescence centers (LCs) associated with oxygen deficiencies that are formed as a result of the non-stoichiometric composition of Si-rich SiO_2.[39-42] Note that as the annealing temperature is increased, the intensity of this band decreases, possibly due to the gradual removal of the luminescence centers upon annealing. Contrary to previously published results on ion beam induced defects in SiO_2,[43] hydrogen passivation was found to result in an intensity increase of the LC-related band by a factor of ~2 for all samples (not shown). The reason for this different behavior of the LC photoluminescence upon passivation is not fully understood at this time, however it seems likely that different LCs are formed depending on the sample preparation method. At annealing temperatures above 900°C a broad emission band peaking between 800 and 900 nm is observed in XSO samples. Photoluminescence decay measurements of this band at an emission wavelength of 900 nm reveal lifetimes in the range of 12 – 142 μs for samples annealed at temperatures in the range of 1000 – 1200ºC. Such slow emission at these wavelengths is commonly attributed to radiative exciton recombination in relatively large silicon nanocrystals (NC) (diameter $d > 4$ nm)[44-46] formed in the Si-rich SiO_2 matrix upon annealing. Note that the observed emission wavelength is too long to be attributed to the recombination of electrons and holes at Si=O surface states as discussed in Refs. 45 and 47.

Figure 2.3 also includes emission spectra from samples containing excess Si and Er (labeled XSE). Note that the signal from these samples has been divided by a factor of ten for clarity. Both the short wavelength LC-related emission and the NC-related emission drop by approximately an order of magnitude in the presence of erbium for all annealing temperatures. This type of drop in the NC emission upon Er incorporation has been previously attributed to

energy transfer from quantum confined excitons to erbium[12] resulting in a reduced NC emission efficiency. Analogously, the reduced LC emission at short wavelengths suggests that the luminescence centers also interact with Er^{3+} ions on a time scale that is significantly faster than the lifetime of the LC emission observed in XSO samples of τ_{LC} <80 ns. The possibility of LC-mediated Er^{3+} excitation is discussed in more detail below.

In addition to the LC- and NC-related emission bands observed in Figure 2.3, an Er^{3+}-related signal is observed at 981nm for XSE samples, corresponding to the transition from the second excited state to the ground state of Er^{3+} ($^4I_{11/2} \rightarrow {}^4I_{15/2}$). Figure 2.4 shows the NIR spectra for the XSE samples under the same excitation conditions.

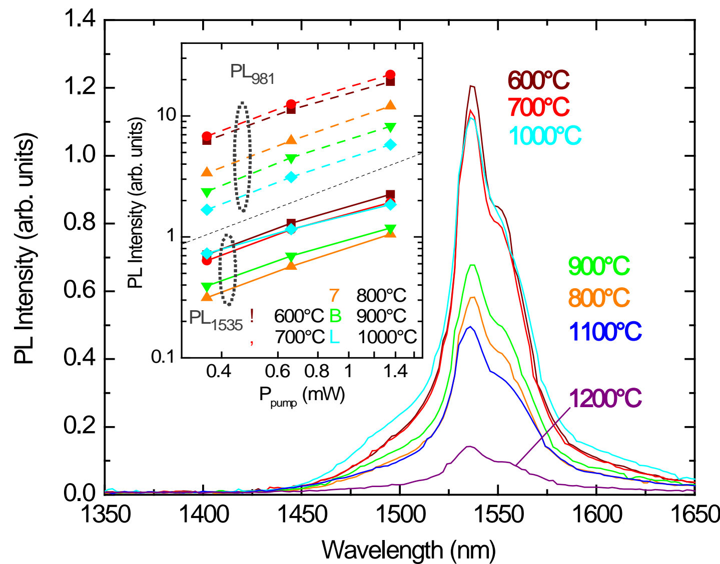

Figure 2.4. (Color) Near-infrared photoluminescence spectra of passivated Er-doped Si-rich SiO_2 samples annealed at temperatures in the range 600 – 1200°C. Inset: the Er^{3+}-related peak emission intensity at 981 nm and 1535 nm as a function of pump power. The dashed line indicates a linear dependence.

A clear Er^{3+}-related emission spectrum peaking at 1535 nm is observed, corresponding to the transition from the first excited state to the ground state of Er^{3+} ($^4I_{13/2} \rightarrow {}^4I_{15/2}$). Neither of these Er^{3+}-related features were observed in XSO samples (i.e. in the samples not containing Er). Although the excitation wavelength of 351 nm used in the present experiments lies in the vicinity of an Er^{3+} absorption line at 355nm ($^4I_{15/2} \rightarrow {}^2G_{7/2}$), [48, 49] no Er^{3+}-related emission was detected at the same pump power in Er-doped SiO_2 (EO samples). This clearly indicates that the observed Er^{3+} PL in Figure 2.3 and Figure 2.4 is the result of indirect excitation.

The inset in Figure 2.4 shows the pump power dependence of the background corrected 981nm emission as well as the 1535 nm emission for samples annealed at different temperatures up to a pump power of 1.35 mW. For reference a linear pump power dependence is indicated by the dashed line. Note that no Er^{3+}-related 981nm emission could be resolved in samples annealed at $T_{ann} > 1000°C$. Both Er^{3+}-related peaks exhibit approximately the same near-linear dependence for all annealing temperatures in this pump power range, indicating that the 981 nm emission is not caused by excited state absorption or cooperative upconversion. These observations demonstrate that a finite fraction of the Er^{3+} ions is excited into the $^4I_{11/2}$ level or into higher lying levels followed by nonradiative relaxation.

2.3.3 Evidence for Luminescence Center Mediated Excitation

Figure 2.5 shows excitation spectra of the PL intensity at 650 nm (squares) and 875 nm (circles) from XSO samples, as well as the PL intensity at 1535 nm (triangles) from XSE samples. These emission wavelengths correspond to PL predominantly from the luminescence centers, the Si

nanocrystals, and the Er^{3+} ions respectively. Results for the as-deposited samples as well as the samples annealed at 600°C and 1100°C are shown. The PL intensity was corrected for the system response at the detection wavelength, and normalized to the incident photon flux. For the sample annealed at 600°C (solid lines) both the Er^{3+} emission and the LC emission intensities show a gradual increase as the excitation wavelength is decreased, increasing by more than a factor 20 over this measurement range. The corresponding excitation spectra of the as-deposited unpassivated sample (dashed lines) are seen to exhibit a very similar spectral dependence.

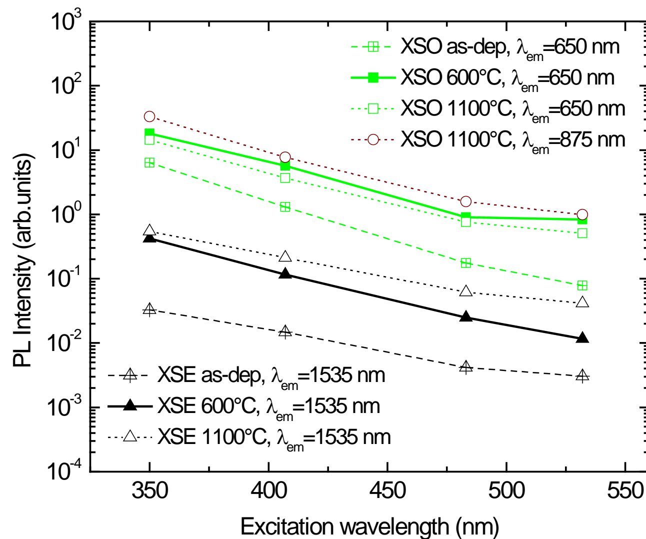

Figure 2.5. (Color) Photoluminescence excitation spectra of passivated Si rich SiO_2 films with (XSE) and without (XSO) erbium for an as-deposited sample as well as samples annealed at 600°C and at 1100°C, measured at emission wavelengths predominantly corresponding to luminescence center emission (650 nm), Si nanocrystal emission (875 nm), and Er^{3+} emission (1535 nm).

The gradual increase of the Er^{3+} emission intensity with decreasing wavelength is commonly attributed to Er^{3+} excitation by quantum confined excitons in Si NCs. This interpretation is

indeed compelling, since the observed Er^{3+} excitation spectrum rather closely follows the expected Si absorption spectrum (not shown). However, no Si nanocrystals were observed in the TEM measurements of as-deposited samples and samples annealed at 600°C, and no distinguishable NC-related emission is observed at T_{ann}=600°C (see Figure 2.3). The similarity between the Er^{3+} excitation spectrum and the LC excitation spectrum in these samples suggests that at these annealing temperatures the erbium is excited via isolated luminescent states in the SiO_2 bandgap or via (surface states on) small Si aggregates. The shape of the excitation spectrum suggests that these states either individually exhibit a broad absorption spectrum, or that the density of these states (or more precisely the joint density of states) increases as a function of increasing photon energy. This aspect will be addressed in more detail in Chapter 6 of this thesis. In the sample annealed at 1100°C (dotted lines), the Er^{3+} emission, the NC emission and the LC emission all show a virtually identical increase in intensity as the excitation wavelength is decreased. The behavior of the Er^{3+} PL and the NC PL in these samples is similar to that observed in numerous other studies . The similarity of the NC and Er^{3+} excitation spectra in this sample could indicate that in samples annealed at 1100°C the Er^{3+} ions are excited via quantum confined excitons. However due to the similarity of the excitation spectra of the NC band and the LC band, the relative contribution of NC and LC-mediated Er^{3+} excitation cannot be determined.

To further investigate the nature of the indirect Er^{3+} excitation in these samples an extensive set of PL measurements was carried out on XSO and XSE samples annealed at different temperatures. The results of these measurements are summarized in Figure 2.6. Unless stated otherwise, all the data were acquired using an excitation wavelength of 351 nm and an excitation power of 0.66 mW.

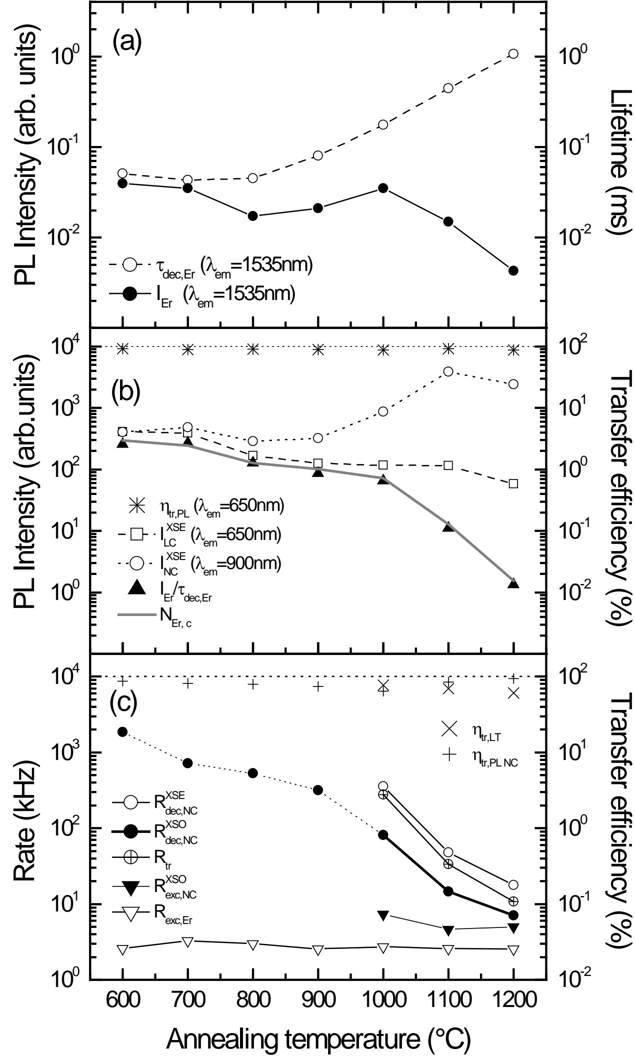

Figure 2.6. Measured and deduced photoluminescence (PL) parameters of passivated Si-rich SiO_2 films with (XSE) and without (XSO) erbium as a function of annealing temperature, showing (a) the Er PL peak intensity (I_{Er}) and the decay time (τ_{Er}) at 1535 nm in XSE samples. (b) the PL intensities at 650 nm (I_{LC}^{XSE}) and 900 nm (I_{NC}^{XSE}) in XSE samples, the derived Er^{3+} excitation density in XSE samples (I_{Er}/τ_{Er}), the relative concentration of Er^{3+} ions coupled to sensitizers ($N_{Er,c}$), and the transfer efficiency at 650 nm derived from the spectral measurements ($\eta_{tr,PL}$). (c) The decay rate of the emission at 900 nm in XSO and XSE samples ($R_{dec,\mathrm{NC}}^{XSO}$ and $R_{dec,\mathrm{NC}}^{XSE}$ respectively), the derived transfer rate at 900 nm (R_{tr}), the excitation rate of the nanocrystals measured at 900 nm in XSO samples ($R_{\mathrm{exc,NC}}^{XSO}$), the Er^{3+} excitation rate measured in XSE samples ($R_{exc,Er}$), the transfer efficiency at 900 nm derived from the lifetime measurements ($\eta_{tr,LT}$), and the transfer efficiency at 900 nm derived from spectral measurements ($\eta_{tr,PL,NC}$).

Figure 2.6 (a) shows the measured photoluminescence peak intensity (I_{Er}, solid circles) as well as the 1/e lifetime ($\tau_{dec,Er}$, open circles) of the Er^{3+}-related emission at λ=1535 nm for XSE samples. The Er^{3+} peak intensity at 1535 nm exhibits a moderate drop as the annealing temperature is increased from 600°C to 800°C. This drop is followed by a brief gradual increase and subsequently a rather steep Er^{3+} PL decrease at T_{ann} > 1000°C. Note that the location of the steep drop coincides with the temperature of the observed nanocrystal formation. The measured Er^{3+} decay traces all exhibited a small degree of multi-exponentiality that is well described by stretched exponential decay of the form $I_{Er}(t) \propto \exp[-(t/\tau_{dec,Er})^{\beta}]$ with a dispersion factor $\beta \approx 0.80 \pm 0.02$. The Er^{3+} lifetime is found to increase significantly as the annealing temperature is increased, which is generally attributed to the removal of defects, relaxation of bond angles and reduction of bond length distortions that can cause non-radiative decay of Er^{3+}-related emission in SiO_2.[50, 51]

Figure 2.6 (b) shows the annealing temperature dependence of the PL intensity at λ_{em} = 650 nm which is predominantly representative of the LC emission (open squares) and the intensity at λ_{em} = 900 nm which is predominantly representative of the NC emission intensity for $T_{ann} \geq$ 1000°C (open circles). The LC emission is seen to *decrease* by a factor ~10 over the shown temperature range, while the PL intensity at 900 nm is seen to *increase* rapidly as T_{ann} is increased beyond 900°C due to the development of the strong NC-related PL band (see spectra in Figure 2.3). In order to correlate the Er^{3+} emission with either the LC emission or the NC emission, we first derive the Er^{3+} excitation density $\rho_{exc,Er}$, defined as the number of Er^{3+} excitation events per second per unit volume. The Er^{3+} excitation density can be found from the

Er^{3+} PL intensity and the Er^{3+} lifetime: assuming a constant Er^{3+} radiative emission rate, the Er^{3+} emission efficiency is known to be linearly proportional to the Er^{3+} lifetime. In the linear intensity vs. pump power regime, the total Er^{3+} PL intensity is given by:

$$I_{Er} \propto R_{exc,Er}\tau_{dec,Er}N_{Er,c} = \tau_{dec,Er}\rho_{exc,Er} , \tag{2.1}$$

with $N_{Er,c}$ (cm^{-3}), the density of Er^{3+} ions that are coupled to a sensitizer and can be excited indirectly; $R_{exc,Er}$ (s^{-1}), the Er^{3+} excitation rate; and $\tau_{dec,Er}$ (s), the Er^{3+} lifetime. This shows that the Er^{3+} excitation density is proportional to $I_{Er}/\tau_{dec,Er}$. This quantity is included in Figure 2.6 (b) (solid triangles). Intriguingly, the Er^{3+} excitation density is found to follow the LC emission almost perfectly up to T_{ann} = 1000°C, after which it is found to drop steeply. The clear correlation of the Er^{3+} excitation density with the LC emission as well as the anti-correlation of the Er^{3+} excitation density with the NC PL intensity suggest that in these samples LC-mediated Er^{3+} excitation dominates over the NC-mediated Er^{3+} excitation.

Figure 2.6 (c) shows the measured Er^{3+} excitation rate ($R_{Er,exc}$) as a function of annealing temperature. These values were obtained from the measured Er^{3+} rise times $\tau_{rise,Er}$ and decay times $\tau_{dec,Er}$ taken at 1535 nm, using the well-known relation

$$R_{exc,Er} = \frac{1}{\tau_{rise,Er}} - \frac{1}{\tau_{dec,Er}} . \tag{2.2}$$

The obtained values correspond to the *indirect* Er^{3+} excitation rate, since the excitation spectra in Figure 2.5 showed no sign of direct Er^{3+} excitation, and no Er^{3+} PL was observed in EO samples when excited at 351 nm. The indirect Er^{3+} excitation rate is found to be remarkably independent of the annealing temperature, varying by less than 30% over the entire temperature range. This is

a highly surprising result given the fact that in this same temperature range the sample microstructure evolves dramatically from predominantly amorphous to clearly phase separated, as observed in the TEM analysis (Figure 2.2). This observation leads us to conclude that the Er^{3+} excitation is due to a sensitizer whose nature does not change significantly for all annealing temperatures shown, *ruling out NC- mediated excitation as the predominant excitation mechanism*. Instead, it appears that the Er^{3+} excitation in these samples occurs predominantly via isolated excess-silicon-related luminescence centers.

The important role of LC-mediated Er^{3+} excitation is further confirmed by a calculation of the total concentration of Er^{3+} ions that are coupled to a sensitizer $N_{Er,c}$. This value can be derived from the Eq. 2.1 in relative units based on the measured values of $R_{exc,Er}$. The resulting $N_{Er,c}$ values have been included in Figure 2.6 (b) (solid grey line). The relative concentration of the indirectly excitable Er^{3+} is found to follow the LC emission almost perfectly up to 1000°C, further supporting our conclusion that the Er^{3+} is predominantly excited via LCs in this temperature range. It should also be noted that the concentration of indirectly excitable Er^{3+} decreases by a factor of ~190 upon increasing T_{ann} from 600°C to 1200°C. This implies that the concentration of indirectly excited Er^{3+} in samples annealed at 1200°C is as low as 0.63 atomic % / 190 = 3.3×10^{-3} atomic %.

The sharp decrease of $N_{Er,c}$ at temperatures above 1000°C at relatively constant excitation rate and relatively constant LC emission suggests that at annealing temperatures above 1000°C either Er^{3+} ions become optically inactive due to the onset of a process known as Er clustering,[51] or that the LC-mediated Er^{3+} excitation process is affected by the presence of Si nanocrystals.

The latter theory seems to be supported by the rapid drop in the LC excited Er^{3+} emission at 981 nm for T_{ann} > 1000°C, however further studies are needed to determine the exact origin of the reduced $N_{Er,c}$ at high annealing temperatures.

2.3.4 *Evidence for Nanocrystal Mediated Excitation*

Although the previous discussion demonstrates that LC-mediated Er^{3+} excitation *dominates* in these measurements, the reduction of the NC PL upon Er^{3+} incorporation suggests that a finite amount of NC-mediated Er^{3+} excitation occurs in these samples as well. To learn about the efficiency of this parallel process, lifetime measurements were performed on XSE and XSO samples annealed at 1000°C, 1100°C, and 1200°C, all of which exhibited clear NC luminescence. These decay traces were measured at an emission wavelength of 900 nm to minimize the PL contribution from the LC band and to ensure that the photoluminescence measurements represent a fixed nanocrystal size. The measured decay traces exhibited multi-exponential decay with dispersion factors, β, between 0.5 and 0.8 for samples annealed at temperatures between 1000°C and 1200°C. The corresponding 1/e decay rates have been included in Figure 2.6 (c). The NC decay rate of the XSO samples ($R_{dec,NC}^{XSO}$, solid circles) is seen to decrease approximately by a factor of 12 as T_{ann} increases from 1000°C to 1200°C. This type of decay rate decrease with increasing T_{ann} is commonly attributed to an increasingly indirect bandgap as the NC diameter increases.[52] Comparing these decay rates with those observed in XSE samples ($R_{dec,NC}^{XSE}$, open circles), an increase in the total decay rate by a factor ~3 – 4 is observed for these temperatures, suggesting the introduction of an additional non-radiative

exciton recombination path due to the presence of Er^{3+} ions. This strongly suggests that despite the fact that most of the observed Er^{3+} PL is due to LC-mediated excitation, Si nanocrystals *do* participate in Er^{3+} excitation in these samples. The Er^{3+} induced difference in nanocrystal lifetime provide further information about the nature of the nanocrystal-mediated excitation process. Based on the measured decay rates it is possible to determine the total NC energy transfer rate $R_{tr}=1/\tau_{tr}$. Here τ_{tr} is the total transfer time which we define as the time required for an exciton confined in a silicon NC to recombine nonradiatively, exciting a nearby Er^{3+} ion. The total NC decay rate in the presence of Er^{3+} is then given by

$$\frac{1}{\tau_{dec,NC}^{XSE}} = \frac{1}{\tau_{dec,NC}^{XSO}} + R_{tr}\,, \tag{2.3}$$

where $\tau_{dec,NC}^{XSE}$ and $\tau_{dec,NC}^{XSO}$ are the measured 1/e lifetimes of the nanocrystal PL at 900 nm. Note that this relation assumes that all additional non-radiative decay observed in the XSE sample is due to energy transfer. The resulting total transfer rate (R_{tr}) has been included in Figure 2.6 (c) (crossed circles). The total transfer rate is found to decrease by more than an order of magnitude as T_{ann} is increased from 1000°C to 1200°C, and is found to be approximately proportional to the NC rate of the XSO sample. These findings seem to suggest that the NC-to-Er^{3+} transfer rate depends on the oscillator strength of the exciton recombination in Si nanocrystals as one would expect for a Förster type energy transfer. Note that in order to fully demonstrate the correlation between the oscillator strength and the transfer rate, the nanocrystal radiative rate should be determined independently.

Based on the measured NC lifetime data the quantum efficiency of the nanocrystal-mediated energy transfer can be found using:

$$\eta_{tr,LT} = \frac{R_{tr}}{R_{dec,NC}^{XSE}} = \frac{\tau_{dec,NC}^{XSE}}{\tau_{tr}}, \tag{2.4}$$

where we have again assumed that all non-radiative decay introduced by the Er^{3+} ions is related to energy transfer events. The thus obtained transfer efficiency is shown in Figure 2.6 (c) ($\eta_{tr,LT}$, crosses). Note that the nanocrystal-mediated transfer efficiency is in the range of 60 – 75%, in agreement with earlier efficiency estimates.[26]

For comparison we have also determined the energy transfer quantum efficiency based on the photoluminescence spectra shown in Figure 2.3. In the following we briefly describe how this can be done without explicit knowledge of PL lifetimes. For a fixed pump power in the linear pump regime using a fixed excitation and collection geometry, the collected signal intensity for the XSO sample at a given emission wavelength is proportional to:

$$I_i^{XSO} \propto \sigma_{abs,i} N_i \frac{R_{rad,i}}{R_{rad,i} + R_{nr,i}}, \tag{2.5}$$

where i represents the type of sensitizer (LC or nanocrystals), $\sigma_{abs,i}$ is the corresponding absorption cross-section, N_i is the corresponding volume density of these sensitizers, and $R_{rad,i}$ and $R_{nr,i}$ are the radiative and non-radiative recombination rates for the corresponding sensitizer. As discussed above, the addition of Er^{3+} ions is assumed to lead to the introduction of an additional non-radiative decay process at a rate R_{tr}. The intensity observed from an XSE sample is reduced due to this additional decay, and is given by:

$$I_i^{XSE} \propto \sigma_{abs,i} N_i \frac{R_{rad,i}}{R_{rad,i} + R_{nr,i} + R_{tr}}, \tag{2.6}$$

Assuming that the presence of Er^{3+} does not affect the density or the absorption cross-section of the sensitizer, we can use these measured PL intensities to derive the transfer efficiency as follows:

$$\eta_{tr,i,PL} = \frac{R_{tr}}{R_{rad,i} + R_{nr,i} + R_{tr}} = \frac{(R_{rad,i} + R_{nr,i} + R_{tr}) - (R_{rad,i} + R_{nr,i})}{R_{rad,i} + R_{nr,i} + R_{tr}} = 1 - \frac{I_i^{XSE}}{I_i^{XSO}}. \tag{2.7}$$

Based on the Eq. 2.7 we can obtain a value for the transfer efficiency as a function of emission wavelength. The results have been included in Figure 2.3 for samples annealed at 600°C (dotted line) and 1100°C (dashed line). Note that results for $\lambda_{em} > 940$ nm are not included in the graph since the formulas used do not take into account the appearance of the observed Er^{3+}-related emission at this wavelength. The PL based transfer efficiency is found to be > 80% throughout the entire spectral range, confirming that both LCs and NCs can efficiently excite Er^{3+}. Surprisingly the transfer efficiency is found to be approximately constant across the emission spectrum of the LCs and the NCs, implying that the obtained efficiency value at a fixed wavelength can be taken to represent the total transfer efficiency. The values for the energy transfer efficiency based on the PL intensities at $\lambda_{em} = 650$ nm corresponding to predominantly LC-mediated excitation have been included in Figure 2.6 (b) (stars). The values for $\lambda_{em} = 900$ nm corresponding to predominantly NC-mediated Er excitation at $T_{ann} \geq 1000$°C have been included in Figure 2.6 (c) (plus symbols). Using this method the NC-mediated transfer efficiency at $T_{ann} =$ 1100°C is found to be 84%, in reasonable agreement with the value of 70% that was obtained

using the lifetime analysis described above. We attribute the discrepancy to the fact that 1/e lifetimes were used in the analysis, which does not take into account the multi-exponential nature of the nanocrystal PL decay traces.

A final point that needs to be addressed is the effective Er^{3+} absorption cross-section. In previous studies the similarity between the magnitude of the indirect Er^{3+} absorption cross-section and the measured Si nanocrystal absorption cross-section seemed to indicate that the NC excitation and the Er^{3+} excitation had the same origin. However from constant Er^{3+} excitation rate in Figure 2.5 (c) it is clear that the same effective absorption cross-section is observed at all annealing temperatures, even well below the temperatures needed for nanocrystal formation. From the excitation rate data and the known pump power, the LC-mediated effective Er^{3+} excitation cross-section at an excitation wavelength of λ_{exc} = 351nm is $\sigma_{Er,LC}(351\text{nm}) \approx 2 \times 10^{-14}\ \text{cm}^2$. To compare the results in the present samples with previous studies, we also measured the nanocrystal excitation rate for XSO samples annealed at T_{ann} between 1000°C and 1200°C based on the emission at 900 nm and the well-known relation:

$$R^{XSO}_{exc,NC} = R^{XSO}_{rise,NC} - R^{XSO}_{dec,NC} \,. \tag{2.8}$$

The resulting nanocrystal excitation rate has been included in Figure 2.5 (c) (solid triangles). For these three temperatures the nanocrystal excitation rate is found to be 5700 ± 900 s^{-1}. Based on the measured excitation rate the nanocrystal absorption cross-section at 351 nm is calculated to be $\sigma_{NC}(351\text{nm}) \approx 5 \times 10^{-14}\ \text{cm}^2$, in good agreement with the literature.[13] Comparing these results with the Er^{3+} excitation rate determined above, we find that the effective Er^{3+} absorption cross-section is approximately constant and a factor ~2 lower than the nanocrystal absorption cross-

section, similar to the results obtained in previous studies.[16, 26] However, in contrast with previous studies, this Er^{3+} excitation rate does not necessarily indicate nanocrystal-mediated excitation, but instead is due to a combination of LC and NC-mediated excitation.

2.3.5 Discussion

Based on the experimental observations presented in this chapter we have arrived at the physical model shown in Figure 2.7. At low annealing temperatures the SiO_2 film contains Er^{3+} ions and a high concentration of luminescence centers, as indicated schematically in Figure 2.7 (a). Figure 2.7 (b) shows the corresponding band diagram, with LC-related levels in the SiO_2 bandgap indicated by horizontal gray lines. After optical excitation of an electron into an LC-related level, electronic relaxation from this level (downward arrow) to a lower lying level leads to the observed indirect Er^{3+} excitation (upward arrow) with a time constant substantially faster than 80 ns. Note that the sketch indicates Er^{3+} excitation into the $^4I_{11/2}$ level, however the fraction of excitation into the $^4I_{11/2}$ level, the $^4I_{13/2}$ level, and possibly other Er^{3+} levels cannot be determined from the present data. At higher annealing temperatures but before the onset of nanocluster formation, the density of LCs is reduced substantially (Figure 2.7 (c)), leading to a reduced number of excitable Er^{3+} ions and a reduced PL intensity, but exhibiting an unmodified indirect Er^{3+} excitation cross-section. At temperatures above the onset of nanocluster formation, the density of LCs continues to decrease, while the formation of Si nanocrystals could lead to the generation of similar electronic states at the nanocrystal surface (Figure 2.7 (d)). The corresponding band diagram is shown in Figure 2.7 (e). Despite the presence of Si nanocrystals,

LC-mediated excitation (dark downward arrow) continues to dominate over nanocrystal-mediated excitation (light downward arrow). Note that the ratio between these processes most likely depends on the excitation wavelength, which is not explicitly investigated here.

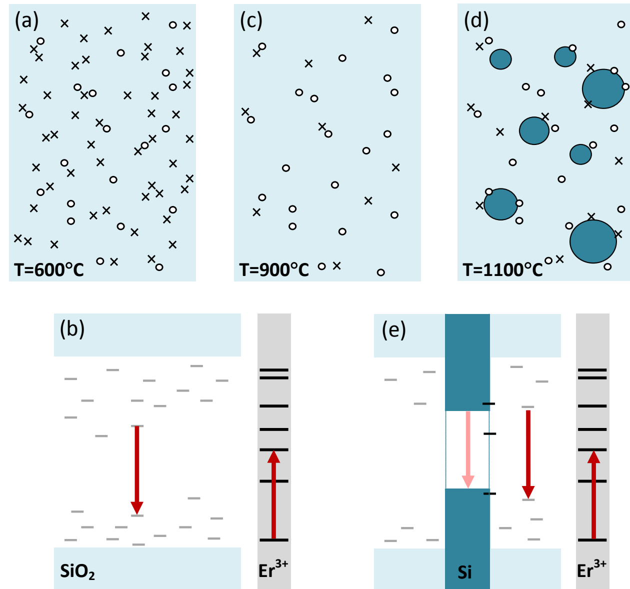

Figure 2.7. (Color) Schematic representation of the Er^{3+} excitation processes in Er-doped Si rich SiO_2 samples (a) at low annealing temperatures, showing a high concentration of excess-Si-related luminescence centers (LCs) indicated by crosses, as well as Er^{3+} ions, indicated by open circles, and (b) the corresponding schematic band diagram, indicating the SiO_2 valence band and conduction band, LC-related electronic levels in the band gap indicated by the horizontal lines, as well as the Er^{3+} energy levels. LC-mediated excitation is indicated by the vertical arrows; (c) at intermediate annealing temperatures, showing a reduced concentration of LCs. (d) at high annealing temperatures, showing the formation of Si nanocrystals (dark circles), and (e) the corresponding band diagram indicating the presence of Si nanocrystals with a quantum confined bandgap. A weak exciton-mediated contribution to the Er^{3+} excitation is indicated by the light vertical arrow.

The observations described above have several implications for the interpretation of data already present in the literature. First, a dominant LC-mediated excitation mechanism could resolve a long standing controversy: in measurements of the indirect Er^{3+} excitation rate as a

function of Er^{3+} concentration it was observed that the Er^{3+} excitation rate remained approximately constant as the Er^{3+} concentration was increased by more than an order of magnitude.[16] It was therefore concluded that Si NCs can excite only 1 – 2 Er atoms. In light of our new observations, it seems likely that in those measurements a single sensitizer indeed could excite no more than 1 – 2 Er^{3+} ions. However the observed sensitization may not have been directly caused by Si nanocrystals, but rather by isolated LCs, resulting in an Er^{3+} excitation rate approximately independent of the Er^{3+} concentration. Due to the 'atomic' size scale that such LCs could have, the limitation of 1 – 2 Er^{3+} ions per LC would seem physically reasonable. Second, the presence of a dominant LC-mediated Er^{3+} excitation process could in part explain the experimentally observed independent behavior of the nanocrystal PL and the Er^{3+} PL as a function of sample temperature in the temperature range of 20 – 300 K.[26, 29] In these studies the nanocrystal lifetime and intensity were found to vary significantly as a function of temperature, while the Er^{3+} PL intensity remained approximately constant. A fast exciton-Er^{3+} energy transfer process was assumed to be responsible for this behavior, rendering nanocrystals coupled to Er^{3+} inefficient ('dark'). Although the existence of relatively dark nanocrystals is confirmed by the PL spectra observed in this study, it now seems likely that part of the insensitivity of the Er^{3+} PL to the sample temperature observed in literature is related to the existence of a significant fraction of LC-mediated Er^{3+} excitation. Third, our observations show that two distinct transfer processes are present with a fast process (τ_{tr} < 80ns) dominant over a slow process (τ_{tr} ~ 4 – 100 μs) which is in good agreement with the findings of Fujii et al.[24] who also observed that two energy transfer processes exist: a fast process (τ_{tr} < 100 ns) and a slow process (τ_{tr} ~ 1 – 70 μs), with the fast process always dominant. This was explained in a later publication by the same team[25] by

assuming that the energy transfer mechanism depends on the distance of the Er^{3+} ions from the nanocrystal surface. Note that this model does not predict the existence of a fast transfer process at temperatures below the onset of nanocrystal formation, nor the observation of an annealing temperature independent Er^{3+} excitation rate. In light of the present results it appears that the observed fast transfer in those studies may also have been associated with Er^{3+} sensitization by discrete luminescence centers in the oxide, while the slow transfer process could have been related to the known and efficient (but less prevalent) energy transfer via excitons confined in Si nanocrystals. However, work presented in Chapter 4 involving time resolved measurements of the emission from both the $^4I_{11/2}$ and the $^4I_{13/2}$ levels strongly suggests that the slow excitation process is a consequence of the LC mediated excitation of the Er^{3+} ions into the $^4I_{11/2}$ state, followed a relatively slow relaxation into the $^4I_{13/2}$ state. The measured relaxation rate from the $^4I_{11/2}$ level very closely matches the time constant of the slow rise of the $^4I_{13/2}$ emission in the same sample observed under pulsed excitation, and consequently internal relaxation is very likely the origin of the slow excitation component, both in our work and in related studies in the literature.

Our interpretation of the present data does not seem to conflict with existing data in literature and resolves some outstanding controversies, however a remaining intriguing coincidence should be pointed out. As mentioned earlier, the effective LC-mediated Er^{3+} cross-section under excitation with 351 nm light was estimated to be of the order of 2×10^{-14} cm^2. In our present interpretation this value represents the LC absorption cross-section, multiplied by the near unity transfer efficiency. Coincidentally, the absorption cross-section associated with the NC emission as found from lifetime measurements in the present study is found to be of a very

similar magnitude, given by $\sigma_{NC} \approx 5 \times 10^{-14}$ cm^2, corresponding very well with values found in the literature.[13] A similar absorption cross-section for these apparently entirely different physical entities (an isolated electronic state vs. a collection of ~ 10^3 atoms) seems surprising, and suggests that a direct physical link may exist between the LC and NC emission. A tempting explanation is that the observed LC PL is mediated by Si nanocrystal excitation, however since this model requires the existence of Si nanocrystals it cannot explain the observation of a nearly constant Er^{3+} absorption cross-section as a function of annealing temperature. An alternate explanation is that Si nanocrystals are excited via LCs, resulting in a similar absorption cross-section and a similar excitation spectrum for both PL features. The latter possibility would also explain the approximately constant NC absorption cross-section for the three highest annealing temperatures (1000°C, 1100°C, and 1200°C). Finally, it could partly explain the strong overall reduction of the NC photoluminescence spectrum without the introduction of clear dips in the NC emission spectra at emission energies resonant with Er^{3+} transition energies, since energy transfer from LCs to Er^{3+} would compete with energy transfer from LCs to Si nanocrystals. Note that this explanation only involves the *excitation* mechanism for the NC emission band, *i.e.* it does allow for this emission to be caused by quantum confined excitons, as convincingly demonstrated by many studies in the literature. Despite matching several experimental observations, it is not clear how such an LC-mediated NC excitation process could dominate over the direct Si nanocrystal excitation, which based on a typical nanocrystal diameter between 3 – 10 nm and the known bulk Si absorption coefficient can be estimated to be of the order of $10^{-14} - 10^{-12}$ cm^2 at $\lambda_{exc} = 351$nm. While these models could explain the observed similarity in absorption cross-section for Si NC excitation and Si sensitized Er excitation, none of the models

could be definitively confirmed or disproven in subsequent measurements. At the time of the completion of this thesis, the origin of this result remains an open question.

The observations made in this study could have a major impact on the maximum gain that can be achieved in Si sensitized Er^{3+} based waveguide amplifiers. As mentioned in the introduction, confined carrier absorption is considered to be a severe challenge in Si nanocrystal sensitized systems due to the relatively long exciton lifetime and large anticipated confined carrier absorption cross-section at 1.54 μm compared to the small Er^{3+} emission cross-section at that same wavelength.[1, 20, 53-55] It is now clear that fast ($\tau_{tr} < 80$ ns) indirect Er^{3+} excitation can occur in these materials *without the presence Si nanocrystals* and therefore without the presence of long lived excitons, while retaining the large effective Er^{3+} excitation cross-sections observed in literature. Secondly the concentration of indirectly excitable Er^{3+} ions $N_{Er,\mathrm{c}}$ obtained at low annealing temperatures is shown to be a factor 10 – 100 higher than that obtained at the annealing temperatures required to form nanocrystals. Since the optical gain coefficient scales linearly with the Er^{3+} concentration, our results suggest that maximum gain can be achieved at low processing temperatures, albeit with a reduced Er^{3+} emission quantum efficiency associated with the relatively short Er^{3+} lifetime.

2.4 Conclusions

The indirect excitation of Er^{3+} ions in Er-doped Si-rich SiO_2 samples annealed at temperatures in the range of 600 – 1200ºC has been investigated. It was demonstrated that the dominant indirect excitation mechanism involves fast ($\tau_{tr} < 80$ ns) Er^{3+} excitation by isolated luminescence centers

(LCs) at all annealing temperatures, while for annealing temperatures exceeding ~ 1000°C a small fraction of the Er^{3+} excitation events is mediated by exciton recombination in Si nanocrystals, with a typical transfer time in the range 4 – 100 μs. Both excitation processes were found to exhibit a transfer efficiency ≥ 60%. The LC -mediated indirect Er^{3+} excitation cross-section at an excitation wavelength of 351 nm was found to be independent of annealing temperature with a magnitude of 2.4×10^{-14} cm^2, while the nanocrystal absorption cross-section at the same wavelength was found to be 5×10^{-14} cm^2. The proposed interpretation of the measurements was shown to explain several observations in the literature. A maximum concentration of indirectly excitable Er^{3+} was found at the lowest annealing temperature used (600°C), suggesting that Er-doped optical amplification media in Si sensitized SiO_2 hosts will exhibit maximum gain for processing temperatures well below those required for the onset of nanocrystal formation.

2.5 References

[1] P. G. Kik and A. Polman, in Proceedings of the NATO Advanced Research Workshop on Towards the First Silicon Laser, Trento, Italy, 2002, edited by L. Pavesi, S. Gaponenko, L. Dal Negro (Kluwer Academic Publishers, Dordrecht, 2003), p. 383.

[2] M. Lipson, J. Light. Tech. **23**, 4222 (2005).

[3] T. J. Kippenberg, J. Kalkman and A. Polman, and K. J. Vahala, Phys. Rev. A **74**, 051802 (2006).

[4] A. Polman, B. Min, J. Kalkman, T. J. Kippenberg and K. J. Vahala, Appl. Phys. Lett. **84**, 1037 (2004)

[5] A. J. Kenyon, Semicond. Sci. Technol. **20,** R65 (2005).

[6] N. Daldosso, D. Navarro-Urrios, M. Melchiorri, C. García, P. Pellegrino, B. Garrido, C. Sada, G. Battaglin, F. Gourbilleau, R. Rizk, and L. Pavesi, IEEE J. Sel. Top. Quantum Electron. **12**, 1607 (2006).

[7] L. Dal Negro, J. H. Yi, J. Michel, L. C. Kimerling, S. Hamel, A. Williamson, and G. Galli, IEEE J. Sel. Top. Quantum Electron. **12**, 1628 (2006).

[8] W. Miniscalco, in Rare-Earth-Doped Fiber Lasers and Amplifiers, edited by M. Digonnet (Marcel Dekker, Inc, New York, 2001), p.62.

[9] A. Polman and F. C. J. M. van Veggel, J. Opt. Soc. Am. B **21**, 871 (2004).

[10] T. Kimura, A. Yokoi, H. Horiguchi, and R. Saito, T. Ikoma, and A. Sato, Appl. Phys. Lett. **65**, 983 (1994).

[11] G. N. van den Hoven, Jung H. Shin, and A. Polman, S. Lombardo, and S. U. Campisano, J. Appl. Phys. **78**, 2642 (1995).

[12] M. Fujii, M. Yoshida, and Y. Kanzawa, S. Hayashi, and K. Yamamoto, Appl. Phys. Lett. **71**, 1198 (1997).

[13] D. Kovalev, J. Diener, H. Heckler, G. Polisski, N. Künzner, and F. Koch, Phys. Rev. B **61**, 4485 (2000).

[14] G. Franzò, V. Vinciguerra, and F. Priolo, Appl. Phys. A **69**, 3 (1999).

[15] F. Gourbilleau, M. Levalois, C. Dufour, J. Vicens, and R. Rizk, J. Appl. Phys. **95**, 3717 (2004).

[16] P. G. Kik and A. Polman, J. Appl. Phys. **88**, 1992 (2000).

[17] A. J. Kenyon, C. E. Chryssou, and C. W. Pitt, T. Shimizu-Iwayama, D. E. Hole, N. Sharma, and C. J. Humphreys, J. Appl. Phys. **91**, 367 (2002).

[18] M. Wojdak, M. Klik, M. Forcales, O. B. Gusev, T. Gregorkiewicz, D. Pacifici, G. Franzò, F. Priolo, and F. Iacona, Phys. Rev. B **69**, 233315 (2004).

[19] J. Lee, J. H. Shin, and N. Park, J. Light. Tech **23**, 19 (2005).

[20] P. G. Kik and A. Polman, J. Appl. Phys. **91**, 534 (2002).

[21] N. Daldosso, D. Navarro-Urrios, M. Melchiorri, L. Pavesi, F. Gourbilleau, M. Carrada, R. Rizk, C. García, P. Pellegrino, B. Garrido, and L. Cognolato, Appl. Phys. Lett. **86**, 261103 (2005).

[22] D. Pacifici, G. Franzò, F. Priolo, F. Iacona, and L. Dal Negro, Phys. Rev. B **67**, 245301 (2003).

[23] A. Mimura, M. Fujii, S. Hayashi, D. Kovalev, and F. Koch, Phys. Rev. B **62**, 12625 (2000).

[24] M. Fujii, K. Imakita, K. Watanabe, and S. Hayashi, J. Appl. Phys. **95**, 272 (2004).

[25] K. Imakita, M. Fujii, and S. Hayashi, Eur. Phys. J. D **34**, 161 (2005).

[26] P. G. Kik, M. L. Brongersma, and A. Polman, Appl. Phys. Lett. **76**, 2325 (2000).

[27] K. Imakita, M. Fujii, and S. Hayashi, Phys. Rev. B **71**, 193301 (2005).

[28] K. Watanabe, M. Fujii, and S. Hayashi, J. Appl. Phys. **90**, 4761 (2001).

[29] M. Fujii, M. Yoshida, S. Hayashi, and K. Yamamoto, J. Appl. Phys. **84**, 4525 (1998).

[30] G. Franzò, S. Boninelli, D. Pacifici, and F. Priolo, F. Iacona, and C. Bongiorno, Appl. Phys. Lett. **82**, 3871 (2003).

[31] F. Gourbilleau, R. Madelon, C. Dufour, and R. Rizk, Opt. Mat. **27**, 868 (2005).

[32] F. Enrichi, G. Mattei, C. Sada, E. Trave, D. Pacifici, G. Franzò, F. Priolo, F. Iacona, M. Prassas, M. Falconieri, and E. Borsella, Opt. Mat. **27**, 904 (2005).

[33] L.-F. Bian, C. G. Zhang, W. D. Chen, C. C. Hsu, and Tongfei Shi, Appl. Phys. Lett. **89**, 231927 (2006).

[34] J. S. Chang, J.-H. Jhe, M.-S. Yang, J. H. Shin, K. J. Kim, and D. W. Moon, Appl. Phys. Lett. **89**, 181909 (2006).

[35] C. Y. Chen, W. D. Chen, S. F. Song, Z. J. Xu, X. B. Liao, G. H. Li, and K. Ding, J. Appl. Phys. **94**, 5599 (2003).

[36] A. Hryciw, C. Blois, A. Meldrum, T. Clement, R. DeCorby, and Quan Li, Opt. Mat. **28**, 873 (2006).

[37] http://www.genplot.com/

[38] F. Iacona, C. Bongiorno, and C. Spinella, S. Boninelli, and F. Priolo, J. Appl. Phys. **95**, 3723 (2004).

[39] T. Shimizu-Iwayama and K. Fujita, S. Nakao and K. Saitoh, T. Fujita, and N. Itoh, J. Appl. Phys. **75**, 7779 (1994).

[40] M. Ya. Valakh, V. A. Yukhimchuk, V. Ya. Bratus', A. A. Konchits, P. L. F. Hemment, and T. Komoda, J. Appl. Phys. **85**, 168 (1999).

[41] J.-Y. Zhang, X.-M. Bao, N.-S. Li, and H.-Z. Song, J. Appl. Phys. **83**, 3609 (1998).

[42] A. J. Kenyon, P. F. Trwoga, C. W. Pitt, and G. Rehm, J. Appl. Phys. **79**, 9291 (1996).

[43] K. S. Min, K. V. Shcheglov, C. M. Yang, H. A. Atwater, M. L. Brongersma, and A. Polman, Appl. Phys. Lett. **69**, 2033 (1996).

[44] I. N. Yassievich and A. S. Moskalenko, Mater. Sci. Eng. B **105**, 192 (2003).

[45] J. S. Biteen, N. S. Lewis, and H. A. Atwater, and A. Polman, Appl. Phys. Lett. **84**, 5389 (2004).

[46] M. L. Brongersma, P. G. Kik, A. Polman, K. S. Min, and H. A. Atwater, Appl. Phys. Lett. **76**, 351 (2000).

[47] M. V. Wolkin, J. Jorne, and P. M. Fauchet, G. Allan, and C. Delerue, Phys. Rev. Lett.**82**, 197 (1999).

[48] G. H. Dieke and H. M. Crosswhite, Appl. Opt. **2**, 675 (1963).

[49] P. W. France, M. G. Drexhange, J. M. Parker, M. W. Moore, S. F. Carter and J. V. Wright, Fluoride Glass Optical Fibres (Balckie, Boca Raton, Florida, 2000), p.167.

[50] A. Polman, D. C. Jacobson, A. Lidgard J. M. Poate, and G. W. Arnold, Nuc. Instr. Meth. Phys. Res. B **59-60**, 1313 (1991).

[51] A. Polman, D. C. Jacobson, D. J. Eaglesham, R. C. Kistler, and J. M. Poate, J. Appl. Phys. **70**, 3778 (1991).

[52] D. Kovalev, H. Heckler, G. Polisski, J. Diener, and F. Koch, Opt. Mat. **17**, 35 (2001).

[53] W. Miniscalco, J.Light.Tech **9**, 234 (1991).

[54] H. Mertens, A. Polman, I. M. P. Aarts, W. M. M. Kessels, and M. C. M. van de Sanden, Appl. Phys. Lett. **86**, 241109 (2005).

[55] H.-S. Han, S.-Y. Seo, J. H. Shin, and N. Park, Appl. Phys. Lett. **81**, 3720 (2002).

CHAPTER 3. EFFECT OF HYDROGEN PASSIVATION ON LUMINESCENCE-CENTER-MEDIATED Er EXCITATION IN Si-RICH SiO_2 WITH AND WITHOUT Si NANOCRYSTALS

(Based on work published in Physical Review B **77**, 205438 (2008))

The influence of hydrogen passivation on the luminescence-center-mediated excitation of Er^{3+} in samples with significantly different microstructure is studied. Photoluminescence measurements are presented of samples containing no detectable nanocrystals (annealed at 600ºC) and of samples containing silicon nanocrystals (annealed at 1100ºC) as a function of hydrogen passivation temperature. Passivation is found to have little effect on the Er^{3+} photoluminescence intensity in the samples that do not contain nanocrystals. In contrast, a pronounced increase in the Er^{3+} photoluminescence intensity is observed in the samples containing Si nanocrystals, which is accompanied by a similar increase in the nanocrystal photoluminescence intensity and a gradual increase of the Si nanocrystal emission lifetime. This observation is attributed to two interrelated effects, namely (a) an increase in the density of fully passivated optically active nanocrystals due to the passivation-induced removal of silicon dangling bonds, and (b) a concurrent reduction of nonradiative Er^{3+} relaxation from levels above the $^4I_{13/2}$ level due to a direct interaction of excited Er^{3+} ions with silicon dangling bonds. In addition, the observed counterintuitive gradual increase of the nanocrystal photoluminescence decay time upon passivation is successfully explained using a new approach that takes into account the inhomogeneous nature of the nanocrystal-related emission band. It is shown that the

combination of luminescence-center-mediated Er^{3+} excitation and silicon dangling bond induced Er^{3+} de-excitation can explain at least fourteen experimental observations reported by independent authors.

3.1 Introduction

The observation of luminescence-center-mediated Er^{3+} excitation in Si-rich SiO_2 as presented in Chapter 2 [Ref. 1] could provide new opportunities in silicon photonics. Erbium-doped silica has long been considered as one of the possible candidates to provide a silicon compatible light source, which is currently one of the most challenging optical components to realize.[2-7] In its ionized state (Er^{3+}) erbium has a weakly allowed optical transition at 1.54 µm corresponding to the transition from the first excited state ($^4I_{13/2}$) to the ground state ($^4I_{15/2}$). The first excited state typically has a lifetime in the millisecond range,[8] which provides the possibility of using it as a metastable level of a laser system. Er-based lasers have been developed using optical pumping into the $^4I_{11/2}$ and $^4I_{13/2}$ levels. These systems require laser-based pumping due to the narrow Er^{3+} absorption lines with low ($\sim 10^{-20} - 10^{-21}$ cm^2) absorption cross-sections.[9] The Er^{3+} excitation process may be facilitated by the incorporation of sensitizers with a large absorption cross-section and a high energy transfer efficiency.[10] An approach that has received a lot of attention involves the use of silicon nanocrystals incorporated into the Er-doped SiO_2 matrix.[11-18] Such composite systems can provide effective Er^{3+} excitation cross-sections in excess of 10^{-16} cm^2 but also introduce significant confined-carrier optical absorption due to the existence of long-lived exciton states in the Si nanocrystals.[7, 19-21]. Research conducted on the nanocrystal-erbium

interaction has suggested the presence of two different excitation mechanisms of Er^{3+} sensitization in silicon-nanocrystal-doped SiO_2 films: one involving fast energy transfer (transfer time < 100 ns) and one involving relatively slow energy transfer (transfer time ~ 1 – 70 μs).[22] The presence of two types of excitation time scales has been attributed either to a nanocrystal-Er^{3+} distance dependent transfer rate[23] or alternatively to the fast excitation of Er^{3+} by hot electrons generated in Si nanocrystals followed by a relatively slow Er^{3+} excitation via thermalized excitons in Si nanocrystals.[24] In Chapter 2 [Ref. 1] we demonstrated that Si nanocrystals (NC) in fact only provide a small part of the Er^{3+} sensitization, while most of the Er^{3+} excitation occurs through excess-silicon-related luminescence centers in the oxide. The luminescence centers (LC) were found to exhibit high (~90%) transfer efficiency to Er^{3+} ions and to dramatically increase the effective Er^{3+} absorption cross-section.[1] These observations suggest the possibility of engineering greatly enhanced Er^{3+} excitation cross-sections, but without the introduction of nanocrystal induced confined carrier absorption.

While the work discussed in Chapter 2 [Ref. 1] showed that only an insignificant fraction of the Er^{3+} ions is sensitized by nanocrystals, other authors have observed a clear correlation between the nanocrystal and erbium emission intensities,[25] which suggests that a physical link does exist between the NC and Er^{3+} optical properties. In order to investigate the role of Si nanocrystals in LC-mediated Er^{3+} excitation, in this chapter we study the effect of hydrogen passivation on the LC-Er^{3+} interaction. Hydrogen passivation has been shown to significantly improve the optical properties of the nanocrystal emission in Si-rich SiO_2 films.[25-30] The improvement is mostly due to the passivation of silicon dangling bonds (commonly referred to as P_b - centers) that act as efficient exciton traps with inherent capture times < 0.1 nsec.[31, 32] Silicon

dangling bonds are created at the interface between the amorphous silica host and a silicon nanocrystal due to the lattice mismatch between the two materials.[33-36] Annealing a Si-nanocrystal-doped silica film in a hydrogen-rich environment results in the saturation of the dangling bonds with atomic hydrogen. This decreases the concentration of the P_b-centers[25, 33, 37] and consequently increases the density of optically active nanocrystals in the silica host.[27, 30] In addition, passivation has been observed to increase the decay time of the nanocrystal-related band.[27] The latter observation is a counterintuitive result, since it is generally believed that the presence of a single dangling bond renders a nanocrystal optically dark due to the fast exciton capture time by dangling bonds.[31, 32]

The current chapter addresses the effect of hydrogen passivation on the photoluminescence of Si nanocrystals, luminescence centers and erbium. The studies are conducted on two structurally different Er-doped and Si-rich SiO_2 films: films without any detectable silicon nanocrystals and films containing Si nanocrystals. Through an investigation of the passivation-temperature-dependent optical properties of these samples, a model is developed that resolves both the unexplained correlation between the nanocrystal and erbium emission intensities and the unexpected gradual increase of the nanocrystal photoluminescence decay time upon passivation. The proposed model at once accounts for at least fourteen experimental observations presented in independent studies by different scientific groups.

3.2 Experimental Techniques

A silicon and erbium doped SiO_2 layer was deposited onto a P-doped (100) Czochralski grown silicon wafer (resistivity 3–7 Ωcm) by magnetron co-sputtering from Si, SiO_2 and SiO_2:Er_2O_3 targets in a multi-gun sputtering system (AJA International, Inc., ATC-2200V). The composition and thickness of the as-deposited film was verified by Rutherford backscattering spectrometry (RBS) (General IONEX 1.7 MU Tandetron) in conjunction with RUMP software[38] used to fit the RBS spectra. The 110 nm thick film was found to contain 12 at. % of excess Si and 0.63 at. % of Er. A low concentration of Ar (~ 0.4 at. %) was also present as a result of the sputtering process. The samples were annealed for 100 seconds in flowing N_2 (flow rate 3 SLPM) at ambient pressure using a rapid thermal processor (Modular Process Technology Corp., RTP-600S). For this study, two different annealing temperatures were used: one set of samples labeled LTA ('low-temperature anneal') was annealed at 600°C, while another set of samples labeled HTA ('high-temperature anneal') was annealed at 1100°C. As was demonstrated in Ref.[1] annealing at temperatures above 1000ºC results in the formation of silicon nanocrystals, while annealing at a temperature of 600ºC does not produce silicon aggregates detectable by transmission electron microscopy. The samples were subsequently passivated for 30 minutes in flowing forming gas (N_2:H_2 = 95%:5%, flow rate 65 SCCM) in a tube furnace (Lindberg, 58114) at temperatures in the range 300 - 600°C and 300 - 800°C for LTA and HTA samples respectively. The samples were allowed to cool down to room temperature in the cold zone of the furnace under continued flowing forming gas flow for 10 min. Unpassivated reference samples were included in all measurements, and the results have been added to the corresponding graphs at a passivation temperature of 20°C. Photoluminescence measurements were taken at room temperature using

the 351 nm emission line of a Kr-ion laser (Spectra-Physics, BeamLok 2060) as the excitation source. The pump power used was 1.32 mW and the spot-size on the sample was ~ 0.5 mm^2 in all the measurements. A single monochromator (Acton, SpectraPro 2300i) was used to disperse the collected signal, and a long pass filter (cut-off wavelength 400 nm) was placed in front of the entrance slits to remove any collected laser signal. A thermo-electrically-cooled CCD camera (Andor, DU401-BR-DD) was used to record the spectra in the visible region. A liquid-nitrogen-cooled Ge-detector (Applied Detector Corp., 403S) in combination with standard lock-in techniques was used for spectral measurements in the near infra-red region. The obtained spectra were corrected for the system response. The time-dependence of the photoluminescence intensity was measured by modulating the pump beam using an acousto-optic modulator (NEOS Technologies, 38210-6AS). Photoluminescence traces at 800 nm, 900 nm, and 1535 nm were obtained respectively using an avalanche photodiode (Perkin Elmer SPCM-AQR), a visible-near-infrared photomultiplier tube (Hamamatsu R4330-02), and a near-infrared photomultiplier tube (Hamamatsu 5509-73), in combination with a multi-channel scaler (Stanford Research Systems, SR430). The spectral resolution in all photoluminescence measurements was ~15 nm. The time resolution in all measurements presented in this study was better than 80 ns.

3.3 Results and Discussion

3.3.1 Experimental Results

Figure 3.1 shows the measured photoluminescence (PL) spectra in the visible-near-infrared region of the LTA samples passivated at temperatures in the range 300 - 600ºC. The spectrum of

the unpassivated sample is included as a reference. Note that all PL spectra in this study are displayed on a logarithmic scale set to the same dynamic range (four orders of magnitude) to facilitate comparison of the relative intensity changes upon passivation. The PL spectra in Fig. 3.1 show two distinct bands that are present at all passivation temperatures: a broad emission band peaking around 550 nm, and a relatively sharp emission band peaking at 981 nm.

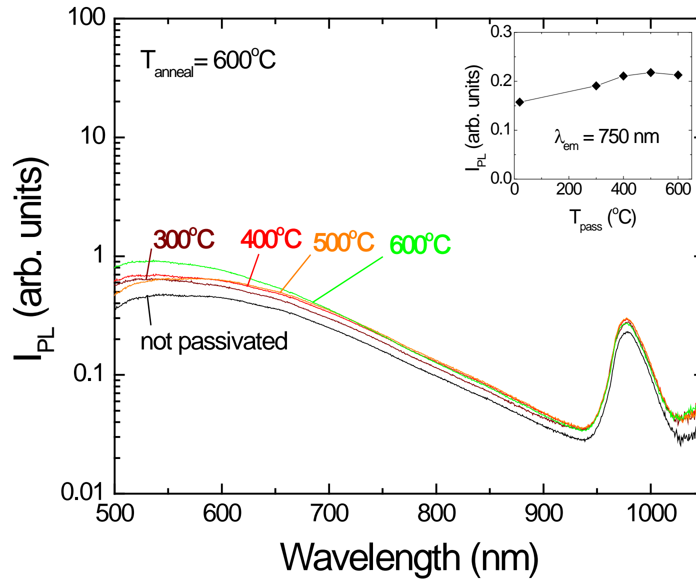

Figure 3.1. (Color) Photoluminescence spectra in the visible-near-infrared region of LTA samples passivated in the temperature range 300 - 600ºC. The PL spectrum of an unpassivated sample is included as a reference. Inset: PL intensity of the luminescence center emission of LTA samples at 750 nm as a function of passivation temperature**.**

The broad emission band is characterized by a resolution-limited decay time τ ($\tau < 80$ ns at $\lambda = 550$ nm) and is ascribed to the emission from luminescence centers (LC) in the Si-rich SiO_2 related to oxygen deficiencies.[1, 39-42] Similar broad visible emission bands have been observed in Si-implanted thermally grown SiO_2 films[29, 30, 39-41] as well as deposited Si-rich SiO_2 films,[42]

(present study), supporting the notion that stoichiometry rather than implantation damage is responsible for the formation of the luminescent centers. The photoluminescence peak at 981 nm is related to the optical transition of Er^{3+} ions from the second excited state ($^4I_{11/2}$) to the ground state ($^4I_{15/2}$). The spectral shape of the LC emission shows very little change as a function of passivation temperature. The emission at a wavelength of 750 nm was chosen to represent the LC intensity and is shown in the inset of Fig. 3.1. Passivation at temperatures up to 600ºC is seen to result in a gradual increase of the LC emission intensity by up to a factor of ~ 1.4 as compared to the unpassivated sample.

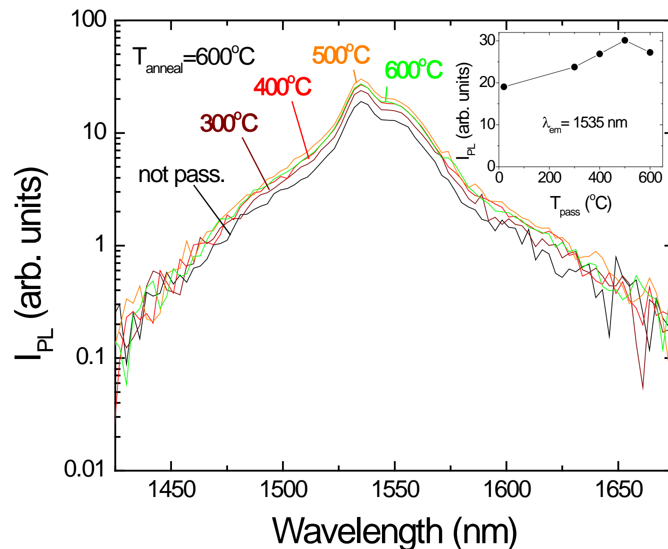

Figure 3.2. (Color) Photoluminescence spectra in the near-infra-red region of LTA samples passivated in the temperature range 300 - 600ºC. The PL spectrum of an unpassivated sample is included as a reference. Inset: PL intensity of the Er^{3+}-related emission of LTA samples at 1535 nm as a function of passivation temperature.

It is worth mentioning that this increase of the LC-related emission upon passivation is different from observations on Si-implanted SiO_2 films[30] where a *decrease* of a similar broad emission

feature was observed upon passivation using deuterium implantation and subsequent annealing. This difference is not well understood, but may be related to the different sample preparation and passivation methods used.

Figure 3.2 shows the photoluminescence spectra of the LTA samples in the near-infrared region. The observed emission band peaking at 1535 nm corresponds to the transition of Er^{3+} ions from their first excited state ($^4I_{13/2}$) to the ground state ($^4I_{15/2}$). The inset in Fig. 3.2 displays the PL intensity at 1535 nm as a function of passivation temperature. Similarly to the moderate intensity increase of the LC-related emission (see inset of Fig. 3.1) an increase of up to a factor ~ 1.6 in the Er-related emission intensity at 1535 nm is observed with increasing passivation temperature.

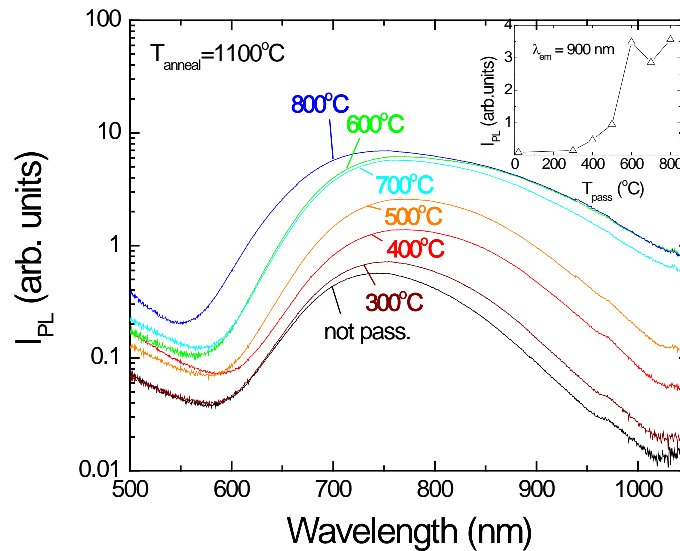

Figure 3.3. (Color) Photoluminescence spectra in the visible-near-infrared region of HTA samples passivated in the temperature range 300 - 800ºC. The PL spectrum of an unpassivated sample is included as a reference. Inset: PL intensity of nanocrystal-related emission of HTA samples at 900 nm as a function of passivation temperature.

Figure 3.3 shows the PL spectra in the visible-near-infrared region of the HTA samples passivated at temperatures in the range 300 - 800ºC. The PL spectrum of the unpassivated sample is included for comparison. Again a broad emission band is observed, in this case peaking around 750 - 800 nm. This band is characterized by a relatively long decay time (τ = 13 - 36 μs at λ = 900 nm) and is attributed to radiative exciton recombination in silicon nanocrystals (NC).[43-46] The inset in Fig. 3.3 shows the behavior of the NC-related signal at 900 nm for different passivation temperatures. This wavelength was chosen in the present analysis to minimize the influence of nanocrystal-to-nanocrystal energy transfer on the photoluminescence properties. The probability of energy transfer is known to be lower for nanocrystals emitting at long wavelengths.[47, 48] The nanocrystal-related emission intensity exhibits a significant increase upon passivation (up to a factor of ~ 40 at a wavelength of 900 nm). Contrary to the case of LTA samples, no Er^{3+}-related emission is observed at 981 nm. It should be noted that passivation leads to a significant change in the spectral shape of the Si NC emission: a higher passivation temperature leads to a relatively large increase in the long wavelength PL intensity as compared to the increase observed at shorter wavelengths.

Figure 3.4 shows the emission spectra of the HTA samples in the near-infrared region. Similarly to the case of LTA, a clear Er^{3+} emission spectrum is observed peaking at 1535 nm. The dependence of the Er^{3+} PL intensity at 1535 nm on passivation temperature is shown in the inset of Fig. 3.4. A significant increase in the Er-related emission intensity of up to a factor ~ 9 is observed upon passivation.

Figure 3.5 (a) shows the measured PL liftetime of the Er^{3+} emission at 1535 nm ($\tau_{dec,Er}$) as a function of passivation temperature of the LTA samples (closed circles) and HTA samples (open circles). Error bars are included for data sets with a relative error in excess of 5%.

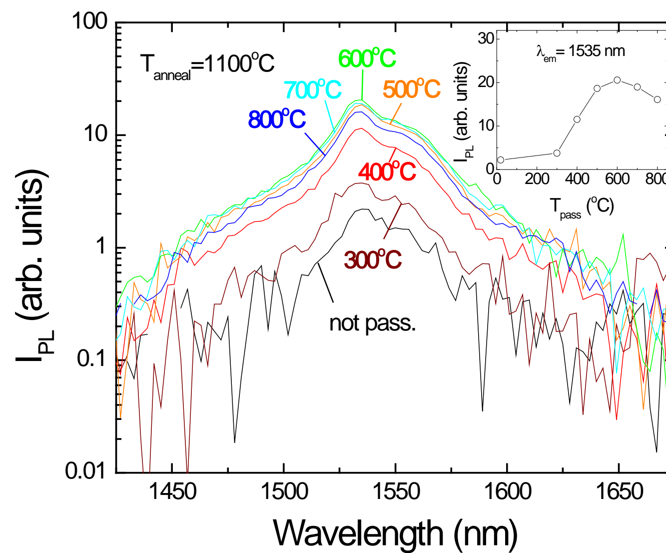

Figure 3.4. (Color) Photoluminescence spectra in the near-infrared region of HTA samples passivated in the temperature range 300 - 800ºC. The PL spectrum of an unpassivated sample is included as a reference. Inset: PL intensity of Er^{3+}-related emission of HTA samples at 1535 nm as a function of passivation temperature.

Note that all panels in Fig. 3.5 display the same dynamic range (three orders of magnitude) to facilitate comparison of the relative changes in each of the measured parameters. All Er^{3+} decay traces were found to exhibit a degree of multi-exponentiality, and could be accurately described by the Kohlrausch–Williams–Watts (KWW) function $I(t) \propto \exp\left\{-(t/\tau_{dec})^{\beta}\right\}$ with a dispersion factor β in the range 0.75 - 0.82.

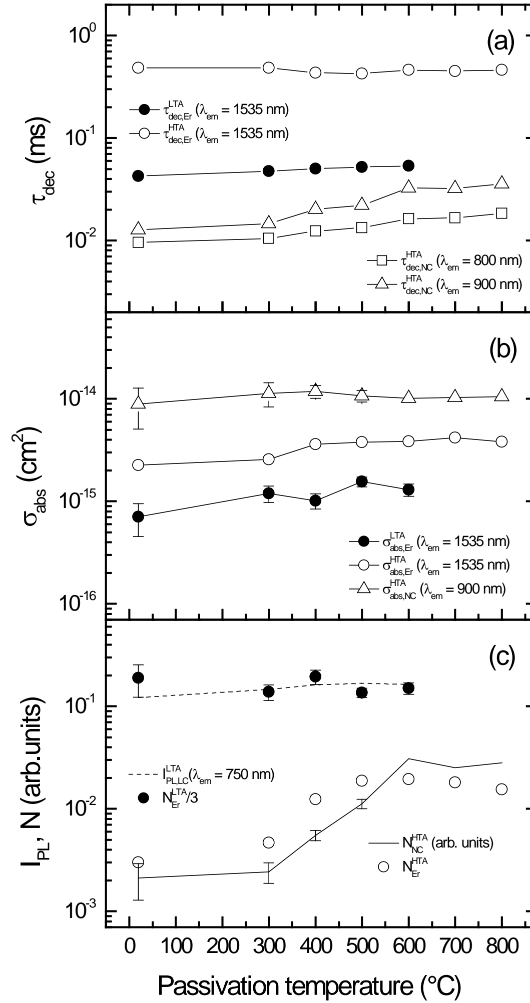

Figure 3.5. Measured and deduced photoluminescence parameters of LTA (solid symbols) and HTA samples (open symbols) as a function of passivation temperature: (a) Er^{3+} PL decay times at 1535 nm of LTA and HTA samples ($\tau_{dec,Er}^{LTA}$ and $\tau_{dec,Er}^{HTA}$ respectively), silicon nanocrystal PL decay times at 800 nm and 900 nm in HTA samples ($\tau_{dec,NC}^{HTA}$), (b) the effective absorption cross-section of the Er^{3+} PL at 1535nm in the LTA and HTA samples ($\sigma_{abs,Er}^{LTA}$ and $\sigma_{abs,Er}^{HTA}$ respectively), and of the silicon nanocrystal PL at 900 nm in the HTA samples ($\sigma_{abs,NC}^{HTA}$), (c) luminescence center PL intensity at 750 nm in LTA samples ($I_{PL,LC}^{LTA}$), the relative density of the sensitized optically active Er^{3+} ions in LTA and HTA samples (N_{Er}^{LTA} and N_{Er}^{HTA} respectively), the relative density of the optically active silicon nanocrystals contributing to the emission at 900 nm (N_{NC}^{HTA}). The arbitrary units of the relative density of the sensitized optically active Er^{3+} ions and optically active silicon nanocrystals are not related

The Er^{3+} lifetimes are seen to remain relatively constant as a function of passivation temperature in both sample types, and are of the order of ~ 50 μs and ~ 450 μs in LTA and HTA samples respectively. The longer Er^{3+} lifetime after high temperature annealing is commonly attributed to the thermally activated removal of non-radiative recombination centers in the oxide matrix directly affecting the Er^{3+} decay rate.[49, 50] The presence of a significant luminescence center induced increase in the total Er decay rate in LTA samples also becomes apparent in Chapter 5, where it explains the observation of a relatively constant $^4I_{11/2}$ lifetime at sample temperatures ranging from 15K to 300K.

The nanocrystal PL decay times in HTA samples ($\tau_{dec,NC}^{HTA}$) measured at 800 nm and at 900 nm are included in Fig. 3.5 (a). Similar to the Er^{3+} PL decay traces the nanocrystal PL decay traces also exhibit multi-exponential behavior with a dispersion factor in the range 0.60 - 0.76. A gradual increase of the nanocrystal lifetime with increasing passivation temperature is observed at both detection wavelengths. The lifetimes of the luminescence–center-related band measured at 550 nm are not included in Fig. 3.5 since they were found to be shorter than the time resolution of 80 ns.

Figure 3.5 (b) shows the effective absorption cross-section σ_{abs} for Er^{3+} excitation in the LTA (closed circles) and HTA samples (open circles) as found based on the measured excitation rate R_{exc} using the well-known relation

$$R_{exc} = \sigma_{abs}\varphi = \frac{1}{\tau_{rise}} - \frac{1}{\tau_{dec}} \tag{3.1}$$

where φ is the known incident pump photon flux, and τ_{rise} and τ_{dec} are the experimentally determined rise and decay times respectively. The measured Er^{3+} and nanocrystal rise times (not shown) exhibit a similar dependence on passivation temperature as the corresponding decay times. The effective Er^{3+} excitation cross-sections are found to be similar in magnitude for both sample types and are relatively independent of the passivation temperature, varying by a factor ~ 2 across the entire temperature range. The effective Er^{3+} absorption cross-sections are found to be (0.7 - 1.6) × 10^{-15} cm^2 in the LTA samples, and (2.3 - 4.2) × 10^{-15} cm^2 in the HTA samples. Note that the values reported here for the HTA sample are a factor of ~ 6 lower than the values reported in Chapter 2 [Ref. 1] due to a more accurate determination of the laser spot size in the present study. Additionally, in Chapter 2 [Ref. 1] the Er^{3+} excitation cross-section in the LTA samples was found to be approximately equal to that in the HTA sample, whereas in the present chapter a lower effective Er^{3+} absorption cross-section is observed in LTA samples by a factor ~ 2 – 3 as compared to that in HTA samples. The reason of this discrepancy is not known, but may be caused by a small degree of sample aging particularly for samples annealed at low temperatures.

The effective nanocrystal absorption cross-section in the HTA samples was also determined as a function of passivation temperature using Eq. 3.1, based on the 1/e rise times and decay times measured at a wavelength of 900 nm. The corresponding cross-section values are included in Fig. 3.5 (b) (open triangles), and are found to be relatively independent of passivation temperature. The measured NC cross-section of $\sigma_{NC} \approx 1 \times 10^{-14}$ cm^2 under 351 nm excitation is in good agreement with known literature values.[51]

The relatively small variation in the measured lifetimes in Fig. 3.5 (a) and absorption cross-sections in Fig. 3.5 (b) suggests that most of the observed changes in the Er^{3+} and nanocrystal PL intensity are related to the number of contributing emitters. In order to verify this, the concentration of optically active Si nanocrystals as well as the concentration of sensitized optically active Er^{3+} ions were determined as a function of passivation temperature. In the case of finite signal saturation and for a fixed film thickness and excitation and collection geometry, the PL intensity I_{PL} depends on the density of active emitters N according to

$$I_{PL} \propto \frac{R_{exc}\tau_{dec}}{1 + R_{exc}\tau_{dec}} N \quad , \tag{3.2}$$

This equation relies on the common assumption that the Er^{3+} ions and the Si nanocrystals can be modeled as a quasi three level system. The concentration of emitters is thus proportional to:

$$N \propto \left(1 + \frac{1}{R_{exc}\tau_{dec}}\right) I_{PL} \quad . \tag{3.3}$$

The term $R_{exc}\tau_{dec}$ is an indication of the excited state population of the emitter, with a value of 1 corresponding to the onset of population inversion. The magnitude of this term depends on the origin of the photoluminescence and on the measurement conditions, and in these studies is ~ 0.02 – 0.03 in the Er^{3+} PL measurements in LTA samples, ~ 0.06 – 0.19 in the NC PL measurements in HTA samples and ~ 0.54 – 0.93 in the Er^{3+} PL measurements in HTA samples. Figure 3.5 (c) shows the behavior of the density of sensitized optically active Er^{3+} ions obtained from Eq. 3.3 as a function of passivation temperature for LTA (closed circles) and HTA samples (open circles), as well as the concentration of optically active nanocrystals (solid line) based on

the measured PL intensities, cross-sections, and lifetimes. For comparison the luminescence center emission intensity observed in the LTA samples at 750 nm has been included (dashed line) in Fig. 3.5 (c). For the LTA samples a relatively small increase of the density of sensitized optically active Er^{3+} ions by a factor of ~ 1.4 is observed as the passivation temperature is increased up to 600ºC. Notably, a similar increase is observed in the LC PL intensity (measured at λ_{em} = 750 nm) in this same passivation temperature range. In contrast, for the HTA samples an increase of the density of sensitized optically active Er^{3+} ions and of optically active Si nanocrystals contributing to the emission at λ_{em} = 900 nm by factors of ~ 6.5 and ~ 14.6 respectively is observed in the same temperature range. Note that the exact change in density of optically active Si nanocrystals most likely depends on the nanocrystal size and therefore on the emission wavelength. However from the spectra shown in Fig. 3.3 it is clear that a significant increase in nanocrystal emission occurs for all wavelengths shown.

The observations made above appear to challenge several existing theories. First, in Chapter 2 [Ref. 1] we demonstrated that LCs are responsible for the majority of Er^{3+} excitation events for all annealing temperatures up to 1200°C, whereas the present data show a clear correlation between the Si nanocrystal PL intensity and the Er^{3+} PL intensity. Second, the observation of a gradual improvement of the NC lifetime upon passivation appears to contradict the existing theory that hydrogen passivates surface traps at the Si-SiO_2 interface, activating previously entirely 'dark' nanocrystals.[27] This kind of 'dark'/'bright' classification would predict a nanocrystal lifetime that is independent of the passivation temperature, rather than the experimentally observed gradual increase of the NC decay time with increasing passivation temperature. Both these apparent contradictions can be resolved, as discussed below.

3.3.2 Discussion

3.3.2.1 Effect of Passivation on Er^{3+} Excitation

Based on the experimental results presented here, as well as those present in the literature, a model is needed that can simultaneously account for all of the following observations:

(i) the similarity between the LC excitation spectrum and the Er^{3+} excitation spectrum, [Chapter 2, [Ref. 1]]

(ii) the correlation between the Er^{3+} excitation density and the LC emission intensity as a function of *annealing* temperature up to 1000ºC, [Chapter 2, [Ref. 1]]

(iii) the similarity in the measured effective absorption cross-section for Er^{3+} excitation in samples with and without Si nanocrystals, [Chapter 2, [Ref. 1]], (present study),

(iv) the relative insensitivity of the effective Er^{3+} absorption cross-section to the Er concentration,[16]

(v) the presence of fast and slow Er^{3+} excitation mechanisms,[22]

(vi) the decrease of the NC lifetime upon Er^{3+} incorporation, [Chapter 2, [Ref. 1]]

(vii) the correlation between the density of sensitized optically active Er^{3+} ions and the LC emission intensity as a function of *passivation* temperature in samples without Si nanocrystals (present study),

(viii) the correlation between the density of sensitized optically active Er^{3+} ions and the density of optically active Si nanocrystals as a function of *passivation* temperature in samples containing Si nanocrystals (present study),

(ix) the larger sensitivity of the Er^{3+} PL to passivation in samples containing nanocrystals as compared to samples where no nanocrystals are present (present study),

(x) the increase of the Er-related emission intensity at lower *passivation* temperatures as compared with the NC-related emission intensity (present study),

(xi) the significant reduction of the NC PL intensity[1, 12, 16, 21, 52] and the LC PL intensity[1] as a result of Er incorporation,

(xii) the absence of resonance features in the NC emission spectrum in Er-doped samples at wavelengths corresponding to optical transitions of Er,[1, 12, 52, 53]

(xiii) the similarity in magnitude of the measured Si nanocrystal absorption cross-section and the effective Er^{3+} absorption cross-section in samples containing Si nanocrystals [Chapter 2, [Ref. 1]], (present study),

(xiv) the similarity between the LC excitation spectrum and the NC excitation spectrum [Chapter 2, [Ref. 1]].

In Chapter 2 [Ref. 1] based on observations (i), (ii), and (iii) we concluded that the Er^{3+} excitation in these silicon-doped SiO_2 samples occurs predominantly through a luminescence-center-mediated process, while a small fraction of the excitation events occurs via nanocrystals. This interpretation also accounted for observations (iv), (v), and (vi), and is further supported by our observation in the present chapter showing that passivation affects the LC emission and the Er^{3+} emission in the same way (observation (vii)). Despite this correspondence a number of observations are present that appear to contradict the model proposed in the previous study. First

of all, the correlation between the density of sensitized optically active Er^{3+} ions and the density of optically active Si nanocrystals as a function of passivation temperature (observation (viii)) suggests that the presence of nanocrystals can significantly affect the Er^{3+} photoluminescence. The influence of nanocrystals on the Er^{3+} PL is further confirmed by the fact that the Er^{3+} PL intensity and the density of sensitized optically active Er^{3+} ions are found to be sensitive to passivation only when nanocrystals are present (observation (ix)). This leaves us with a paradox: while annealing studies[1] strongly suggest that nanocrystals are not required for Er^{3+} excitation, our passivation studies show that their presence can strongly influence the optical properties of the Er^{3+} ions.

To resolve this paradox, the excitation model presented in Chapter 2 [Ref. 1] needs to be extended without introducing any conflicts with earlier observations. We first consider the effect of passivation on the nanocrystal PL intensity. Electron paramagnetic resonance (EPR) studies on Si-rich SiO_2 samples have shown that P_b-type defects (silicon dangling bonds) form predominantly at the Si-SiO_2 interface due to lattice mismatch between the Si nanocrystals and the amorphous SiO_2 matrix.[35, 36] The experimentally observed anti-correlation of the NC PL intensity and the density of P_b-type defects measured by EPR as a function of passivation temperature[25] and of passivation time[54] has demonstrated that the presence of silicon dangling bonds results in a reduced nanocrystal PL intensity. We therefore conclude that the observed nanocrystal PL increase seen in Fig. 3.3 is due to the saturation of silicon dangling bonds with hydrogen upon passivation at elevated temperatures. Second, we consider the behavior of the Er^{3+} PL intensity. From Fig. 3.5 (c) we see that the dependence of the concentration of indirectly excitable and optically active Er^{3+} ions on passivation is similar to that of the concentration of

optically active Si nanocrystals. Since Chapter 2 [Ref. 1] demonstrated that LC mediated Er^{3+} excitation is the dominant Er^{3+} excitation mechanism in these samples, we must conclude that the observed improvement of the Er^{3+} PL intensity upon passivation *cannot be related to a change in a nanocrystal mediated excitation process*. Instead, we propose that the presence of unpassivated nanocrystals leads to either suppression of the LC-mediated Er^{3+} excitation process or to a non-radiative Er^{3+} relaxation process in HTA samples. Based on the relatively long lifetimes of the Er^{3+} excited states, the latter possibility appears the most likely. Since no significant passivation-dependent changes were observed in the Er^{3+} decay traces at 1.54 μm of HTA samples, it appears that this non-radiative interaction does not involve the Er^{3+} first excited state. We therefore propose that the presence of silicon dangling bonds at the nanocrystal surface can introduce a rapid non-radiative Er^{3+} relaxation from one or more of the Er^{3+} energy levels above the first excited state to the ground state. In this way, dangling bonds could reduce the excitation efficiency of the Er^{3+} first excited state, leading to the experimentally observed lower Er^{3+} emission intensity. Based on our experimental observations we propose that the presence of a dangling bond enables an Auger process in which non-radiative Er^{3+} relaxation is accompanied by the promotion of an electron from a neutral P_b center to the quantum confined conduction band of a Si nanocrystal. Based on the known location of the neutral dangling bond state relative to the silicon valence band (~ 0.3 eV above the valence band of bulk silicon)[55, 56] it is expected that this process would require 0.8 eV in unconfined silicon systems with a band gap of 1.1 eV, and more in quantum confined systems due to the additional confinement energy that would need to be overcome. Based on the known emission energies of 0.8 eV, 1.3 eV, and 1.5 eV of the first, second, and third excited states of Er^{3+} respectively, it indeed is physically reasonable to assume

that the first excited state would not have sufficient energy to induce such an Auger process in our nanocrystal doped samples, which fits with our experimental observations. Note that this process would also result in a lower apparent Er^{3+} excitation rate at low passivation temperatures, since the LC-mediated excitation into higher lying states would have a reduced probability of bringing Er^{3+} into the first excited state. A reduced Er^{3+} excitation rate is indeed observed in Fig. 3.5 (b) for the unpassivated HTA sample and for the HTA sample passivated at 300°C. While these arguments appear reasonable, it should be noted that Chapter 4 and Chapter 5 will show that a significant fraction (~ 50%) of the LC mediated Er^{3+} excitation events appear to occur directly into the first excited state, which would imply that hydrogen passivation and the presumed suppression of non-radiative relaxation of the $^4I_{11/2}$ level could not increase the Er^{3+} emission intensity by more than a factor 2. These observations together seem to indicate that the apparent observed 'direct' excitation into the $^4I_{13/2}$ level discussed in Chapter 4 in fact corresponds to excitation into the $^4I_{11/2}$ level, followed by rapid internal relaxation to the $^4I_{13/2}$ on a time scale that exceeds our time resolution limit (~ 27 ns). Further experiments at higher time resolution will be needed to definitively resolve this issue, however this is beyond our current experimental capability.

With the model proposed above, we can now understand the passivation temperature dependence of the photoluminescence properties of HTA samples in Fig. 3.5 (c). As the passivation temperature is increased, the average number of silicon dangling bonds on Si nanocrystals is reduced, and the number of fully passivated nanocrystals increases. This leads to a simultaneous increase in the nanocrystal and Er^{3+} PL intensity: the nanocrystal PL increases

due to an increased density of fully passivated optically active nanocrystals, while the Er^{3+} PL increases due to a reduced non-radiative coupling of the Er^{3+} ions to silicon dangling bonds.

Using the data in Fig. 3.5 (c) we can estimate a lower bound on the fraction of sensitized optically active Er^{3+} ions in HTA samples that is affected by the presence of silicon dangling bonds. As was shown before, the density of sensitized optically active Er^{3+} ions in HTA samples increased by a factor of ~ 6.5 upon passivation. This implies that before passivation a large fraction of the indirectly excitable Er^{3+} ions was affected by the presence of unpassivated nanocrystals. We can determine an upper bound on the fraction of affected Er^{3+} ions by noting that the fully passivated sample contains at most 100% active Er^{3+} ions. This implies that at most 100% / 6.5 = 15% of the Er^{3+} ions were unaffected by the presence of unpassivated nanocrystals, or conversely, that at least 85% of the indirectly excitable Er^{3+} ions were affected by the presence of unpassivated nanocrystals. A consequence of this model is thus that a large fraction of the Er^{3+} ions is in close proximity to at least one silicon dangling bond in unpassivated samples. This can be considered as a viable scenario given the high Si concentration in the samples under study.

Based on the proposed model it may be expected that a complete recovery of the nanocrystal PL intensity will require higher passivation temperatures or longer passivation times than those required for recovery of the Er^{3+} PL intensity, since the former requires the complete removal of *all* silicon dangling bonds at the Si-SiO_2 interface of a particular nanocrystal. The experimental results presented in Fig. 3.5 (c) indeed seem to indicate that the density of sensitized optically active Er^{3+} ions in HTA samples stabilizes at a passivation temperature of 500°C, while the density of optically active nanocrystals stabilizes at a passivation temperature of 600°C.

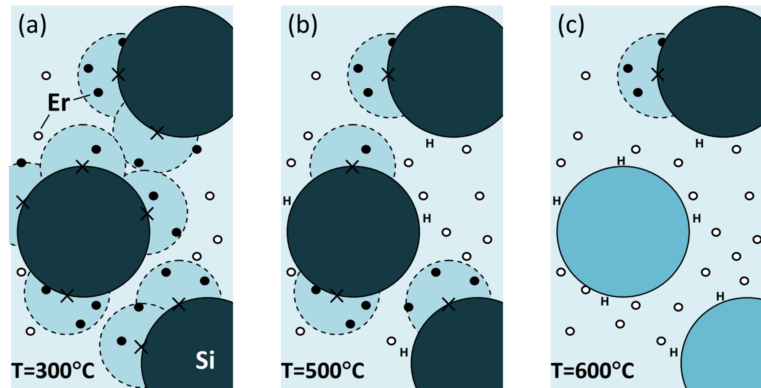

Figure 3.6. (Color) Proposed model of the effect of hydrogen passivation on the Si nanocrystal and Er^{3+} emission at three different passivation temperatures: (a) 300°C, (b) 500°C, and (c) 600°C. The large dark and bright solid circles represent Si nanocrystals with low and high emission efficiency respectively. The crosses represent dangling bonds, the dashed circles schematically indicate the interaction range of a dangling bond, and the letter H represents a hydrogen terminated dangling bond. The small solid and open circles represent Er^{3+} ions that are affected or unaffected by a dangling bond respectively.

This was also observed by Fukata et al.[25] in combined PL and EPR studies but in their case as a function of hydrogen diffusion. A possible physical origin for these observations is schematically shown in Fig. 3.6. At low passivation temperatures (Fig. 3.6 (a)) Si nanocrystals (large circles in Fig. 3.6) may contain multiple dangling bonds, as indicated by the crosses at the Si-SiO_2 interface, rendering the nanocrystals 'dark'. In our model, these dangling bonds can affect the Er^{3+} ions within a certain interaction range, as indicated by the dashed circles around the dangling bonds.

The Er^{3+} ions are known to be located inside the silica matrix[57] or at the nanocrystal-silica interface,[57, 58] as shown schematically in Fig. 3.6. At low passivation temperatures, a large fraction of the Er^{3+} ions is affected by dangling bonds, as indicated by the dark small circles, while a small fraction of the Er^{3+} ions is unaffected, as indicated by the small open circles. As the

passivation temperature is increased (Fig. 3.6 (b)), dangling bonds become hydrogen passivated, as indicated by the letter H in Fig. 3.6. This leads to a decrease of the number of affected Er^{3+} ions and a corresponding increase of the Er^{3+} emission intensity. Importantly, at this same passivation temperature the nanocrystal emission intensity does not show a similar increase, since the presence of a single dangling bond can render a nanocrystal optically 'dark'. Only at higher passivation temperatures the number of nanocrystals that are fully passivated increases significantly, as indicated by the light-colored circles in Fig. 3.6 (c), resulting in the observed increase of the nanocrystal emission intensity.

The argument that dangling bonds affect the Er^{3+} ions directly also explains the observed weak sensitivity to passivation of the Er^{3+} and LC PL in the LTA samples. According to published EPR studies no P_b-centers are present in unannealed Si-rich SiO_2 samples[59] and dangling bonds are formed only at crystalline silicon-SiO_2 interfaces[35, 36] with their concentration increasing in the process of nanocrystal formation.[60] Taking into account that no crystalline phase has been observed in LTA samples as was shown in Chapter 2 [Ref. 1], dangling bonds are expected to be absent in these samples. As a result, passivation only has a minor effect on the Er^{3+} emission as well as on the LC emission efficiency in samples where no nanocrystals are present.

The arguments given above provide an explanation for observations (vii)-(x), and since our model maintains the LC mediated nature of the Er^{3+} excitation, observations (i)-(vi) are still in agreement with this model. Intriguingly, the remaining unexplained observations (xi)-(xiv) can all be accounted for by assuming that luminescence centers can excite not only Er^{3+} ions but can also generate excitons in Si nanocrystals. If we consider LCs to be an important source of

nanocrystal excitation, then addition of Er^{3+} could lead to a reduced probability of nanocrystal excitation, resulting in a reduced nanocrystal emission intensity, as commonly observed in literature,[1, 12, 16, 21, 52] but without introducing any resonance features in the nanocrystal emission spectrum associated with NC→ Er^{3+} excitation. The absence of such resonance features was reported in numerous PL studies on Er-doped Si-rich SiO_2.[1, 12, 52, 53] This would also naturally explain the similar values of the typical nanocrystal absorption cross-section and of the effective Er^{3+} absorption cross-section[1, 13] as well as the good correspondence between the LC and NC excitation spectra.[1]

3.3.2.2 Effect of Passivation on the Nanocrystal Lifetimes

Figure 3.5 (a) shows that the nanocrystal emission lifetime at 800 nm and at 900 nm both increase gradually as the passivation temperature is increased. This is a surprising result that cannot readily be understood in terms of passivation-induced changes in the emission lifetime of individual nanocrystals. To clarify this statement, we consider the possible exciton decay channels. The total exciton lifetime is governed by (a) radiative exciton recombination,[61] (b) non-radiative exciton trapping by silicon dangling bonds,[27, 31, 32] (c) energy transfer to a nearby nanocrystal,[62-64] and (d) energy transfer to a nearby Er^{3+} ion.[1, 22, 65] The total decay rate of excitons in nanocrystals of a specific size is therefore given by:

$$R_{dec,NC} = R_{rad,NC} + N_{DB} \times R_{DB} + R_{NC-NC,tot} + R_{NC-Er,tot} \tag{3.4}$$

where $R_{rad,NC}$ is the exciton radiative reconbimation rate, R_{DB} is the exciton capture rate by a single silicon dangling bond, N_{DB} is the number of silicon dangling bonds per nanocrystal,

$R_{NC\,NC,tot}$ is the total energy transfer rate to nearby larger nanocrystals, and $R_{NC\text{-}Er,tot}$ is the total energy transfer rate from the nanocrystal to nearby Er^{3+} ions. These rates affect the nanocrystal emission efficiency given by $\eta_{NC} = \frac{R_{rad,NC}}{R_{dec,NC}}$. Of all the decay contributions, the number of silicon dangling bonds is expected to depend most strongly on the passivation treatment. The other three contributions ($R_{rad,NC}$, $R_{NC\text{-}NC,tot}$ and $R_{NC\text{-}Er,tot}$) are thought to depend on respectively the nanocrystal size and shape, the nanocrystal density, and the Er^{3+} distribution, none of which are expected to change significantly for passivation temperatures well below the annealing temperature used.

Based on theoretical works[31, 32] the exciton capture rate of a silicon dangling bond at the Si-SiO_2 interface was calculated to be ~ 10^{10} - 10^{11} sec^{-1} for nanocrystals with peak PL intensities around ~ 750 nm. By comparison, the other possible decay channels are dramatically slower. The typical room temperature radiative decay rate of excitons in nanocrystals emitting at these wavelengths is $R_{rad,\,NC}$ ~ 10^3 – 10^4 sec^{-1} [Ref. 46, 61, 65] while the experimentally observed nanocrystal-to-erbium energy transfer rate constant is ~ 10^4 – 10^6 sec^{-1} [Ref. 1, 22, 65]. This suggests that the presence of a single silicon dangling bond ($N_{DB} = 1$) can reduce the nanocrystal emission efficiency by several orders of magnitude, rendering the nanocrystals effectively 'dark', i.e. virtually undetectable in photoluminescence spectra and in lifetime measurements. We thus expect Si nanocrystal doped samples to contain (a) *unpassivated nanocrystals with one or more silicon dangling bonds* that are optically undetectable due to an extremely low emission efficiency given by

$$\eta_{NC,unpass} = \frac{R_{rad,NC}}{R_{rad,NC} + N_{DB} \times R_{DB} + R_{NC-NC,tot} + R_{NC-Er,tot}} \approx 0, \quad (3.5)$$

as well as (b) *fully passivated nanocrystals that do not have a silicon dangling bond*, and have relatively high emission efficiency given by

$$\eta_{NC,pass} = \frac{R_{rad,NC}}{R_{rad,NC} + R_{NC-NC,tot} + R_{NC-Er,tot}}. \quad (3.6)$$

These arguments suggest that the total nanocrystal photoluminescence intensity and therefore the measured decay rate will reflect only the lifetime of fully passivated nanocrystals. Consequently, the measured nanocrystal lifetime is expected to be independent of passivation temperature. This is in clear contradiction with the observations in Fig. 3.5 (a).

To resolve the apparent contradiction described above, we consider the inhomogeneous nature of the nanocrystal emission spectrum. As was observed in Fig. 3.5 (a), the nanocrystal lifetime at an emission wavelength of 800 nm is found to be a factor of 1.3 – 2 shorter than that observed at 900 nm. Such wavelength dependent emission lifetime has been attributed to two different phenomena: (i) the size-dependent oscillator strength of the transitions in the nanocrystals resulting in the size dependent radiative decay rates of the nanocrystals,[66, 67] and (ii) the presence of energy transfer from small nanocrystals that have a large bandgap to larger nanocrystals that have a smaller bandgap.[47, 48, 62-64] Both these effects lead to a shorter lifetime for smaller nanocrystals.[1, 22, 65, 66] As will be shown below, this size-dependent emission lifetime can lead to an *apparent* gradual change in the nanocrystal lifetime at a single emission wavelength due to the inhomogeneous nature of the nanocrystal emission spectrum. The nanocrystal emission spectra in this type of sample are well-known to be inhomogeneously

broadened, with the short wavelength emission being largely due to emission by small (rapidly decaying) nanocrystals, and the long wavelength emission originating predominantly from large (slowly decaying) nanocrystals. As demonstrated in previous studies[68] the homogeneous emission linewidth of a silicon nanocrystal with a diameter of ~ 3 - 4 nm is ~ 120 meV (~ 50 nm) at the peak emission energy of ~ 1.7 eV (~ 730 nm). The significant inhomogeneous broadening enables the observation of different lifetimes in different parts of the spectrum. More importantly, the nanocrystal emission detected at a wavelength of 900 nm contains a significant PL contribution from nanocrystals that exhibit a slightly different peak emission wavelength and that have a different lifetime. A gradual change in the apparent emission lifetime may thus be expected at a specific emission wavelength if the *relative photoluminescence contribution of nanocrystals with different sizes changes as a function of passivation temperature*. This effect is illustrated in Fig. 3.7 using the measured emission spectra.

The left inset shows the measured NC emission spectrum (thick solid line) for an unpassivated HTA sample, normalized at a wavelength of 900 nm. The Gaussian curves underneath the PL spectrum schematically depict the individual PL contributions of nanocrystals with different sizes. The linewidth of all Gaussian curves was chosen to be equal to the known homogeneous linewidth[68] of ~ 120 meV. Note that emission by nanocrystals with a center wavelength of 850 nm (curve A) leads to a finite contribution to the PL intensity observed at 900 nm (curve B). This PL contribution, indicated by the short vertical line, will lead to the addition of a small fast lifetime component in PL decay traces recorded at 900 nm. Experimentally this appears as a relatively short lifetime at λ_{em} = 900 nm, and a low β value due to the stronger deviation from single-exponential decay.

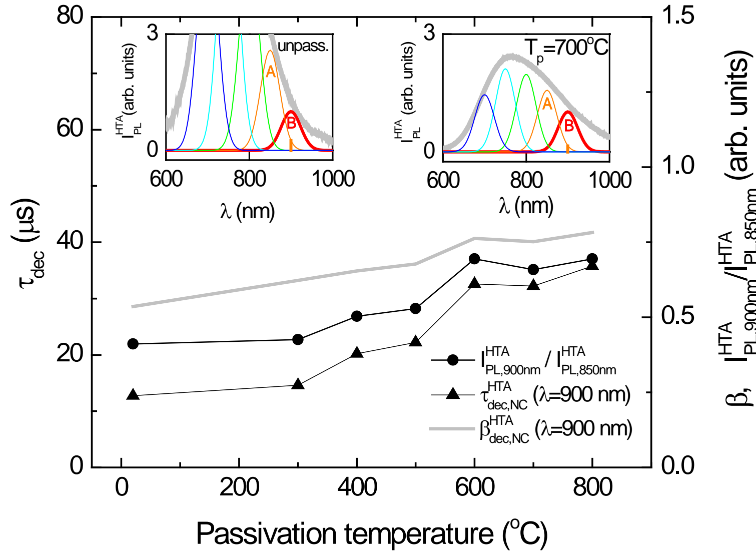

Figure 3.7. (Color) Measured and deduced photoluminescence parameters of the silicon-nanocrystal-related emission in HTA samples as a function of passivation temperature: silicon nanocrystal PL decay times of the HTA samples at 900 nm ($\tau_{dec,NC}^{HTA}$), silicon nanocrystal PL decay time dispersion factor of HTA samples at 900 nm ($\beta_{dec,NC}^{HAT}$), the ratio of the silicon nanocrystal PL intensity at 900 nm to that of 850 nm ($I_{PL,900nm}^{HTA}/I_{PL,850nm}^{HTA}$). Insets: measured silicon nanocrystal emission spectrum (thick solid line) for an unpassivated (left) and passivated at 700ºC (right) HTA samples, normalized at a wavelength of 900 nm. The Gaussian curves underneath the PL spectrum schematically depict the individual PL contributions of silicon nanocrystals with different sizes.

Note that the relatively weak emission from nanocrystals with a peak emission wavelength of 950 nm also adds a small contribution to the PL detected at 900 nm. For simplicity we do not consider this minor contribution here. The right inset shows the NC emission spectrum (thick solid line) for a HTA sample passivated at 700ºC. According to the model introduced above, passivation has led to a change in the number of optically active nanocrystals emitting at various wavelengths, while their individual lifetimes are unchanged. Similar to what was observed in the left inset, nanocrystals with a peak emission wavelength of 850 nm add a finite PL contribution

at a detection wavelength of 900 nm. However, due to the change in the shape of the NC emission spectrum, the *relative contribution of emission from these nanocrystals to the photoluminescence at 900 nm is reduced.* This reduction in the short-wavelength contribution, and the concurrent reduction in the short-lifetime contribution at 900 nm, leads to a longer 1/e lifetime at λ_{em} = 900 nm, and an increased β value. Both of these effects are clearly observed experimentally. Note that the analysis above only considered two discrete peak emission wavelengths, while in reality the emission at 900 nm contains contributions from nanocrystals with a range of peak emission wavelengths near 900 nm that is given by the homogeneous linewidth.

To further verify the proposed role of inhomogeneous broadening on the measured nanocrystal decay traces, Fig. 3.7 includes the measured nanocrystal decay time at an emission wavelength of 900 nm (triangles), the corresponding dispersion factor $\beta_{dec,NC}^{HTA}$ (solid line) and the ratio of the nanocrystal-related photoluminescence intensity observed at 900 nm and at 850 nm (circles), labeled $I_{PL,900nm}^{HTA} / I_{PL,850nm}^{HTA}$. The experimental error is less than 5% in all these data sets, and has not been included in the graph. The plotted intensity ratio is approximately proportional to the local slope of the PL spectrum, and as such is a measure of the relative contribution of short wavelength emission (850 nm) to the PL detected at 900 nm. An excellent qualitative correspondence is observed between the measured nanocrystal decay time and the local slope of the PL spectrum, despite the very different nature of these quantities. Further support for this interpretation is provided by the behavior of the dispersion factor $\beta_{dec,NC}^{HTA}$. As the local slope of the PL spectrum decreases, the dispersion factor is seen to gradually increase, which can be

attributed to the reduced influence of smaller nanocrystals on the PL decay traces measured at 900 nm: as the relative PL contribution from smaller nanocrystals is reduced, fast lifetime components are being removed from the PL decay trace at 900 nm, leading to a more single-exponential decay, and a β value closer to 1.

Based on the clear correlation of the local slope of the photoluminescence spectra with the passivation induced changes in the PL lifetime and in the measured β values we conclude that the gradual nanocrystal lifetime increase observed upon passivation is *not* due to a gradual improvement of the nanocrystal emission efficiency, but rather are a result of the inhomogeneous nature of the nanocrystal PL spectrum combined with a size-dependent degree of nanocrystal passivation at each temperature. This model also explains the relatively small increase of the NC lifetime with passivation temperature observed both in the current and independent studies[27] compared to the large changes in nanocrystal PL intensity. A final observation is that the change in the shape of the nanocrystal emission spectrum upon passivation (Fig. 3.3) implies that large nanocrystals responsible for the long wavelength shoulder of the NC emission spectra require higher temperatures to become fully passivated as compared with the smaller nanocrystals. This could be a reflection of the fact that large nanocrystals have a larger Si-SiO_2 interface area. This leads to a larger number of silicon dangling bonds for large nanocrystals[26, 28, 69] and may therefore require longer passivation times or higher passivation temperatures in order to reach full saturation of all dangling bonds.

The findings presented in this study are of significant importance for the realization of gain in Er-doped Si-rich SiO_2 waveguides. First, Er^{3+} in Si rich SiO_2 films is excited predominantly via luminescence centers. This implies that one can obtain the large Er^{3+}

excitation cross-section enhancements that have been observed in literature, but without the need for silicon nanocrystals. This is an important result, since Si nanocrystals are known[7, 19] to induce a significant amount of confined carrier absorption at 1.54 μm due to the presence of long lived excitons in the nanocrystals during excitation. The ability to enhance Er^{3+} excitation without introducing significant free carrier absorption would therefore be a major step forward in the development of silicon sensitized Er^{3+} gain media. Secondly, a low annealing temperature (600ºC) was found to lead to a higher concentration of indirectly excitable Er^{3+} as compared with a high annealing temperature (1100ºC). The observed higher concentration of sensitized optically active Er^{3+} ions in the samples annealed at low temperature (600ºC) implies a reduction in the concentration of optically active Er^{3+} ions that are not sensitized. This in turn reduces the degree of ground state absorption due to unsensitized Er^{3+} ions. Additionally, due to the direct relation between optical gain and the density of excited emitters, the larger concentration of sensitized optically active Er^{3+} ions observed in the LTA samples implies that a higher gain can be achieved in LTA samples as compared with HTA samples. Third, it was found that dangling bonds at the Si-SiO_2 interface can efficiently quench the Er^{3+} PL. This implies that any nanocrystals present in the matrix need to be fully passivated in order to obtain maximum gain. All these observations indicate that annealing temperatures below the onset of nanocrystal formation are preferred in order to achieve maximum gain. It should be noted that the Er^{3+} lifetime in samples annealed at low temperature is significantly shorter than that observed in samples annealed at high temperatures. Although this would lead to higher required pump powers for population inversion, this drawback may be outweighed by the significant advantages of purely luminescence center mediated Er^{3+} excitation.

3.4 Conclusions

The effect of hydrogen passivation at different temperatures on the luminescence-center-mediated sensitization of Er^{3+} has been studied in Er-doped Si-rich SiO_2 films containing no detectable Si nanocrystals (annealed at 600ºC) and containing Si nanocrystals (annealed at 1100ºC). Passivation is shown to have a minor effect on the photoluminescence properties of samples without nanocrystals, which is ascribed to the absence of dangling bonds in these samples. In contrast, samples containing silicon nanocrystals exhibit a significant increase in the density of optically active silicon nanocrystals, which is accompanied by a gradual change in the nanocrystal lifetime and a significant increase in the density of sensitized optically active Er^{3+} ions. The observed concurrent increase in the densities of active silicon nanocrystals and sensitized optically active Er^{3+} ions is ascribed to a passivation temperature dependent concentration of dangling bonds, which influences the emission from Si nanocrystals and Er^{3+} ions in different ways. In the case of nanocrystal photoluminescence, the presence of a dangling bonds results in the rapid trapping of excitons followed by nonradiative decay. In the case of Er^{3+} photoluminescence, we conclude that an Er^{3+} ion excited via a luminescence center can relax non-radiatively via a direct interaction with dangling bonds present on the surface of nanocrystals. This interaction appears to predominantly affect excited states above the $^4I_{13/2}$ level, and is accompanied by a reduced excitation rate of the $^4I_{13/2}$ level. In addition, the gradual increase of the lifetime of the nanocrystal-related photoluminescence is attributed to a passivation-induced change in the concentration of optically active nanocrystals with different sizes. This change, combined with the inhomogeneous nature of the nanocrystal emission

spectrum in these samples, leads to a change in the measured nanocrystal photoluminescence decay time.

3.5 References

[1] O. Savchyn, F. R. Ruhge, P. G. Kik, R. M. Todi, K. R. Coffey, H. Nukala, and H. Heinrich, Phys. Rev. B **76**, 195419 (2007).

[2] M. Lipson, J. Lightwave Technol. **23**, 4222 (2005).

[3] N. Daldosso, D. Navarro-Urrios, M. Melchiorri, C. García, P. Pellegrino, B. Garrido, C. Sada, G. Battaglin, F. Gourbilleau, R. Rizk, and L. Pavesi, IEEE J. Sel. Top. Quantum Electron. **12**, 1607 (2006).

[4] T. J. Kippenberg, J. Kalkman, A. Polman, and K. J. Vahala, Phys. Rev. A **74**, 051802 (2006).

[5] A. Polman, B. Min, J. Kalkman, T. J. Kippenberg, and K. J. Vahala, Appl. Phys. Lett. **84**, 1037 (2004).

[6] A. J. Kenyon, Semicond. Sci. Technol. **20**, R65 (2005).

[7] P. G. Kik and A. Polman, in Proceedings of the NATO Advanced Research Workshop on Towards the First Silicon Laser, Trento, Italy, 2002, edited by L. Pavesi, S. Gaponenko, and L. Dal Negro (Kluwer Academic, Dordrecht, 2003), p. 383.

[8] A. Polman, D. C. Jacobson, D. J. Eaglesham, R. C. Kistler, and J. M. Poate, J. Appl. Phys. **70**, 3778 (1991).

[9] W. Miniscalco, J.Light.Tech. **9**, 234 (1991).

[10] A. Polman and F. C. J. M. van Veggel, J. Opt. Soc. Am. B **21**, 871 (2004).

[11] A. J. Kenyon, P. F. Trwoga, M. Federighi, and C. W. Pitt, J.Phys.: Condens. Matter **6**, L319 (1994).

[12] M. Fujii, M. Yoshida, and Y. Kanzawa, S. Hayashi, and K. Yamamoto, Appl. Phys. Lett. **71**, 1198 (1997).

[13] P. G. Kik, M. L. Brongersma, and A. Polman, Appl. Phys. Lett. **76**, 2325 (2000).

[14] G. Franzò, V. Vinciguerra, and F. Priolo, Appl. Phys. A **69**, 3 (1999).

[15] F. Gourbilleau, M. Levalois, C. Dufour, J. Vicens, and R. Rizk, J. Appl. Phys. **95**, 3717 (2004).

[16] P. G. Kik and A. Polman, J. Appl. Phys. **88**, 1992 (2000).

[17] A. J. Kenyon, C. E. Chryssou, C. W. Pitt, T. Shimizu-Iwayama, D. E. Hole, N. Sharma, and C. J. Humphreys, J. Appl. Phys. **91**, 367 (2002).

[18] M. Wojdak, M. Klik, M. Forcales, O. B. Gusev, T. Gregorkiewicz, D. Pacifici, G. Franzò, F. Priolo, and F. Iacona, Phys. Rev. B **69**, 233315 (2004).

[19] A. Mimura, M. Fujii, S. Hayashi, D. Kovalev, and F. Koch, Phys. Rev. B **62**, 12625 (2000).

[20] P. G. Kik and A. Polman, J. Appl. Phys. **91**, 534 (2002).

[21] D. Pacifici, G. Franzò, F. Priolo, F. Iacona, and L. Dal Negro, Phys. Rev. B **67**, 245301 (2003).

[22] M. Fujii, K. Imakita, K. Watanabe, and S. Hayashi, J. Appl. Phys. **95**, 272 (2004).

[23] K. Imakita, M. Fujii, and S. Hayashi, Eur. Phys. J. D **34**, 161 (2005).

[24] I. Izeddin, A. S. Moskalenko, I. N. Yassievich, M. Fujii, and T. Gregorkiewicz, Phys. Rev. Lett. **97**, 207401 (2006).

[25] N. Fukata, C. Li, H. Morihiro, K. Murakami, M. Mitome, and Y. Bando, Appl. Phys. A **84**, 395 (2006).

[26] S. Cheylan, and R. G. Elliman, Nucl. Instrum. Methods Phys. Res.B **175-177**, 422 (2001).

[27] A. R. Wilkinson and R. G. Elliman, Phys. Rev. B **68**, 155302 (2003).

[28] S. Cheylanand and R. G. Elliman, Appl. Phys. Lett. **78**, 1225 (2001).

[29] S. P. Withrow, C. W. White, A. Meldrum, J. D. Budai, D. M. Hembree, Jr., and J. C. Barbour, J. Appl. Phys. **86**, 396 (1999).

[30] K. S. Min, K. V. Shcheglov, C. M. Yang, Harry A. Atwater, M. L. Brongersma and A. Polman, Appl. Phys. Lett. **69**, 2033 (1996).

[31] M. Lannoo, C. Delerue, and G. Allan, J. Lumin. **70**, 170 (1996).

[32] C. Delerue, G. Allan, and M. Lannoo, Phys. Rev. B **48**, 11024 (1993).

[33] A. Stesmans, J.Appl.Phys. **92**, 1317 (2002).

[34] P. J. Caplan, E. H. Poindexter, B. E. Deal, and R. R. Razouk, J. Appl. Phys. **50**, 5847 (1979).

[35] Y. Nishi, J.J. Appl. Phys.10, 52 (1971).

[36] P. M. Lenahan and J. F. Conley, Jr., J. Vac.Sci. Technol.B 16, 2134 (1998).

[37] K. L. Brower, Phys. Rev. B **38**, 9657 (1988).

[38] http://www.genplot.com/

[39] T. Shimizu-Iwayama, K. Fujita, S. Nakao, K. Saitoh, T. Fujita, and N. Itoh, J. Appl. Phys. **75**, 7779 (1994).

[40] M. Ya. Valakh, V. A. Yukhimchuk, V. Ya. Bratus', A. A. Konchits, P. L. F. Hemment, and T. Komoda, J. Appl. Phys. **85**, 168 (1999).

[41] J.-Y. Zhang, X.-M. Bao, N.-S. Li, and H.-Z. Song, J. Appl. Phys. **83**, 3609 (1998).

[42] A. J. Kenyon, P. F. Trwoga, C. W. Pitt, and G. Rehm, J. Appl. Phys. **79**, 9291 (1996).

[43] J. S. Biteen, N. S. Lewis, H. A. Atwater, and A. Polman, Appl. Phys. Lett. **84**, 5389 (2004).

[44] I. N. Yassievich and A. S. Moskalenko, Mater. Sci. Eng. B **105**, 192 (2003).

[45] M. V. Wolkin, J. Jorne, P. M. Fauchet, G. Allan, and C. Delerue, Phys. Rev. Lett. **82**, 197 (1999).

[46] M. L. Brongersma, P. G. Kik, A. Polman, K. S. Min, and H. A. Atwater, Appl. Phys. Lett. **76**, 351 (2000).

[47] F. Priolo, G. Franzò, D. Pacifici, V. Vinciguerra, F. Iacona, and A. Irrera, J. Appl. Phys. **89**, 264 (2001).

[48] A. Polman and R. G. Elliman, in Proceedings of the NATO Advanced Research Workshop on Towards the First Silicon Laser, Trento, Italy, 2002, edited by L. Pavesi, S. Gaponenko, and L. Dal Negro (Kluwer Academic, Dordrecht, 2003), p. 209.

[49] A. Polman, D. C. Jacobson, A. Lidgard and J. M. Poate, and G. W. Arnold, Nuc. Instr. Meth. Phys. Res. B **59-60**, 1313 (1991).

[50] A. Polman, D. C. Jacobson, D. J. Eaglesham, R. C. Kistler, and J. M. Poate, J. Appl. Phys. **70**, 3778 (1991).

[51] D. Kovalev, J. Diener, H. Heckler, G. Polisski, N. Künzner, and F. Koch, Phys. Rev. B **61**, 4485 (2000).

[52] F. Priolo, G. Franzó, F. Iacona, D. Pacifici, and V. Vinciguerra, Mater.Sci.Eng. B **81**, 9 (2001).

[53] P.G. Kik and A. Polman, Mater.Sci.Eng. B **81**, 3 (2001).

[54] P. Pellegrino, B. Garrido, C. García, R. Ferré, J. A. Moreno, and J. R. Morante, Physica E **16**, 424 (2003).

[55] E. H. Poindexter, G. J. Gerardi, M.-E. Rueckel, P. J. Caplan, N. M. Johnson, and D. K. Biegelsen, J. Appl. Phys. **56**, 2844 (1984).

[56] N. M. Johnson, D. K. Biegelsen, M. D. Moyer, S. T. Chang, E. H. Poindexter, and P. J. Caplan, Appl. Phys. Lett. **43**, 563 (1983).

[57] G. Franzò, D. Pacifici, V. Vinciguerra, F. Priolo, and F. Iacona, Appl. Phys. Lett. **76**, 2167 (2000).

[58] X. L. Wu, Y. F. Mei, G. G. Siu, K. L. Wong, K. Moulding, M. J. Stokes, C. L. Fu, and X. M. Bao, Phys. Rev. Lett. 86, 3000 (2001).

[59] M. López, B. Garrido, C. Bonafos, A. Pérez-Rodríguez, J. R. Morante, and A. Claverie, Nucl. Instr. Meth. Phys. Res. Sec. B **178**, 89 (2001).

[60] M. López, B. Garrido, C. García, P. Pellegrino, A. Pérez-Rodríguez, J. R. Morante, C. Bonafos, M. Carrada, and A. Claverie, Appl. Phys. Lett. **80**, 1637 (2002).

[61] M. S. Hybertsen, Phys. Rev. Lett. **72**, 1514 (1994).

[62] M. L. Brongersma, A. Polman, K. S. Min, E. Boer, T. Tambo, and H. A. Atwater, Appl. Phys. Lett. **72**, 2577 (1998).

[63] J. Linnros, N Lalic, A. Galeckas, and V. Grivickas, J. Appl. Phys. **86**, 6128 (1999).

[64] L. Pavesi, J. Appl. Phys. **80**, 216 (1996).

[65] K. Watanabe, M. Fujii, and S. Hayashi, J. Appl. Phys. **90**, 4761 (2001).

[66] T. Takagahara and K. Takeda, Phys. Rev. B **46**, 15578 (1992).

[67] D. Kovalev, H. Heckler, G. Polisski, J. Diener, and F. Koch, Opt. Mat. **17**, 35 (2001).

[68] J. Valenta, R. Juhasz, and J. Linnros, Appl. Phys. Lett. **80**, 1070 (2002).

[69] D. Kovalev, H. Heckler, G. Polisski, and F. Koch, Phys. Stat. Sol. (b) **215**, 871 (1999).

CHAPTER 4. MULTI-LEVEL SENSITIZATION OF Er^{3+} IN LOW-TEMPERATURE-ANNEALED Si-RICH SiO_2

(Based on work published in Applied Physics Letters **93**, 233120 (2008))

The dynamics of Er^{3+} excitation in low-temperature-annealed Si-rich SiO_2 are studied. It is demonstrated that Si-excess-related indirect excitation is fast (transfer time $\tau_{tr} < 27$ ns) and occurs into higher lying Er^{3+} levels as well as directly into the first excited state ($^4I_{13/2}$). By monitoring the time-dependent Er^{3+} emission at 1535 nm the multi-level nature of the Er^{3+} sensitization is shown to result in two types of excitation of the $^4I_{13/2}$ state: a fast excitation process ($\tau_{tr} < 27$ ns) directly into the $^4I_{13/2}$ level and a slow excitation process due to fast excitation into Er^{3+} levels above the $^4I_{13/2}$ level, followed by internal Er^{3+} relaxation with a time constant $\tau_{32} > 2.3$ μs. The fast and slow excitation of the $^4I_{13/2}$ level account for an approximately equal fraction of the excitation events: 45 – 50 % and 50 – 55 % respectively.

4.1 Introduction

The continued technological implementation of Si photonics requires the development of a cost effective Si-compatible light source.[1-4] The use of Si nanocrystals (NCs) as sensitizers of Er^{3+} ions[5] and subsequent demonstration of Si-sensitized gain at 1.54 μm [Ref. 6] have drawn significant attention, since this approach could potentially enable the realization of an on-chip laser under excitation with a low-cost broadband light source. Despite significant promise of this

approach, the presence of Si nanocrystals was found to result in a low concentration of optically active erbium ions[7, 8] and to introduce significant confined carrier absorption[9-11] as well as scattering.[12] In Chapter 2 [Ref. 7] and Chapter 3 [Ref. 8] it was shown that broadband sensitization of Er^{3+} can also occur in Si-doped SiO_2 annealed at temperatures well below those required for NC formation (see also Refs. 7, 8, and 13). As described in Chapter 2 [Ref. 7] and Chapter 3 [Ref. 8] this phenomenon was attributed to Er^{3+} excitation by Si-excess-related luminescence centers (LC) in the SiO_2 matrix. Low-temperature-annealed samples were found to contain a higher density of optically active Er^{3+} ions compared to Si-nanocrystal-doped samples with similar total Si and Er concentration [Chapter 2 [Ref. 7] and Chapter 3 [Ref. 8]]. In addition, the absence of Si NCs in low-temperature annealed samples could minimize scattering and confined carrier absorption typically introduced by Si NCs during optical pumping.[9, 10] These two factors make low-temperature-annealed Er-doped Si-rich SiO_2 an interesting candidate for the realization of amplification at 1.54 μm under broadband excitation. The evaluation of this material as a gain medium requires a detailed understanding of the observed Er^{3+} excitation process. This chapter discusses the dynamics of the LC-mediated Er^{3+} excitation mechanism in low temperature annealed Er-doped Si-rich SiO_2.

4.2 Experimental Techniques

An Er-doped Si-rich SiO_2 film containing 12 at. % of excess Si and 0.63 at. % of Er was deposited by magnetron co-sputtering onto a Si wafer. The sample was annealed for 100 seconds in N_2 at 600°C and subsequently passivated for 30 min. in forming gas (N_2:H_2 = 95%:5%) at

500°C. No Si aggregates could be detected in transmission electron microscopy measurements on this sample [Chapter 2 [Ref. 7]]. For optical measurements the sample was attached to the cold finger of a closed-loop He cryostat, and held at 15 K at a pressure of 5×10^{-7} mbar. Photoluminescence (PL) spectra were taken using the 351 nm line of a Kr-ion laser as the excitation source (0.26 W/cm^2). PL spectra in the regions 500 - 1100 nm and 950 - 1750 nm were recorded using respectively a charge-coupled device array and a Ge-detector with a spectral resolution of 10 nm. The PL spectra were corrected for the system spectral response, and concatenated at λ = 1025 nm. The time-dependent PL signal was measured under pulsed excitation using the 355 nm line of a Nd:YAG laser. The full width at half maximum pulse length Δt, the pulse energy, the repetition rate and the $1/e^2$ spot-size were 5 ns, 1.9 μJ, 30 Hz and 1.9 mm^2 respectively. PL decay traces at emission wavelengths of 981 nm and 1535 nm were obtained using a photomultiplier tube. Unless otherwise stated the PL decay traces were recorded with a time resolution of 80 ns. The maximum time resolution in the PL decay measurements was ~ 27 ns most likely due to pulse timing jitter. In all measurements the samples were scanned to minimize the possibility of light-induced changes to the optical properties of the samples upon exposure to UV light.[12] Further details on the experimental procedures can be found in Chapter 2 [Ref. 7] and Chapter 3 [Ref. 8].

4.3 Results and Discussion

Figure 4.1 shows the PL spectrum in the region 500 - 1700 nm. The spectrum shows four emission bands: a broad emission band peaking around ~ 600 nm corresponding to the emission

from Si-excess-related LCs in the Si-rich SiO_2 matrix[15, 16] two narrow bands peaking at 981 nm and 1535 nm corresponding to the transition from respectively the second ($^4I_{11/2}$) and first ($^4I_{13/2}$) excited state of the Er^{3+} ions to the ground state ($^4I_{15/2}$), and a weak emission peak at 1128 nm, most likely due to radiative exciton recombination in the Si substrate. At this pump power no Er-related PL signal could be detected during either continuous wave (CW) or pulsed excitation from a reference sample containing a similar concentration of Er (0.49 at.%) but no excess Si.

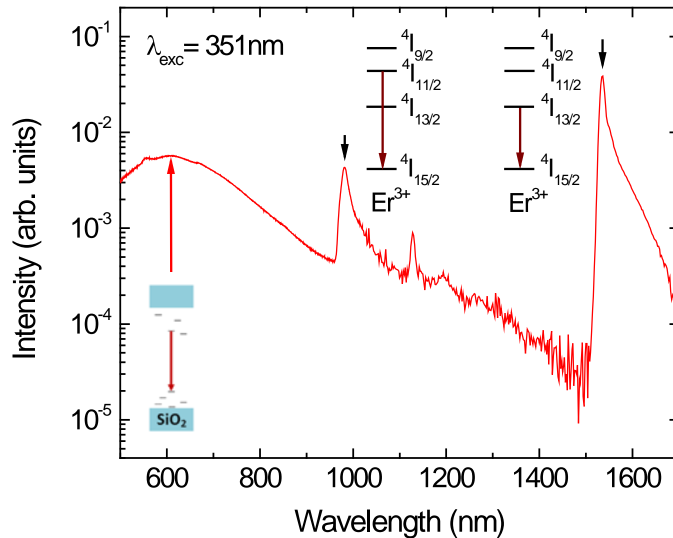

Figure 4.1. (Color) Photoluminescence spectrum of low-temperature-annealed Er-doped Si-rich SiO_2 measured at 15K. Emission from luminescence centers and Er^{3+} ions is indicated schematically on energy diagrams.

This demonstrates that the observed Er^{3+} emission is predominantly excited indirectly via a Si-excess-related mechanism. Power-dependent CW and pulsed PL measurements (not shown) indicated that second order processes such as co-operative upconversion and excited state absorption do not significantly contribute to the observed 981 nm emission in these experiments.

Figure 4.2 shows the PL decay trace detected at 981 nm under pulsed excitation. The signal shows a sharp initial peak, followed by a much slower multi-exponential decay. The decay after the initial peak was fitted with a stretched exponential function of the form $I_3(t) = I_3(0)\times\exp(-(t/\tau_3)^{\beta_3})$, with a decay time $\tau_3 = 2.38 \pm 0.07$ μs and dispersion factor $\beta_3 = 0.79 \pm 0.01$ (dashed line).

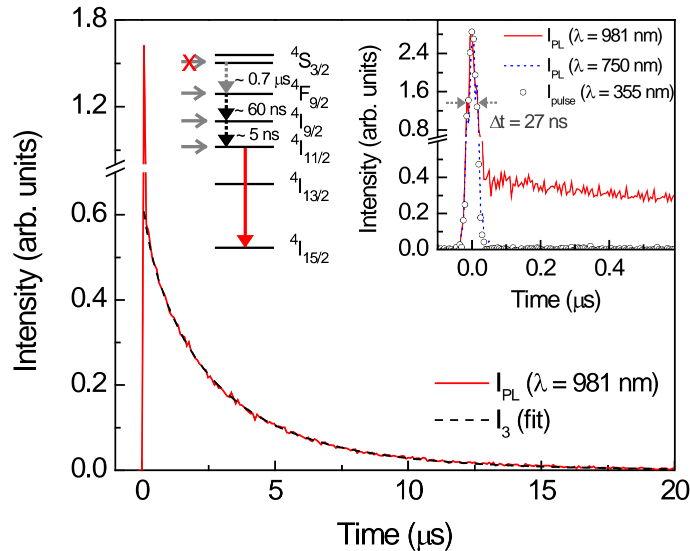

Figure 4.2. (Color) Time-dependent photoluminescence intensity at 981 nm under pulsed excitation (I_{PL}, solid line) with the corresponding fit (I_3, dashed line). The Er^{3+} level diagram indicates possible excitation pathways and typical multi-phonon relaxation times. Inset: Er^{3+} emission at 981 nm (I_{PL}, solid line), the LC emission at 750 nm (I_{PL}, dotted line) and the pump pulse (I_{pulse}, open circles) scaled to the same maximum value.

The inset of Fig. 4.2 shows the same signal measured with a detection resolution of 5 ns as well as the laser pulse shape (open circles, $\Delta t \approx 27$ ns) and the LC emission at 750 nm (dotted line) scaled to the same peak value. The LC emission can be seen to have a lifetime < 27 ns. The initial peak detected at 981 nm exhibits the same jitter-limited length of 27 ns, and is attributed to

background emission from LCs at 981 nm (see Fig.4.1). At this same wavelength scattered laser light was estimated to contribute less than ~ 2 % to the total signal.

The absence of a resolvable Er^{3+} signal rise after the excitation pulse in Fig. 4.2 demonstrates that the energy transfer time of the fast excitation process of Er^{3+} into the second excited state τ_{tr} is shorter than ~ 27 ns. Based on this observation, possible excitation channels leading to the 981 nm emission include excitation by LCs directly into the Er^{3+} $^4I_{11/2}$ level, or excitation into higher lying Er^{3+} levels followed by internal relaxation of the Er^{3+} ion on a time scale of < 27 ns. The Er^{3+} energy level diagram in Fig. 4.2 lists typical room-temperature non-radiative relaxation times for Er^{3+} in glass hosts.[17] Taking into account the predominantly multiphonon nature of the relaxation, the relaxation times at 15K are expected to be longer than the listed values.[18] Of the shown relaxation paths, only the $^4S_{3/2} \rightarrow {}^4F_{9/2}$ relaxation is significantly slower than 27 ns. We therefore conclude that the most likely excitation paths of the 981 nm emission are LC-mediated excitation either directly into the $^4I_{11/2}$ level, or into the $^4I_{9/2}$ or $^4F_{9/2}$ levels followed by rapid relaxation to the $^4I_{11/2}$ level.

Figure 4.3 shows the PL decay trace taken at 1535 nm. The signal shows a fast rise followed by a slow decay. The inset of Fig. 4.3 shows the signal in the first 27 μs after excitation. Two different excitation processes can be distinguished: fast excitation (< 27 ns) resulting in the rise of the signal up to ~ 80% of its maximum value, and slow excitation taking place on the time scale of ~ 2 – 3 μs. Reference measurements taken at wavelengths in the range 1200 - 1500 nm (not shown) revealed only the resolution-limited initial peak, but no slow rise and decay. This demonstrates that all emission at 1535 nm observed after the initial peak is due to Er^{3+} emission from the first excited state. The similarity between the decay time of the second

excited state (~ 2.38 μs) and the duration of the slow excitation of the first excited state (~ 2 - 3 μs) suggests that the slow excitation results from internal relaxation of the Er^{3+} ion from the $^4I_{11/2}$ to the $^4I_{13/2}$ level.

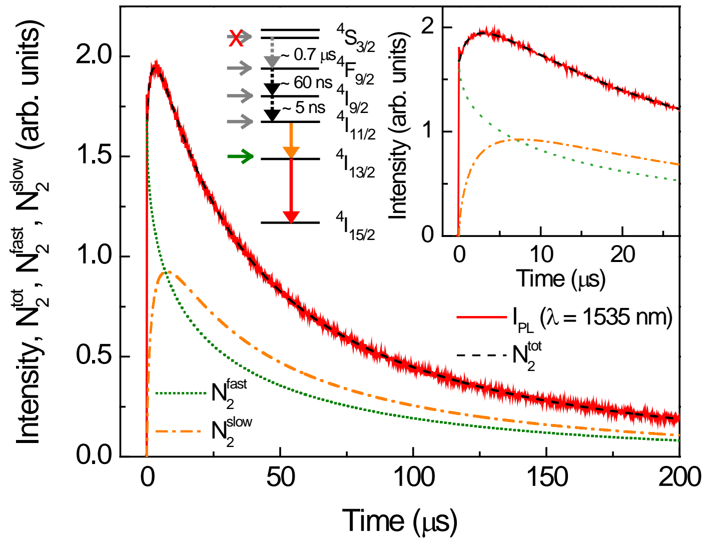

Figure 4.3. (Color) Time-dependent photoluminescence intensity at 1535 nm under pulsed excitation (I_{PL}, solid line) with the corresponding fit (N_2^{tot}, dashed line), including the individual time-dependent contributions due to excitation by the fast (N_2^{fast}) and slow (N_2^{slow}) mechanisms. The Er^{3+} level diagram indicates possible excitation pathways. The inset shows the same data in the range 0 – 27 μs.

Based on the experimental observations, it appears that the time-dependent emission from the first excited state (and thus its total population N_2^{tot}(t)) contains two contributions: emission from Er^{3+} ions excited into the first excited state via a fast excitation mechanism (N_2^{fast}) and emission from Er^{3+} ions excited via a slow excitation mechanism (N_2^{slow}) due to the relaxation of Er^{3+} ions from the second excited state (characterized by the population N_3) to the first excited state. The time dependent populations are described by the following rate equations:

$$\frac{dN_3(t)}{dt} = -\frac{N_3(t)}{\tau_3}$$
$$\frac{dN_2^{slow}(t)}{dt} = \frac{N_3(t)}{\tau_{32}} - \frac{N_2^{slow}(t)}{\tau_2} \tag{4.1}$$
$$\frac{dN_2^{fast}(t)}{dt} = -\frac{N_2^{fast}(t)}{\tau_2}$$

where τ_2 is the decay time of first excited state and τ_{32} is the relaxation time from the second to the first excited state. These equations lead to the following time-dependent total intensity I_2^{tot} of the ${}^4I_{13/2} \rightarrow {}^4I_{15/2}$ transition:

$$I_2^{tot}(t) \propto N_2^{fast}(0) e^{-(\frac{t}{\tau_2})^{\beta_2}} + \frac{N_3(0)}{\tau_{32}(\tau_3^{-1} - \tau_2^{-1})} \left[e^{-(\frac{t}{\tau_2})^{\beta_2}} - e^{-(\frac{t}{\tau_3})^{\beta_3}} \right] \tag{4.2}$$

where the dispersion factors β_2 and β_3 have been added to account for the multi-exponentiality of the decay. Setting both dispersion factors to 1 reduces Eq. 4.2 to the analytical solution of Eqs. 4.1. Fitting the trace measured at 1535 nm with Eq. 4.2 yields the following parameter values: $\tau_2 = 20.7 \pm 1.9$ μs, $N_3(0)/(\tau_{32} N_2^{fast}(0)) = (4.93 \pm 0.52) \times 10^5$ s^{-1}, $\tau_3 = 2.33 \pm 0.05$ μs, $\beta_2 = 0.49 \pm 0.01$, and $\beta_3 = 0.63 \pm 0.02$. The corresponding fit to the experimental trace and the respective time-dependent contributions to the population of the first excited state N_2^{fast} and N_2^{slow} are included in Fig.4.3. The decay time $\tau_3 = 2.33$ μs found from this fit and the value $\tau_3 = 2.38$ μs found independently in Fig. 4.2 are equal within the experimental error. This observation provides strong support for the attribution of the slow excitation process to internal

$^4I_{11/2} \rightarrow {}^4I_{13/2}$ relaxation, and not to a slow LC-mediated excitation process. Taking into account that $\tau_3^{-1} = \tau_{31}^{-1} + \tau_{32}^{-1}$ with τ_{31}^{-1} the relaxation rate from level $^4I_{11/2}$ to the ground state, we find that the relaxation time τ_{32} is longer than 2.3 μs. Time-integration of the functions N_2^{fast} and N_2^{slow} yields a quantity proportional to the number of Er^{3+} ions excited into the first excited state via the two excitation mechanisms. Performing this integration shows that ~ 45 - 50 % of the optically active sensitized Er^{3+} ions are excited directly into the $^4I_{13/2}$ level by LCs, while ~ 50 - 55 % are excited into the $^4I_{13/2}$ after LC-mediated excitation of the $^4I_{11/2}$ level followed by internal relaxation of the Er^{3+} ions. Note that the apparent direct excitation into the $^4I_{13/2}$ could result from excitation into higher lying levels followed by internal relaxation on a time scale that exceeds our temporal resolution. The presence of a large contribution of excitation via the $^4I_{11/2}$ level implies that the inter-level relaxation rate τ_{32}^{-1} will have a significant effect on the maximum net LC-mediated excitation rate of the $^4I_{13/2}$ level.

4.4 Conclusions

In summary, the mechanism of Er^{3+} excitation in low temperature annealed Er-doped Si-rich SiO_2 was studied. Er^{3+} excitation by luminescence centers appears to occur directly into the $^4I_{13/2}$ level, as well as into higher lying levels, with a typical time constant < 27 ns. The presence of such a multilevel sensitization results in two types of excitation of the $^4I_{13/2}$ level of Er^{3+}: fast direct excitation (τ_{tr} < 27 ns) by the LCs, and slow excitation due to the fast excitation of Er^{3+} ions into the higher energy levels with subsequent relaxation to the first excited state with a time

constant $\tau_{32} > 2.3$ μs. It is shown that an approximately equal percentage of Er^{3+} ions are excited into the $^4I_{13/2}$ level by the fast (45 – 50 %) and slow (50 – 55%) processes.

4.5 References

[1] M. Lipson, J. Lightwave Technol. **23**, 4222 (2005).

[2] T. J. Kippenberg, J. Kalkman, A. Polman, and K. J. Vahala, Phys. Rev. A **74**, 051802 (2006).

[3] Q. Lin, T. J. Johnson, R. Perahia, C. P. Michael, and O. J. Painter, Optics Express, **16**, 10596 (2008).

[4] M. Makarova, V. Sih, J. Warga, R. Li, L. Dal Negro, and J. Vuckovic, Appl. Phys. Lett. **92**, 161107 (2008).

[5] M. Fujii, M. Yoshida, and Y. Kanzawa, S. Hayashi and K. Yamamoto, Appl. Phys. Lett. **71**, 1198 (1997).

[6] H.-S. Han, S.-Y. Seo, and J. H. Shin, Appl. Phys. Lett. **79**, 4568 (2001).

[7] O. Savchyn, F. R. Ruhge, P. G. Kik, R. M. Todi, K. R. Coffey, H. Nukala, and H. Heinrich, Phys. Rev. B **76**, 195419 (2007).

[8] O. Savchyn, P. G. Kik, R. M. Todi, and K. R. Coffey, Phys. Rev. B **77**, 205438 (2008).

[9] P. G. Kik and A. Polman, J. Appl. Phys. **91**, 534 (2002).

[10] R. D. Kekatpure and M. L. Brongersma, Nano Lett. **8**, 3787 (2008).

[11] D. Navarro-Urrios, A. Pitanti, N. Daldosso, F. Gourbilleau, R. Rizk, G.Pucker, and L. Pavesi, Appl. Phys. Lett. **92**, 051101 (2008).

[12] R. D. Kekatpure and M. L. Brongersma, Phys. Rev. A **78**, 023829 (2008).

[13] G. Franzó, S. Boninelli, D. Pacifici, F. Priolo, F. Iacona, and C. Bongiorno, Appl. Phys. Lett. **82**, 3871 (2003).

[14] S. Godefroo, M. Hayne, M. Jivanescu, A. Stesmans, M. Zacharias, O. I. Lebedev, G. Van Tendeloo, and V. V. Moshchalkov, Nat. Nanotechnol. **3**, 174 (2008).

[15] M. Zhu, Y. Han, R. B. Wehrspohn, C. Godet, and R. Etemadi, J. Appl. Phys. **83**, 5386 (1998).

[16] A. J. Kenyon, P. F. Trwoga, and C. W. Pitt, and G. Rehm, J. Appl. Phys. **79**, 9291 (1996).

[17] E. Desurvire, C. R. Giles, and J. R. Simpson, J. Lightwave Technol. **7**, 2095 (1989).

[18] C. B. Layne, W. H. Lowdermilk, and M. J. Weber, Phys. Rev. B 16, 10 (1977).

CHAPTER 5. OBSERVATION OF TEMPERATURE-INDEPENDENT INTERNAL Er^{3+} RELAXATION EFFICIENCY IN Si-RICH SiO_2 FILMS

(Based on work published in Applied Physics Letters **94**, 241115 (2009))

Time-dependent photoluminescence measurements of low-temperature-annealed Er-doped Si-rich SiO_2 were conducted at sample temperatures 15 – 300K. The erbium internal relaxation efficiency from the second ($^4I_{11/2}$) to the first ($^4I_{13/2}$) excited state upon luminescence-center-mediated Er^{3+} excitation is investigated. Despite the observation of temperature-dependent relaxation rates, the erbium internal relaxation efficiency is found to be remarkably temperature-independent, which suggests that the internal relaxation efficiency is near-unity. Internal relaxation is shown to account for 50 - 55% of the $^4I_{13/2}$ excitation events in the entire temperature range. These results demonstrate that high pump efficiency and stable operation of devices based on this material will be possible under varying thermal conditions.

5.1 Introduction

Currently a significant amount of work is dedicated to the realization of a silicon-based light source for optical on-chip interconnects.[1-5] The discovery of luminescence-center-mediated sensitization of Er^{3+} in Si-rich SiO_2 as discussed in Chapter 2 [Ref. 6] and Chapter 3 [Ref. 7] and the presence of Er^{3+} sensitization even in samples containing excess silicon but no Si nanocrystals (NCs)[6, 7, 8] opens up new opportunities to achieve this goal. The use of Er-doped Si-

rich SiO_2 without Si NCs could potentially overcome several challenges, including free carrier absorption,[9, 10] NC-related scattering losses[11] and the low density of sensitized Er^{3+} ions[6] inherent to Er-doped Si-rich SiO_2 with Si NCs. In Chapter 4 [Ref. 12] we demonstrated that the excitation of Er^{3+} in Si-rich SiO_2 without Si NCs likely occurs not only into higher energy levels but also directly into the first excited state ($^4I_{13/2}$). As a result, the first excited state of Er^{3+} is populated via two channels: through direct excitation by Si-related luminescence centers (LC), and through LC-related excitation into higher lying levels followed by internal relaxation of the Er^{3+} ions to the first excited state. As was demonstrated in Chapter 4 [Ref. 12] these two excitation pathways account for an approximately equal number of excitation events at T=15K. For room temperature operation of devices based on this material, it is crucial to understand the temperature-dependent contribution of these two excitation channels. In the current study we monitor temperature-dependent excitation and relaxation rates to obtain information on the internal relaxation efficiency of Er^{3+} and its effect on the net Er^{3+} excitation as a function of temperature, and demonstrate that the internal relaxation remains an efficient excitation channel up to room temperature.

5.2 Experimental Techniques

Er-doped Si-rich SiO_2 films containing 12 at. % excess Si and 0.63 at. % of Er were prepared by magnetron co-sputtering onto a Si substrate. The samples were annealed for 100 seconds in N_2 at 600°C or 1100°C (labeled LTA and HTA respectively for Low and High Temperature Anneal) and subsequently passivated for 30 minutes in forming gas (N_2:H_2 = 95%:5%) at 500°C. No Si

aggregates could be detected in transmission electron microscopy measurements on LTA samples, while measurements on HTA samples clearly showed the presence of NCs [Chapter 2 [Ref. 6]]. Optical measurements were performed in a closed-loop He cryostat in the temperature range 15 - 300K. Photoluminescence (PL) spectra were taken under 351 nm excitation with a Kr-ion laser (pump irradiance 1.40 W/cm^2). The PL spectra were corrected for the system spectral response. The time-dependent PL signal was measured either under modulated continuous wave (cw) pumping using the excitation parameters described above, or using pulsed excitation with the 355 nm line of a Nd:YAG (neodymium doped yttrium aluminum garnet) laser with a pulse width of 5 ns and a pulse energy of 1.9 μJ. The excitation and detection conditions were held constant during all measurements. All measured PL parameters have an experimental error smaller than ± 5%. A more detailed description of the experimental procedures can be found in Chapter 2 [Ref. 6], Chapter 3 [Ref. 7] and Chapter 4 [Ref. 12].

5.3 Results and Discussion

The PL spectra of the LTA sample shown in Fig.5.1 (a) exhibit 4 emission bands: a band peaking at ~ 600 nm corresponding to the emission from silicon-excess-related LCs,[13] a band peaking at 1128 nm most likely corresponding to radiative exciton recombination in the Si substrate, and two Er-related emission bands at 981 nm and 1535 nm corresponding to the transitions $^4I_{11/2} \rightarrow {}^4I_{15/2}$ and $^4I_{13/2} \rightarrow {}^4I_{15/2}$ respectively. The PL spectra of the HTA sample shown in Fig. 5.1 (b) exhibit three emission bands: a broad emission band peaking at ~ 750 nm typically attributed to emission from Si NCs formed in the Si-rich SiO_2 matrix, and the two Er-related emission bands

that were also observed in the LTA sample. In both samples the Er-related emission at 1535 nm shows pronounced spectral broadening with increasing temperature due to the temperature-dependent redistribution of the excited states over the Stark-split $^4I_{13/2}$ level. No Er^{3+} emission could be detected in samples containing a similar Er concentration (0.49 at.%) but no Si excess under cw or pulsed excitation. This clearly demonstrates that the excitation of Er^{3+} in the LTA and HTA samples is predominantly indirect and Si-excess-related. To ensure similar excitation conditions the measurements under both cw and pulsed excitation were taken at sufficiently low pump power to avoid significant signal saturation.

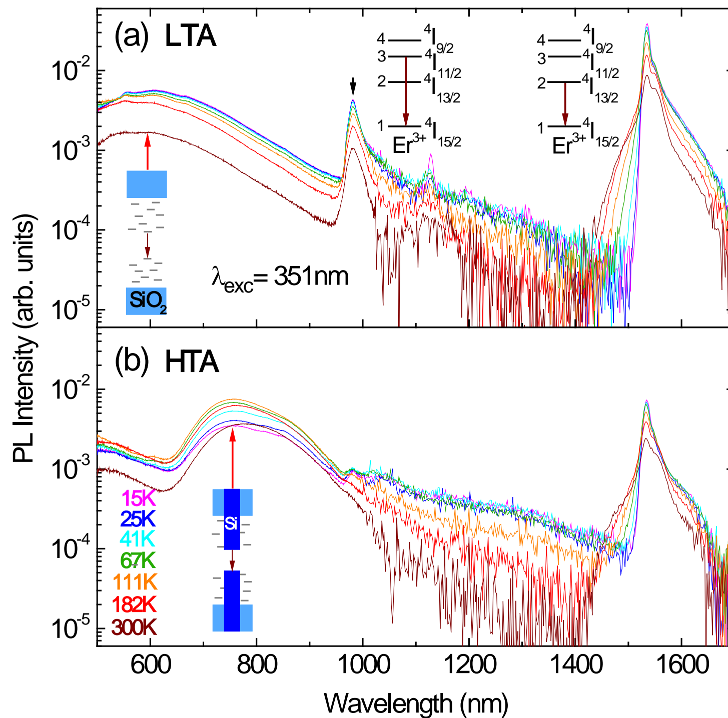

Figure 5.1. (Color) Temperature-dependent photoluminescence spectra of Er-doped Si-rich SiO_2 annealed at 600°C (LTA) (a) and at 1100°C (HTA) (b). The corresponding optical transitions are schematically indicated.

Power-dependent cw and pulsed measurements (not shown) demonstrated that second order processes (cooperative upconversion, excited state absorption) are insignificant under the pump powers used in the current study.

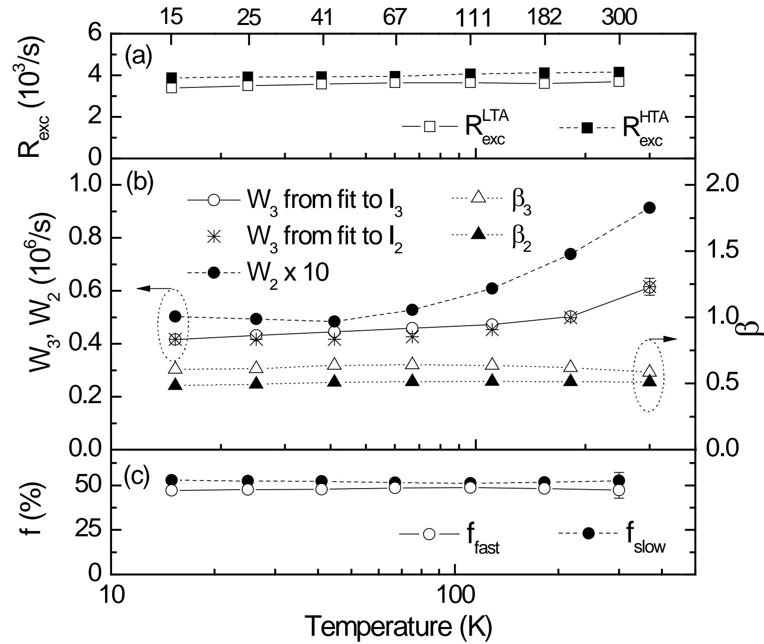

Figure 5.2. Temperature dependence of (a) the Er^{3+} first excited state excitation rate in LTA (R_{exc}^{LTA}) and HTA (R_{exc}^{HTA}) samples, (b) the Er^{3+} second excited state relaxation rate (W_3) found from the time-dependent intensities at 981 nm (I_3) and 1535 nm (I_2), the first excited state relaxation rate (W_2), and the dispersion factors corresponding to the relaxation from the first (β_2) and second (β_3) excited states, (c) the relative fractions of the first excited state excitation events due to the fast (f_{fast}) and slow (f_{slow}) excitation processes**.**

Based on lifetime measurements at 1535 nm under modulated CW excitation (not shown) the excitation rate of the first excited state of Er^{3+} (R_{exc}) in LTA and HTA samples was determined using the well-known relation $R_{exc} = \tau_{rise}^{-1} - \tau_{dec}^{-1}$ where τ_{rise} and τ_{dec} are respectively the rise and decay times of the emission. The results are shown in Fig. 5.2 (a). Note that despite the significant difference in the stoichiometry of the LTA and HTA samples, the observed

excitation rates are similar in value and are both virtually temperature-independent. This provides further evidence for a similar origin of Er^{3+} sensitization in these different samples.

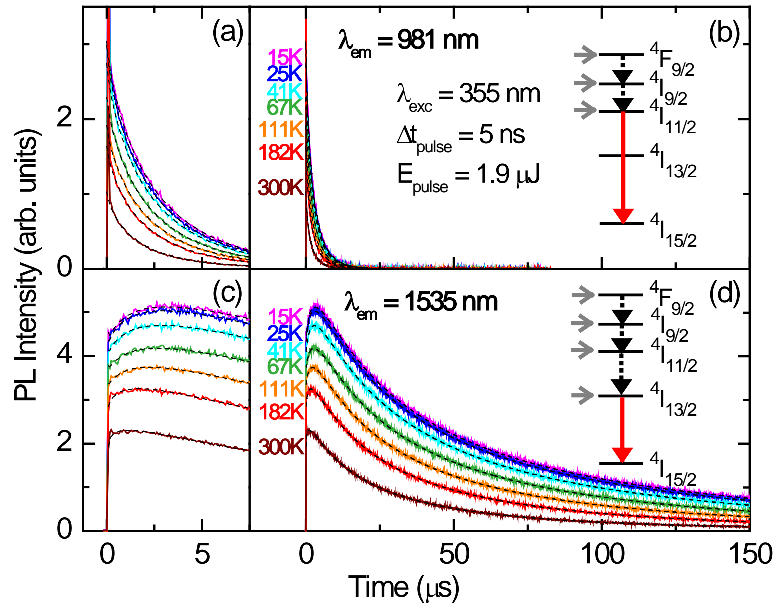

Figure 5.3. (Color) Time-dependent Er^{3+} PL intensity at 981 nm [(a) and (b)] and at 1535 nm [(c) and (d)] under pulsed excitation at 355 nm (solid lines) with the corresponding fits (dashed lines). All intensities are shown on the same relative scale. Contributing excitation channels are schematically indicated by the horizontal and dashed vertical arrows. The relevant optical transitions are indicated by the solid vertical arrows.

Figure 5.3 (a, b) shows the time-dependent PL intensity at 981 nm in the LTA sample taken under pulsed excitation at 355 nm. The excitation of the second excited state was found to take place on a time scale < 27 ns at all temperatures. The relaxation from the second excited state of Er^{3+} ($^4I_{11/2}$) was found to exhibit multi-exponential behavior. The 1/e decay times τ_3 were obtained by fitting the measured decay traces with the function $I_3(t) = I_3(0)\times\exp(-(t/\tau_3)^{\beta_3})$. All decay traces exhibited a temperature-independent value of $\beta_3 = 0.79$ +/- 0.01. The corresponding

decay rate of the second excited state of Er^{3+} in the LTA sample $W_3=1/\tau_3$ is shown in Fig. 5.2 (b) and demonstrates a gradual increase by a factor of ~ 1.5 as the temperature is increased from 15K to 300 K.

Figure 5.3 (c, d) shows the time-dependent PL intensity at 1535 nm in the LTA sample taken under pulsed excitation. As discussed in detail in Chapter 4 [Ref. 12], the shape of these traces results from the presence of two distinct sensitization mechanisms: a fast excitation process taking place on a timescale < 27 ns due to excitation of Er^{3+} by LCs apparently directly into the first excited state, and a slow excitation process taking place on a timescale of several μs due to the LC-mediated excitation of Er^{3+} into higher energy levels followed by relatively slow relaxation to the first excited state. The short time constant (< 27 ns) of the fast excitation of both the first and second excited states at all considered temperatures suggests a similar origin of the fast excitation of both states. The experimental decay traces are characterized by the function:[12]

$$I_2(t) \propto N_2^{fast}(0) e^{-(\frac{t}{\tau_2})^{\beta_2}} + \frac{N_3(0)}{\tau_{32}(\tau_3^{-1} - \tau_2^{-1})} \left[e^{-(\frac{t}{\tau_2})^{\beta_2}} - e^{-(\frac{t}{\tau_3})^{\beta_3}} \right] \tag{5.1}$$

where $N_2^{fast}(0)$ and $N_3(0)$ are the densities of the Er^{3+} ions excited by the fast process into the first excited state and into higher excited states respectively, τ_2, β_2 and τ_3, β_3 are the decay times and the dispersion factors respectively of the first and second excited states and τ_{32} is the relaxation time from the second to the first excited state of Er^{3+}. The thus obtained $W_3=1/\tau_3$ values are in excellent agreement with the corresponding decay rates acquired from the fit to the time-dependent 981 nm emission (Fig. 5.2 (b)), strongly supporting the presented model. The decay rate of the first excited state ($W_2=1/\tau_2$) of the LTA sample is included in Fig. 5.2 (b) and shows a

similar to W_3 increase by a factor of ~ 1.9. The values of the dispersion factors β_2 and β_3 describe the observed multi-exponential decay, which is likely caused by the presence of Er^{3+} ions with different decay rates. The obtained dispersion factors are shown in Fig. 5.2 (b), and can be seen to be relatively constant, suggesting that temperature affects all Er^{3+} ions responsible for the emission in a similar manner.

The relaxation rate W_3 is commonly assumed to be dominated by multiphonon relaxation from the second to the first excited state, with the energy difference bridged predominantly by high energy phonons[14] with energies of ~ 130-150 meV in the case of SiO_2.[15, 16] However using the well-known expression for the multiphonon relaxation rate,[14] the temperature dependence of W_3 could not be accurately described. This suggests that a non-phonon related temperature-dependent nonradiative decay channel is present. This assumption is supported by the room-temperature relaxation rate of $W_3 = 6.2 \times 10^5$ s^{-1} which is much larger than both the room temperature multiphonon rate of ~ 1×10^5 s^{-1} [Ref. 14] and the typical radiative rate of ~ 100 – 130 s^{-1} [Ref. 17] of the second excited state of Er^{3+} in silicate glasses. Note that the first excited state decay rate W_2 which is known to be approximately temperature-independent in SiO_2 [17] also increases by a factor ~ 1.9 in this temperature range. Both observations are likely due to the presence of nonradiative relaxation through coupling with low-energy electronic transitions in this low-temperature processed Si-doped oxide. This suggests that the technical implementation of this material requires thermal processing that minimizes the presence of electronic defects, while avoiding the formation of extended Si nanocrystals.

The temperature dependence of the fractions of Er^{3+} ions excited into the first excited state via the fast (f_{fast}) and slow (f_{slow}) process respectively found from the time integration of the

first and second terms in Eq. 5.1 [Chapter 4 [Ref. 12]] is shown in Fig. 5.2 (c). Surprisingly, for all temperatures the fast and slow excitation mechanisms are responsible for 45 - 50% and 50-55% respectively of the excitation events into the first excited state. Assuming that the fast excitation of the first and second excited state have the same temperature dependence, the observed temperature-independent contribution of each of the excitation pathways of the first excited state suggests that the relaxation efficiency from the second to the first excited state of Er^{3+} (η_{32}) does not change significantly with temperature. However, the total relaxation rate from the second excited state (W_3) *does* vary with temperature by a factor of ~ 1.5, increasing from 4.2×10^5 s^{-1} at 15K to 6.2×10^5 s^{-1} at room temperature (Fig. 5.2 (b)). Since $W_3 = W_{32} + W_{31}$ where $W_{32} = 1/\tau_{32}$ is the relaxation rate from the second to the first excited state and W_{31} is the relaxation rate from the second excited state to the ground state, this increase of W_3 indicates that at least one of the two contributing relaxation rates W_{32} and W_{31} increases with temperature. This in turn would lead to a temperature-dependent relaxation quantum efficiency from the second to the first excited state given by $\eta_{32} = W_{32}/W_3 = (1+W_{31}/W_{32})^{-1}$, which would be accompanied by a change of the excitation rate of the first excited state (R_{exc}), and a change of the relative fraction of Er^{3+} ions excited into the first excited state by the slow excitation mechanism (f_{slow}). Based on the fact that neither of these changes are observed we conclude that the relaxation efficiency is temperature independent. The temperature independent relaxation efficiency can be explained by assuming a relatively slow relaxation from the second excited state to the ground state ($W_{31} << W_{32}$ and thus $W_3 = W_{32} + W_{31} \approx W_{32}$) resulting in $W_{31}/W_{32} << 1$. Under this assumption and realizing that $\eta_{32} = W_{32}/W_3 = (1+W_{31}/W_{32})^{-1}$ we find $\eta_{32} \approx 1$. Alternatively the temperature independent relaxation efficiency could be explained by assuming an identical temperature

dependence of W_{32} and W_{31}. This scenario is considered unlikely due to the significantly different energy of the $^4I_{11/2} \rightarrow {}^4I_{15/2}$ and $^4I_{11/2} \rightarrow {}^4I_{13/2}$ transitions (1.26 eV and 0.45 eV respectively). The latter transition is expected to be more strongly influenced by changes in the multi-phonon relaxation contribution,[14] which would lead to a different temperature dependence of the two rates. Based on these considerations it seems most likely that the decay from the second excited state is dominated by the relaxation to the first excited state ($W_3 \approx W_{32}$), suggesting that the relaxation efficiency η_{32} in this material is near-unity. The observation of high internal relaxation efficiency suggests that high pump efficiency can be achieved in low temperature processed gain media relying on Si-based sensitization of Er^{3+}. Additionally, the observed temperature independence of the relaxation efficiency predicts that stable operation of devices based on this material can be achieved in a wide temperature range.

5.4 Conclusions

In summary, luminescence-center-mediated Er^{3+} excitation is shown to occurs with near-equal probability through direct excitation into the first excited state (45 - 50%), and through excitation into higher levels followed by relaxation to the first excited state (50 - 55%) in the entire temperature range 15 – 300K. The observation of a temperature-independent Er^{3+} excitation rate and a temperature-independent fraction of Er^{3+} excitation events occurring via the second excited state, combined with the observed increasing second excited state relaxation rate suggests a constant near-unity relaxation efficiency from the second to the first excited state of Er^{3+} in low-temperature-annealed Er-doped Si-rich SiO_2 in this temperature range. These results indicate that

high pump efficiency and stable room temperature operation of devices based on this material is possible.

5.5 References

[1] M. Lipson, J. Lightwave Technol. **23**, 4222 (2005).

[2] M. Makarova, V. Sih, J. Warga, R. Li, L. Dal Negro, and J. Vuckovic, Appl. Phys. Lett. **92**, 161107 (2008).

[3] L. Dal Negro, R. Li, J. Warga, and S. N. Basu, Appl. Phys. Lett. **92**, 181105 (2008).

[4] Q. Lin, T. J. Johnson, R. Perahia, C. P. Michael, and O. J. Painter, Opt. Express **16**, 10596 (2008).

[5] T. J. Kippenberg, J. Kalkman, A. Polman, and K. J. Vahala, Phys. Rev. A **74**, 051802 (2006).

[6] O. Savchyn, F. R. Ruhge, P. G. Kik, R. M. Todi, K. R. Coffey, H. Nukala, and H. Heinrich, Phys. Rev. B **76**, 195419 (2007).

[7] O. Savchyn, P. G. Kik, R. M. Todi, and K. R. Coffey, Phys. Rev. B **77**, 205438 (2008).

[8] G. Franzò, S. Boninelli, D. Pacifici, F. Priolo, F. Iacona, and C. Bongiorno, Appl. Phys. Lett. **82**, 3871 (2003).

[9] D. Navarro-Urrios, A. Pitanti, N. Daldosso, F. Gourbilleau, R. Rizk, G. Pucker, and L. Pavesi, Appl. Phys. Lett. **92**, 051101 (2008).

[10] R. D. Kekatpure and M. L. Brongersma, Nano Lett. **8**, 3787 (2008).

[11] R. D. Kekatpure and M. L. Brongersma, Phys. Rev. A **78**, 023829 (2008).

[12] O. Savchyn, R. M. Todi, K. R. Coffey, and P. G. Kik, Appl. Phys. Lett. **93**, 233120 (2008).

[13] M. Ya. Valakh, V. A. Yukhimchuk, V. Ya. Bratus, A. A. Konchits, P. L. F. Hemment, and T. Komoda, J. Appl. Phys. **85**, 168 (1999).

[14] C. B. Layne, W. H. Lowdermilk, and M. J. Weber, Phys. Rev. B 16, 10 (1977).

[15] F. L. Galeener and G. Lucovsky, Phys. Rev. Lett. **37**, 1474 (1976).

[16] C. T. Kirk, Phys. Rev. B **38**, 1255 (1988).

[17] E. Desurvire, Erbium-doped fiber amplifiers: principles and applications (A John Wiley & Sons, Inc., Hoboken, New Jersey, 2002), Chapter 4, pp.223-224.

CHAPTER 6. EXCITATION WAVELENGTH-INDEPENDENT SENSITIZED Er^{3+} CONCENTRATION IN AS-DEPOSITED AND LOW TEMPERATURE ANNEALED Si-RICH SiO_2 FILMS

(Based on work published in Applied Physics Letters **95**, 231109 (2009))

Erbium sensitization is observed in as-deposited Er^{3+} doped Si-rich SiO_2, ruling out the involvement of Si nanocrystals in the Er^{3+} excitation in these samples. The Er^{3+} absorption cross-section in this material is similar within a factor 3 to that of samples annealed at 600°C under 355 nm and 532 nm excitation. The density of excitable Er^{3+} ions is shown to be excitation wavelength independent, while the shape of the Er^{3+} excitation spectra is governed by a wavelength-dependent Er^{3+} absorption cross-section. These findings enable the use of a broad range of wavelengths for the efficient excitation of this gain medium.

6.1 Introduction

Among the different approaches to the realization of a Si laser,[1-5] using the emission from Er^{3+} sensitized in Si-rich SiO_2 (SRSO) received significant attention.[6] In Chapter 2 [Ref. 7] and Chapter 3 [Ref. 8] it was shown that luminescence centers (LCs), not Si nanocrystals (NCs), are the dominant Er^{3+} sensitizer in SRSO. The ability to sensitize Er^{3+} without Si NCs has a number of advantages: a higher density of sensitized Er^{3+} ions,[7] a favorable temperature dependence of the Er^{3+} emission,[9] and a possible reduction of confined carrier absorption[10, 11] and scattering.[12]

While as shown in Chapter 2 [Ref. 7] the sensitization of Er^{3+} by LC is highly excitation wavelength (λ_{exc}) dependent, it is not clear if this is due to a wavelength-dependent concentration of sensitizers (and thus excitable Er^{3+} ions) or due to a wavelength-dependent cross-section of the sensitizers. The former would correspond to excitation via an inhomogeneous distribution of LC related levels in the SRSO bandgap leading to a wavelength-dependent number of possible transitions, while the latter would correspond to excitation through LCs with an intrinsic wavelength-dependent absorption cross-section associated with a broad absorption band of each LC. In the present chapter we demonstrate that the density of sensitized Er^{3+} ions is remarkably constant with changing λ_{exc} while the Er^{3+} effective absorption cross-section shows a significant wavelength dependence.

6.2 Experimental Techniques

An Er-doped Si-rich SiO_2 film (thickness 110 nm) containing 12 at. % of excess Si and 0.63 at. % of Er was sputter deposited onto a Si wafer (sample temperature < 40°C). An as-deposited sample and two samples respectively annealed at 600°C and 1100°C (labeled LTA and HTA) for 100 s in flowing N_2 and subsequently passivated for 30 min. in forming gas (N_2:H_2=95%:5%) at 500°C were studied. X-ray photoelectron spectroscopy (XPS) measurements were performed on etched to a thickness of 50 ± 8 nm samples using the Al Kα line (1486.6 eV) of an X-ray source. Photoluminescence (PL) spectra (resolution ~ 10 nm) were taken at room temperature using the 351 nm line of a Kr-ion laser (2.7 W/cm^2). Excitation spectra were taken using Xe-lamp emission filtered through a monochromator. Time-dependent PL measurements

(resolution 80 ns) were done under pulsed excitation using the 355 nm and 532 nm lines of a Nd-doped yttrium aluminum garnet laser (pulse length 5 ns). The laser spot area was determined with an accuracy better than ± 10 %. All spectral PL measurements were done in the linear regime of PL vs. power and corrected for system response. The absence of pump induced sample damage was verified for the highest pump power used. More information on the experimental techniques can be found in Chapter 2 [Ref. 7] and Chapter 4 [Ref. 13].

6.3 Results and Discussion

Figure 6.1 shows the PL spectra of the as-deposited, LTA and HTA samples taken under continuous wave (cw) excitation at 351 nm.

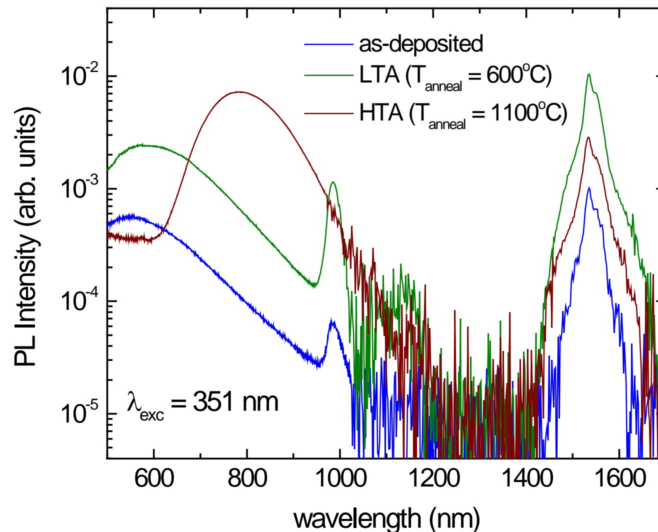

Figure 6.1. (Color) PL spectra of Er-doped SRSO of as-deposited, LTA and HTA samples under cw excitation at 351 nm.

The spectra of as-deposited and LTA samples contain emission bands peaking at ~ 550 nm, 981 nm and 1535 nm corresponding to the emission from the Si-excess-related LCs[14] and Er^{3+} transitions $^4I_{11/2}\rightarrow{}^4I_{15/2}$ and $^4I_{13/2}\rightarrow{}^4I_{15/2}$ respectively. The spectrum of the HTA sample exhibits emission bands peaking at ~ 780 nm and 1535 nm corresponding to the emission from Si NCs and Er^{3+} transition $^4I_{13/2}\rightarrow{}^4I_{15/2}$ respectively. No Er^{3+} emission was observed in the sample containing a similar Er concentration but no silicon excess under cw and pulsed excitation.

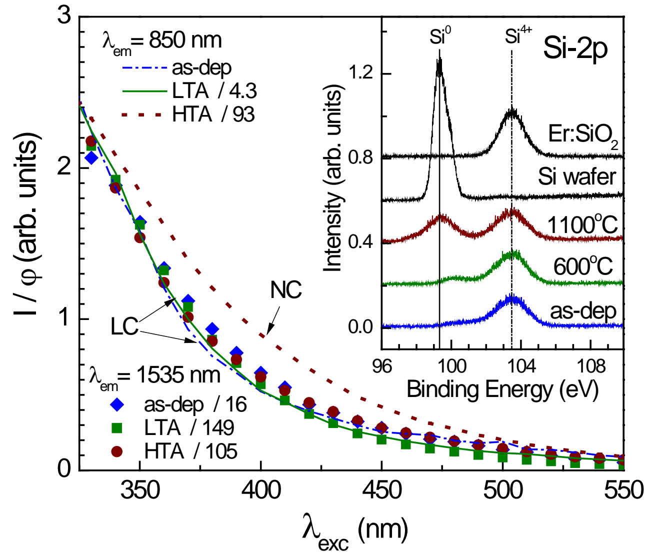

Figure 6.2. (Color) Excitation spectra of Er^{3+} emission at 1535 nm (as-deposited, LTA and HTA samples), LC emission at 850 nm (LTA sample) and Si NCs emission at 850 nm (HTA sample). The corresponding scaling factors are included. Inset: XPS spectra of as-deposited and annealed (600°C and 1100°C) Er-doped SRSO, a Si (100) substrate and a sputtered $Er:SiO_2$ film.

The inset of Fig. 6.2 shows XPS spectra from the Si-2p core level region of Er-doped SRSO films for an as-deposited sample and samples annealed at 600°C and 1100°C as well as reference data from a Si (100) substrate and a co-sputtered unannealed Er-doped SiO_2 film. The

known binding energies (BEs) of Si^0 and Si^{4+} are indicated by the vertical lines. The XPS spectrum of the as-deposited film shows a clear Si^{4+} peak, as well as a small broad shoulder in the BE region where Si^{3+}, Si^{2+} and Si^{+} species are expected (~ 100 - 102 eV).[15] The latter is attributed to the presence of excess Si in the film. In the sample annealed at 600°C no Si^0 signal is observed. The sample annealed at 1100°C does exhibit a clear Si^0 peak, indicative of the nucleation and growth of extended Si inclusions. These results conclusively show that no extended Si aggregates are present in the as-deposited sample and the sample annealed at 600°C.

Figure 6.2 shows the excitation spectra corrected for photon fluence ($I(\lambda_{exc})/\varphi(\lambda_{exc})$, with I the PL intensity and φ (m^{-2}) the pump photon fluence) Er^{3+} PL at 1535 nm in as-deposited, LTA and HTA samples, the LC PL at 850 nm in the as-deposited and LTA samples and the Si NC PL at 850 nm in the HTA sample. The 1535 nm excitation spectra show a gradual increase of the PL intensity for decreasing λ_{exc}. The absence of resonances in the Er^{3+} excitation spectra and their identical behavior confirms that the excitation of Er^{3+} is predominantly indirect and of the same origin in all samples. Furthermore, the similarity between the 1535 nm Er^{3+} excitation spectra and the 850 nm LC PL of the as-deposited and LTA samples strongly suggests that the sensitization is mediated by the LCs, as was previously proposed.[7, 8] Finally, the significantly different spectral shape of the Si NC excitation spectrum of the HTA sample demonstrates that Si NCs are not the dominant source of Er^{3+} excitation in HTA samples.

Figure 6.3 shows the 1535 nm Er^{3+} PL intensity at t=80 ns after the pulse as a function of pump photon fluence per pulse φ (m^{-2}) under 355 nm and 532 nm excitation for the as-deposited and LTA samples, shown on the same relative scale. No significant relaxation at 1535 nm could

be detected on a time scale shorter than ~ 80 ns, and consequently the signal recorded at t = 80 ns is considered to be representative of the Er^{3+} PL intensity immediately after the excitation pulse. Data on the HTA sample are not included due to the presence of a fast background signal at 1535 nm unrelated to Er^{3+}. This fast background was also observed in previous work by independent authors.[16, 17] The exact origin of the background is not known, however its presence only in HTA samples suggests that this component is related to transitions in the Si NC or at the Si NC surface. Figure 6.3 demonstrates the increase and subsequent saturation of the Er^{3+} PL at 1535 nm with increasing photon flux.

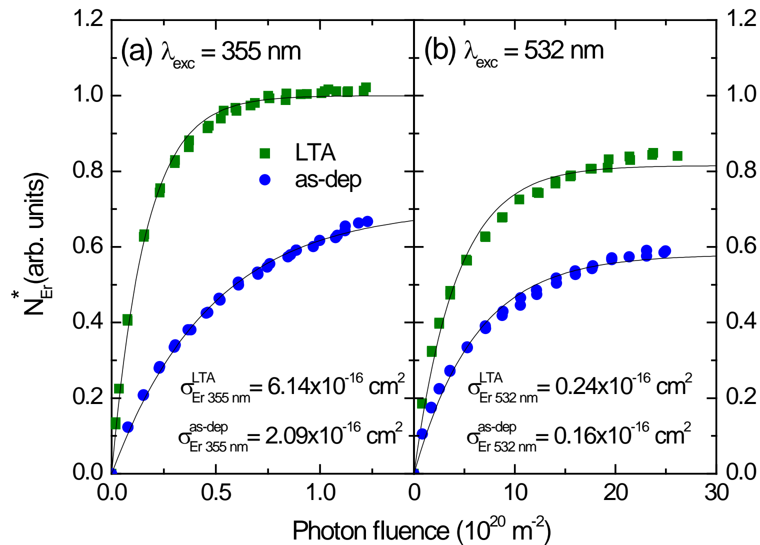

Figure 6.3. (Color) The dependence of the relative density of excited Er^{3+} ions $N_{Er}*$ in LTA (squares) and as-deposited (circles) Er-doped SRSO on pump flux under (a) 355 nm and (b) 532 nm pulsed excitation. The solid lines represent fits to the data.

Assuming that no significant Er^{3+} relaxation takes place during the excitation, the LC-mediated Er^{3+} excitation efficiency is pump fluence independent, and the Er^{3+} radiative rate is

identical in both the samples, the Er^{3+} PL intensity immediately after pulsed excitation is given by

$$I_{Er}(\varphi) \propto N_{Er}^{*} = N_{Er}(1 - e^{-\sigma_{Er}\varphi}) \tag{6.1}$$

with N_{Er}* the density of excited Er^{3+} ions, N_{Er} the density of sensitized Er^{3+} ions, and σ_{Er} the total effective Er^{3+} absorption cross-section. Note that due to the multilevel nature of the Er^{3+} excitation demonstrated in Chapter 4 [Ref. 13] and Chapter 5 [Ref. 18] the value of σ_{Er} represents the sum of the absorption cross-sections of all sensitized Er^{3+} levels due to the fact that the observed saturation results from ground state depletion. The solid lines in Fig. 6.3 represent fits to the measured data using Eq. 6.1, and show good agreement for both λ_{exc} and for both samples.

Table 6.1. Values of σ_{Er} and N_{Er} under pulsed 355 nm and 532 nm excitation for as-deposited and LTA samples

Parameter \ Sample	As deposited	LTA
σ_{Er}*(355 nm),* (10^{-16} cm^2)	2.09±0.22	6.14±0.63
N_{Er}*(355 nm), (arb. units)*	0.70±0.07	1.00±0.10
σ_{Er}*(532 nm),* (10^{-16} cm^2)	0.164±0.018	0.237± 0.025
N_{Er}*(532 nm), (arb. units)*	0.58±0.07	0.82±0.09

Table 6.1 lists the obtained values of σ_{Er} and N_{Er} based on the fits in Fig. 6.3. The value of σ_{Er} at 355 nm in the LTA sample is in agreement with that found from cw measurements in Chapter 3 [Ref. 8]. For both 355 nm and 532 nm excitation the difference in cross-section between the as-deposited and the LTA sample is found to be less than a factor ~ 3. The fact that

similar values of the σ_{Er} are observed in as-deposited, LTA and HTA samples [Chapter 2 [Ref. 7], Chpater 3 [Ref. 8]], combined with the similar Er^{3+} excitation spectra in these samples (Fig. 6.2) provides further evidence that the indirect excitation of Er^{3+} in as-deposited SRSO is the same as in LTA samples and the sample containing Si NCs (HTA).

While the fits in Fig. 6.3 do not provide absolute values for N_{Er}, the relative magnitudes of N_{Er} can be compared. We find that $N_{Er}^{LTA}/N_{Er}^{as\text{-}dep} \approx 1.4$ for both 355 nm and 532 nm excitation. Apparently the 600°C anneal of the LTA sample only slightly increases the density of indirectly excitable Er^{3+} ions. This in turn suggests that the density of Si-excess-related sensitizers present in as-deposited samples is not strongly affected by a low-temperature anneal.

Using the values in Table 6.1 the origin of the wavelength dependent excitation spectra in Fig. 6.2 can be determined. At low power, the excitation spectrum is given by

$$I_{Er}(\lambda_{exc})/\varphi(\lambda_{exc}) \propto \sigma_{Er}(\lambda_{exc}) \times N_{Er}(\lambda_{exc}) \tag{6.2}$$

Note that this relation leaves open the possibility of a wavelength-dependent number of sensitized Er^{3+} ions. Fig. 6.2 shows that $I_{Er}(\lambda_{exc})/\varphi(\lambda_{exc})$ increases by a factor ~ 20 and ~ 32 for as-deposited and LTA samples respectively as λ_{exc} decreases from 532 nm to 355 nm. By comparison, in this same wavelength range the term $\sigma_{Er}(\lambda_{exc}) \times N_{Er}(\lambda_{exc})$ obtained from pulsed measurements increases by a factor ~ 15 and ~ 32 for the as deposited and LTA sample respectively. The good correspondence between these values indicates that we may directly compare the excitation spectra in Fig. 6.2 with the values in Table 6.1 obtained under pulsed excitation. We find that the N_{Er} is approximately independent of λ_{exc} (Table 6.1). It is therefore concluded that the rapid increase in Er^{3+} PL with decreasing λ_{exc} is due predominantly to an

increase of σ_{Er} and thus of the LC absorption cross-section, assuming a fixed number of LCs per Er^{3+} ion.

The fact that the density of indirectly excitable Er^{3+} ions does not change with the λ_{exc} rules out the possibility that the shape of the LC excitation spectrum is related to a varying density of LC levels in the SRSO gap. Instead, we must conclude that the LCs exhibit an increasing optical cross-section as the excitation wavelength is decreased and exhibit a broad absorption band that extends at least from 2.3 eV to 3.5 eV. The fact that all LCs exhibit a similar absorption spectrum while a broad PL spectrum is observed seems to suggest that significant relaxation of the LCs can occur after excitation, leading to homogenous broadening. The absence of resonant features in the LC PL spectra around Er^{3+} transitions seems to indicate that the LC mediated Er^{3+} excitation is non-resonant, however further research is needed to determine the details of the energy transfer mechanism.

6.4 Conclusions

In summary, indirect excitation of Er^{3+} in as-deposited Si-rich SiO_2 has been demonstrated. The observation of similar values of the Er^{3+} effective absorption cross-section and similar excitation spectra in as-deposited samples and samples annealed at 600°C and 1100°C shows that the excitation mechanism is largely independent of annealing treatment. The increase of the Er^{3+} emission intensity at 1535 nm with decreasing excitation wavelength is demonstrated to be predominantly due to an increase of the Er^{3+} effective absorption cross-section rather than due to an increase of the density of sensitized Er^{3+} ions. The demonstrated excitation wavelength

independent density of indirectly excited Er^{3+} ions implies that similar gain could be achieved in amplifiers and lasers based on this material using a broad range of pump wavelengths.

6.5 References

[1] T. J. Kippenberg, J. Kalkman, A. Polman, and K. J. Vahala, Phys. Rev. A **74**, 051802 (2006).

[2] M. Lipson, J. Lightwave Technol. **23**, 4222 (2005).

[3] M. Makarova, V. Sih, J. Warga, R. Li, L. Dal Negro, and J. Vuckovic, Appl. Phys. Lett. **92**, 161107 (2008).

[4] Q. Lin, T. J. Johnson, R. Perahia, C. P. Michael, and O. J. Painter, Opt. Express **16**, 10596 (2008).

[5] L. Dal Negro, R. Li, J. Warga, and S. N. Basu, Appl. Phys. Lett. **92**, 181105 (2008).

[6] M. Fujii, M. Yoshida, Y. Kanzawa, S. Hayashi, and K. Yamamoto, Appl. Phys. Lett. **71**, 1198 (1997).

[7] O. Savchyn, F. R. Ruhge, P. G. Kik, R. M. Todi, K. R. Coffey, H. Nukala, and H. Heinrich, Phys. Rev. B **76**, 195419 (2007).

[8] O. Savchyn, P. G. Kik, R. M. Todi, and K. R. Coffey, Phys. Rev. B **77**, 205438 (2008).

[9] F. Lenz, A. Hryciw, R. DeCorby, and A. Meldrum, Appl. Phys. Lett. **95**, 091909 (2009).

[10] D. Navarro-Urrios, A. Pitanti, N. Daldosso, F. Gourbilleau, R. Rizk, G. Pucker, and L. Pavesi, Appl. Phys. Lett. **92**, 051101 (2008).

[11] R. D. Kekatpure and M. L. Brongersma, Nano Lett. **8**, 3787 (2008).

[12] R. D. Kekatpure and M. L. Brongersma, Phys. Rev. A **78**, 023829 (2008).

[13] O. Savchyn, R. M. Todi, K. R. Coffey, and P. G. Kik, Appl. Phys. Lett. **93**, 233120 (2008).

[14] M. Ya. Valakh, V. A. Yukhimchuk, V. Ya. Bratus, A. A. Konchits, P. L. F. Hemment, and T. Komoda, J. Appl. Phys. **85**, 168 (1999).

[15] N. Koshizaki, H. Umehara, and T. Oyama, Thin Solid Films **325**, 130 (1998).

[16] A. Al Choueiry, A. M. Jurdyc, B. Jacquier, F. Gourbilleau, and R. Rizk, J. Appl. Phys. **106**, 053107 (2009).

[17] D. Navarro-Urrios, A. Pitanti, N. Daldosso, F. Gourbilleau, R. Rizk, B. Garrido, and L. Pavesi, Phys. Rev. B **79**, 193312 (2009).

[18] O. Savchyn, R. M. Todi, K. R. Coffey, and P. G. Kik, Appl. Phys. Lett. **94**, 241115 (2009).

CHAPTER 7. HIGH TEMPERATURE OPTICAL PROPERTIES OF SENSITIZED Er^{3+} IN Si-RICH SiO_2 – IMPLICATIONS FOR GAIN PERFORMANCE

(Based on work published in Optical Materials **32**, 1274 (2010))

The high-temperature photoluminescence of Er-doped Si-rich SiO_2 with and without silicon nanocrystals is studied at sample temperatures in the range 20 – 200°C. The optical properties of Er-doped Si-rich SiO_2 with and without silicon nanocrystals are shown to exhibit a similar temperature dependence. Based on the measured photoluminescence intensities and lifetimes it is predicted that an increase of the sample temperature from 20°C to 200°C results in a decrease of the maximum optical gain at 1535 nm by a factor of ~ 1.8 and ~ 1.6 for samples with and without nanocrystals respectively. Implementation of this material in silicon photonics requires stable operation at typical processor case temperatures up to 80 – 90°C. It is demonstrated that increasing the temperature from room temperature to 90°C leads to a predicted maximum optical gain reduction of ~ 1.26 for both materials. In addition, the predicted erbium related optical gain at significant inversion levels in samples processed at low temperature (600°C) is a factor ~ 9 higher than for samples processed at high temperature (1060°C). These findings demonstrate that relatively thermally stable gain performance of the Er-doped Si-rich SiO_2 up to typical processor operating temperatures is possible and indicate that low-temperature-processed erbium-doped silicon-rich SiO_2 is a technologically viable gain medium for use in silicon photonics.

7.1 Introduction

The implementation of CMOS-compatible photonic devices into integrated circuits is one of the main avenues for increasing the performance of computers.[1-4] In recent years, a number of silicon compatible photonic devices have been demonstrated[5-10] however the realization of a cost efficient on-chip silicon compatible light source remains a challenge. Silicon compatible sources being considered so far are silicon Raman lasers,[11] hybrid evanescent lasers,[12] devices based on germanium-on-silicon,[13] silicon nanocrystal doped SiO_2 [Ref. 14-19], silicon nanocrystal doped silicon nitride,[20] erbium-doped Si-rich silicon nitride,[21] erbium-doped silicon-rich SiO_2 [Ref. 22-29]. In Er-doped Si-rich SiO_2, Er^{3+} ions provide emission at 1.54 μm due to an intra-4f shell transition of Er^{3+} from its first excited state ($^4I_{13/2}$) to the ground state ($^4I_{15/2}$). While the Er^{3+} emission can be quite efficient, efficient excitation of Er^{3+} in SiO_2 is difficult to achieve due to intrinsically narrow absorption lines with low absorption cross-sections. To overcome this challenge, a significant amount of research has focused on sensitization of Er^{3+} ions by adding dopants with strong broadband absorption and efficient energy transfer to Er^{3+} ions. The observation of strong broadband sensitization of Er^{3+} in silicon nanocrystal doped SiO_2 led to the conclusion that Si nanocrystals are promising Er^{3+} sensitizers. Silicon sensitization of Er^{3+} in Si-rich SiO_2 has been shown to result in a dramatic increase (~ 3 – 6 orders of magnitude) of the effective Er^{3+} absorption cross-section as compared to that in stoichiometric SiO_2 films.[29-34] Optical gain [25, 35] and signal enhancement[36] at 1535 nm were demonstrated in waveguides based on this type of material. It should be noted that in these studies gain was achieved in composites containing rather low concentrations of excess silicon. While the presence of excess silicon has been repeatedly shown to produce significant Er^{3+} sensitization, the formation of extended Si

nanocrystals is known to introduce confined carrier absorption[26, 37, 38] and scattering,[39] both of which adversely affect optical gain. It should also be noted that annealing of Er-doped Si-rich SiO_2 at temperatures above 1000°C necessary for silicon nanocrystal formation, results in a significant decrease of the density of optically active Er^{3+} ions,[30] resulting in a significant reduction of the maximum achievable optical gain.

In Chapter 2 [Ref. 30] and Chapter 3 [Ref. 31] we demonstrated that while Si nanocrystals do act as sensitizers, the dominant cause for Er^{3+} sensitization in Si-rich SiO_2 is the presence of silicon-excess related luminescence centers capable of sensitizing Er even in as-deposited Si-rich SiO_2 as was shown in Chapter 6 [Ref. 40]. These results implied that the use of Er-doped Si-rich SiO_2 annealed at low temperatures could provide a significant improvement in the maximum optical gain at 1.54 μm compared to Er^{3+} doped materials containing silicon nanocrystals, due to (i) a higher density of optically active Er^{3+} ions in this material, and (ii) the absence of Si nanocrystal related confined carrier absorption and optical scattering.

In order to evaluate the viability of Er-doped Si-rich SiO_2 as a gain medium in silicon photonics, it is important to consider its performance under realistic operating conditions. One possible approach for combining optical data transfer and processing with present day silicon technology is by incorporating photonic elements on top of the electronic device layer. This approach requires that any on-chip optical components provide reliable and stable performance under exposure to significant temperature variations ranging from room temperature up to maximum processor case temperatures of ~ 80 - 90°C. While several studies have focused on the optical properties of Er-doped Si-rich SiO_2 at cryogenic temperatures,[23, 41-43] little is known about the performance of this material at elevated temperatures. In the present chapter, several key

optical properties directly affecting optical gain are studied in the temperature range 20 – 200°C. Based on the measured temperature dependence of the optical parameters the behavior of the optical gain in the samples with and without silicon nanocrystals is modeled. The results suggest that devices based on Er-doped Si-rich SiO_2 are capable of providing thermally stable gain performance under high temperature operating conditions.

7.2 Experimental Techniques

Er-doped Si-rich SiO_2 films containing 12 at. % excess Si and 0.63 at. % of Er were deposited onto a P-doped Si substrate ((100), resistivity 3 – 7 Ωcm) by magnetron co-sputtering from Si, SiO_2 and SiO_2:Er_2O_3 targets in a multi-gun sputtering system (AJA International, Inc., ATC-2200V). Samples with different microstructure were prepared by annealing the as-deposited films for 100 seconds in flowing N_2 (3 SLPM) at 600°C or 1060°C (labeled LTA and HTA respectively for Low and High Temperature Anneal) using a rapid thermal processor (Modular Process Technology Corp., RTP-600S). No Si aggregates could be detected in transmission electron microscopy (TEM) measurements on LTA samples, while TEM measurements on samples annealed at $T \geq$ 1000C (e.g. HTA sample) clearly showed the presence of NCs [Chapter 2 [Ref. 30]]. The processed samples were attached with silver paint to the cold finger of a closed-loop He cryostat designed for operation in the temperature range 10 - 800 K (ARS DE-202AE-T). Photoluminescence (PL) measurements were performed in the temperature range 20 – 200°C at a pressure of ~ 5×10^{-7} mbar. Note that these temperatures lie well below the applied annealing temperatures. No permanent change of the optical properties was observed after

extended exposure of the samples to temperatures up to 200°C. The maximum sample temperature was limited by the ability to measure the Er^{3+} emission at 1535 nm on top of the thermal radiation background without saturating the near-infrared detectors. Photoluminescence measurements were taken under 351 nm excitation using a continuous wave (cw) Kr-ion laser (Spectra-Physics, BeamLok 2060) (pump irradiance 2.56 W/cm^2). A single monochromator (Acton, SpectraPro 2300i) was used to disperse the collected signal. A thermo-electrically-cooled charge-coupled device camera (Andor, DU401-BR-DD) was used to record the spectra in the region 450 – 1050 nm. A liquid-nitrogen-cooled Ge-detector (Applied Detector Corp., 403S) in combination with standard lock-in techniques was used for spectral measurements in the region 900 – 1750 nm. The obtained spectra were corrected for the system response and concatenated in the region 1030 – 1050 nm. The time-dependence of the photoluminescence intensity was measured by modulating the cw pump beam using an acousto-optic modulator (NEOS Technologies, 38210-6AS). Photoluminescence traces were recorded using a near-infrared photomultiplier tube (Hamamatsu R5509-73), in combination with a multi-channel scaler (Stanford Research Systems, SR430). During all measurements the samples were continuously scanned against the laser beam to prevent possible light-induced changes to their optical properties upon exposure to UV light.[44] The spectral resolution in all photoluminescence measurements was ~ 15 nm. The system time resolution of the lifetime measurements was 40 ns for luminescence center and nanocrystal related emission, 320 ns for the Er emission at 1535 nm in LTA sample and 1.28 μs for the Er emission at 1535 nm in HTA sample.

7.3 Results and Discussion

Figure 7.1 shows the photoluminescence (PL) spectra of the LTA sample taken in the temperature range 20 – 200°C. The PL spectra of the LTA sample are characterized by three emission bands: a broad rapidly decaying (lifetime < 40 ns) band peaking around 550 nm corresponding to the emission from Si-excess related luminescence centers (LC) and two relatively narrow slowly decaying emission bands at 981 nm and 1535 nm corresponding to the transitions from the second ($^4I_{11/2}$) and first ($^4I_{13/2}$) excited states respectively to the ground ($^4I_{15/2}$) state of Er^{3+}.

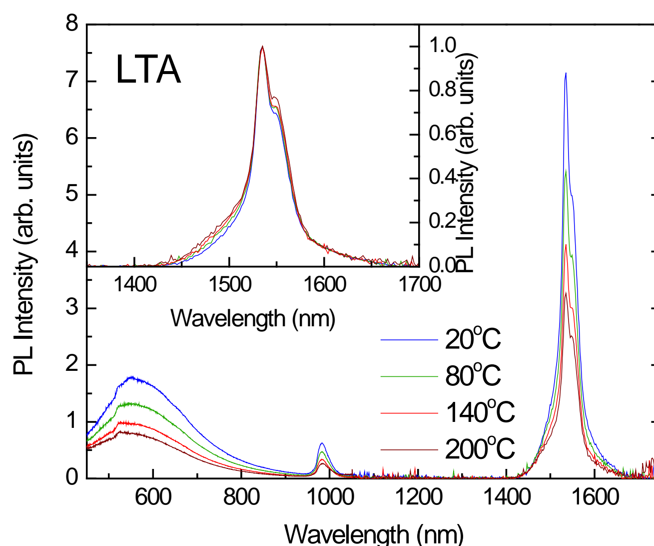

Figure 7.1. (Color) Photoluminescence spectra of Er-doped Si-rich SiO_2 annealed at 600°C (LTA) measured in the temperature range 20 – 200°C. Inset: normalized emission from the first excited state of Er^{3+} ($^4I_{13/2}$).

Figure 7.2 shows the corresponding PL spectra of the HTA samples plotted on the same relative intensity scale as Fig. 7.1. The spectrum of HTA sample is characterized by four emission bands:

a fast (lifetime < 40 ns) broad LC related band peaking around ~ 550 nm, a rather slow (lifetime ~ 2 μs at room temperature) broad Si nanocrystal (NC) related band peaking at ~ 745 nm, and the two Er^{3+} related bands at 981 and 1535 nm also observed in the LTA sample. The insets of Fig. 7.1 and Fig. 7.2 show the spectra of the Er^{3+} transition from the first excited to the ground state, normalized to their peak value at 1535 nm for the LTA and HTA samples respectively. Relatively small changes in spectral shape are observed in the temperature range 20 – 200°C, suggesting that optical cross-sections and therefore the spectral dependence of the gain will be largely temperature independent across the Er^{3+} emission band.

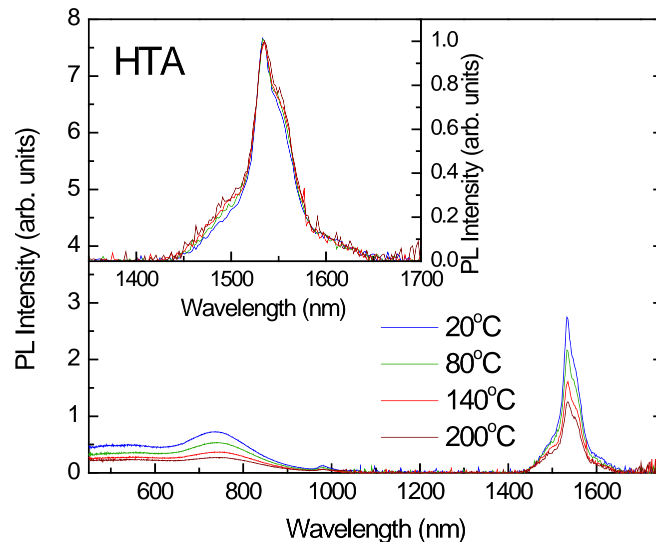

Figure 7.2. (Color) Photoluminescence spectra of Er-doped Si rich SiO_2 annealed at 1060°C (HTA) measured in the temperature range 20 – 200°C. The values of the PL intensity may be compared to the intensities in Fig. 1. Inset: normalized emission from the first excited state of Er^{3+} ($^4I_{13/2}$).

Figure 7.3 (a) shows the PL intensity corresponding to the transition of Er^{3+} from the first excited ($^4I_{13/2}$) state to the ground ($^4I_{15/2}$) state in the LTA and HTA sample, integrated in the region 1350 – 1700 nm (I_{Er}). For both LTA and HTA samples the integrated intensity is observed to decrease by a factor of ~ 1.92 as the sample temperature is increased from 20°C to 200°C. This change was found to be reversible, i.e. upon returning the samples to room temperature, the original room-temperature PL intensity was recovered. The PL decay traces of the Er-related emission at 1535 nm (not shown) in LTA and HTA samples exhibited stretched exponential behavior. The 1/e decay times τ_{dec} were obtained by fitting the measured decay traces with the function $I(t) = I_0(t) \exp(-(t/\tau_{dec})^{\beta})$ where β is the dispersion factor of the stretched exponent. Figure 7.3 (b) shows the behavior of the Er^{3+} decay times τ_{dec} at 1535 nm in LTA and HTA samples.

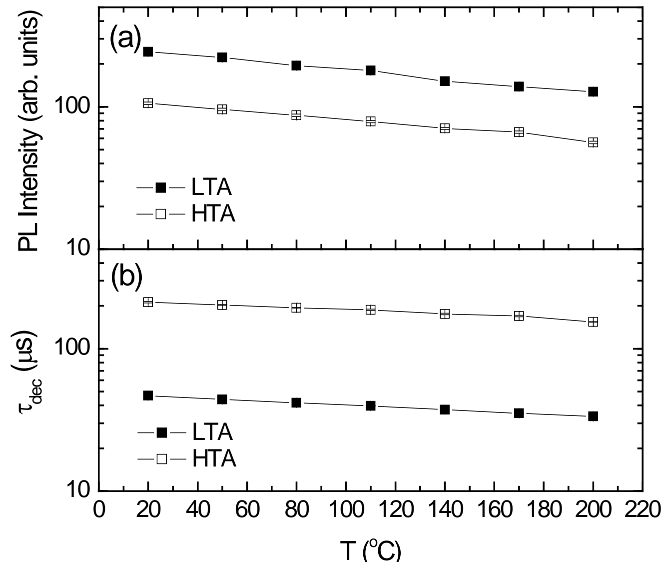

Figure 7.3. Temperature dependence of (a) integrated photoluminescence intensity I_{Er} corresponding to the $^4I_{13/2} \rightarrow {}^4I_{15/2}$ transition of Er^{3+} and (b) decay time τ_{dec} of the first excited state of Er^{3+} ($^4I_{13/2}$) in samples annealed at low (LTA) and high (HTA) temperature.

In the considered temperature range τ_{dec} is found to decrease by a factor of ~1.4 for both LTA and HTA samples. The dispersion factors for both samples were found to be approximately temperature independent and equal to $\beta_{LTA} = 0.73 \pm 0.1$ and $\beta_{HTA} = 0.76 \pm 0.1$.

Figure 7.4 (a) shows the effective absorption cross-section of the first excited state of Er^{3+} in LTA and HTA samples, as found from the rise time and decay time measurements (not shown) using the well-known relation $\sigma_{eff}\ \varphi = 1/\tau_{rise} - 1/\tau_{dec}$, where σ_{eff} is the effective absorption cross-section of the first excited state of Er^{3+}, φ is the excitation photon flux, τ_{rise} is the rise time, and τ_{dec} is the decay time of the Er^{3+} first excited state. For both LTA and HTA samples the Er^{3+} effective absorption cross-section is found to be temperature independent within the experimental error.

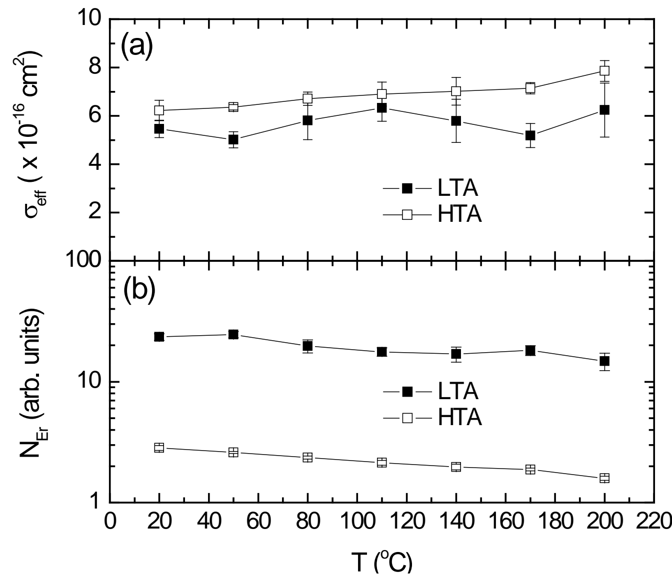

Figure 7.4. Temperature dependence of the (a) effective absorption cross-section of the first excited state of Er^{3+} (σ_{eff}) and (b) the density of optically active sensitized Er^{3+} ions in samples annealed at low (LTA) and high (HTA) temperature.

Based on the experimentally determined values of the integrated emission intensity (I_{Er}), the decay time (τ_{dec}), and the Er^{3+} effective absorption cross-section at 1535 nm (σ_{eff}) the density of optically active sensitized Er^{3+} ions N_{Er} in LTA and HTA samples can be found using the expression $N_{Er,sens} \propto I_{Er} \times (1 + 1/(\sigma_{eff}\ \varphi\ \tau_{dec}))$ [Chapter 2 [Ref. 30], Chapter 3 [Ref. 31]]. Figure 7.4 (b) shows the thus obtained temperature dependent density of sensitized optically active Er^{3+} ions. N_{Er} is found to gradually decrease by a factor of 1.6 and 1.8 for LTA and HTA samples respectively as the sample temperature is increased from 20°C to 200°C.

Based on the temperature dependence of the decay time (τ_{dec}), the Er^{3+} effective absorption cross-section (σ_{eff}), and the density of optically active sensitized Er^{3+} ions (N_{Er}) the effect of heating on the optical gain at 1535 nm in LTA and HTA samples can be estimated assuming a temperature independent peak emission cross-section of Er^{3+}, as suggested by the relatively temperature independent shape of Er^{3+} emission spectra, and excluding upconversion and excited state absorption. Under these assumptions the maximum low-signal gain coefficient can be found from the relation:

$$\gamma = \sigma_{Er,peak} \Delta N = \sigma_{Er,peak} N_{Er} \frac{\sigma_{eff} \varphi\ \tau_{dec} - 1}{\sigma_{eff} \varphi\ \tau_{dec} + 1} \tag{7.1}$$

where γ is the optical gain coefficient at 1535nm, $\sigma_{Er,peak}$ is the peak emission cross-section of the Er^{3+} $^4I_{13/2} \rightarrow {}^4I_{15/2}$ transition, assumed to be equal to the absorption cross-section of the $^4I_{15/2} \rightarrow {}^4I_{13/2}$ transition at this same wavelength,[45] and φ is the pump photon flux. Note that Eq. 7.1 does not take into account the possible effects of cooperative upconversion and excited state absorption. These effects will likely occur at high pump powers [46, 47], resulting in

respectively an increase in the pump power required to achieve Er^{3+} related gain, and a decrease in the value of the maximum gain. However, the required parameters to quantitatively predict these effects are not available for the present sample composition and processing conditions, and their determination is outside the scope of the current study.

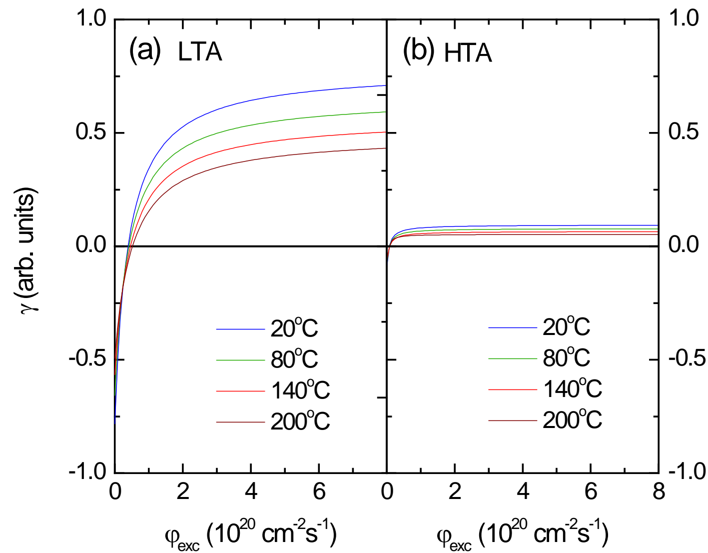

Figure 7.5. (Color) Calculated pump flux dependence of the Er^{3+} related optical gain at 1535 nm under excitation at 351 nm for different sample temperatures, in samples annealed at (a) low (LTA) and (b) high (HTA) temperature.

Figures 7.5 (a) and (b) show the calculated photon flux dependence of γ based on Eq. 7.1 for LTA and HTA samples respectively, obtained for different sample temperatures based on the experimentally determined temperature dependent values of the lifetime, Er^{3+} effective absorption cross-section, and the density of sensitized Er^{3+} ions under 351 nm excitation. It should be noted that these curves do not take into account ground state absorption from any unsensitized Er^{3+} ions that may be present in the film. Several key differences in gain

performance of the LTA and HTA sample can be observed. First, the Er^{3+} related absorption at low pump flux and maximum achievable gain at high population inversion levels ($\sigma_{eff}\ \varphi\ \tau_{dec} \gg 1$) occurring for high pump flux are a factor ~ 9 larger for the LTA sample than for the HTA sample due to the higher N_{Er} at all temperatures for the former. Second, the threshold pump flux is higher for the LTA sample mainly due to a significantly (by a factor of ~ 4.6) lower Er^{3+} lifetime compared to the HTA sample. Third, as the temperature is increased the maximum gain under significant population inversion reduces by a factor of ~ 1.6 and ~ 1.8 in the temperature region 20 – 200°C for LTA and HTA samples respectively. Note that at typical processor operating temperatures of ~ 80 – 90°C the maximum gain is only a factor ~ 1.26 less than at room temperature for both samples. This indicates that a relatively thermally stable gain performance under significant inversion can be achieved using both low (600°C, LTA) and high (1060°C, HTA) temperature annealed Er-doped Si-rich SiO_2 as the gain medium under real-world operating conditions of silicon integrated circuits. Samples annealed at low temperature (LTA) not containing silicon nanocrystals are expected to provide better gain performance in real on-chip devices as compared with samples annealed at high temperature (HTA). This conclusion is based predominantly on the predicted higher optical gain, a lower ground state absorption resulting from a higher concentration of sensitizers and thus a higher fraction of sensitized Er^{3+} ions, and lower confined carrier absorption as compared with the samples with silicon nanocrystals. It should be noted that due to the lower Er^{3+} decay time in LTA samples as compared to HTA samples, higher pump powers will be needed to achieve population inversion in LTA samples. Secondly, it is necessary to take into account that while the concentration of Er is the same in both LTA and HTA samples studied here, the density of optically active sensitized

Er^{3+} ions is factor ~ 9 higher in the LTA sample as compared to HTA sample. This difference is expected to be even higher for the samples annealed at temperatures above 1060°C where a steep drop of the density of optically active indirectly excitable Er^{3+} ions occurs.[30] While the predicted optical gain in the current study does not take into account any remaining unsensitized Er^{3+} in the LTA sample, the much larger density of sensitized Er^{3+} ions in the LTA sample compared to the HTA samples suggests that using low annealing temperatures can minimize ground state absorption from unsensitized Er^{3+} ions. The higher concentration of sensitized Er^{3+} in LTA samples, combined with the absence of Si nanocrystal related optical loss contributions such as confined carrier absorption[37, 38] and scattering[39] make LTA the most viable candidate for the achievement of high optical gain at 1.54 μm. Based on these considerations low-temperature processed Si-sensitized Er-doped SiO_2 has the potential to become an important optical gain medium with thermally stable performance.

7.4 Conclusions

In summary, it was shown that in samples without (annealed at 600°C) and with (annealed at 1060°C) Si nanocrystals the change of the spectral shape of the Er^{3+} band at 1535 nm is insignificant in the temperature range 20 – 200°C, suggesting that optical cross-sections throughout the Er^{3+} emission band at 1.54 μm is relatively thermally stable. Based on measurements of the temperature dependent excitation rate, decay time and density of optically active sensitized Er^{3+} ions, it is predicted that in the temperature range 20 – 90°C the peak optical gain does not change more than by a factor of ~ 1.26 in the case of LTA and HTA samples at

significant inversion levels. This observation proves that relatively stable operation of on-chip photonic devices based on Er-doped Si-rich SiO_2 is possible when the material is exposed to typical processor operating temperatures. While the temperature dependence of the gain is predicted to be similar in the case of LTA and HTA samples, based on the obtained values of the density of optically active sensitized Er^{3+} ions, devices fabricated from low temperature processed Er-doped Si-rich SiO_2 are expected to demonstrate a higher optical gain at 1535 nm as compared with high temperature processed material.

7.5 References

[1] N. Daldosso and L. Pavesi. Laser Photon. Rev. **3**, 508 (2009).

[2] M. Lipson, J. Light. Tech.. **23**, 4222 (2005).

[3] B. Jalali and S. Fathpour, J. Light. Tech. **24**, 4600 (2006).

[4] R. Soref, J. Sel. Top. Quant. Electr. **12**, 1678 (2006).

[5] Y. Kang, H.-D. Liu, M. Morse, M. J. Paniccia, M. Zadka, S. Litski, G. Sarid, A. Pauchard, Y.-H. Kuo, H.-W. Chen, W. S. Zaoui, J. E. Bowers, A. Beling, D. C. McIntosh, X. Zheng, and J. C. Campbell, Nat. Photon. **3**, 59 (2008).

[6] K. Preston, S. Manipatruni, A. Gondarenko, C. Poitras, and M. Lipson, Opt. Express **17**, 5118 (2009).

[7] Y. Vlasov, W. M. J. Green, and F. Xia, Nat. Photon. **2**, 242 (2008).

[8] L. Chen and M. Lipson, Opt. Express **17**, 7901 (2009).

[9] N. Sherwood-Droz, H. Wang, L. Chen, B. G. Lee, A. Biberman, K. Bergman, and M. Lipson, Opt. Express **16**, 15915 (2008).

[10] F. Xia, L. Sekaric, and Y. Vlasov, Nat. Photon. **1**, 65 (2006).

[11] H. Rong, A. Liu, R. Jones, O. Cohen, D. Hak, R. Nicolaescu, A. Fang, and M. Paniccia, Nature **433**, 292 (2005).

[12] A. W. Fang, H. Park, O. Cohen, R. Jones, M. J. Paniccia, and J. E. Bowers, Opt. Express **14**, 9203 (2006).

[13] X. Sun, J. Liu, L. C. Kimerling, and J. Michel, Opt. Lett. **34**, 1198 (2009).

[14] L. Pavesi, L. Dal Negro, C. Mazzoleni, G. Franzò, and F. Priolo, Nature **408**, 440 (2000).

[15] R. J. Walters, G. I. Bourianoff, and H. A. Atwater, Nat. Mater. **4**, 143 (2005).

[16] I. Sychugov, N. Elfström, A. Hallén, J. Linnros, and M. Qiu, Opt. Lett. **32**, 1878 (2007).

[17] R.-J. Zhang, S.-Y. Seo, A. P. Milenin, M. Zacharias, and U. Gösele, Appl. Phys. Lett. **88**, 153120 (2006).

[18] M. L. Brongersma, P. G. Kik, A. Polman, K. S. Min, and H. A. Atwater, Appl. Phys. Lett. **76**, 351 (2000).

[19] J. Ruan, P. M. Fauchet, L. Dal Negro M. Cazzanelli, and L. Pavesi, Appl. Phys. Lett. **83**, 5479 (2003).

[20] K. S. Cho, N.-M. Park, T.-Y. Kim, K.-H. Kim, G. Y. Sung, and J. H. Shin, Appl. Phys. Lett. **86**, 071909 (2005).

[21] S. Yerci, R. Li, S. O. Kucheyev, T. van Buuren, S. N. Basu, and L. Dal Negro, Appl. Phys. Lett. **95**, 031107 (2009).

[22] M. Fujii, M. Yoshida, Y. Kanzawa, S. Hayashi, and K. Yamamoto, Appl. Phys. Lett. **71**, 1198 (1997).

[23] P. G. Kik, M.L. Brongersma, and A. Polman, Appl. Phys. Lett. **76**, 2325 (2000).

[24] A. J. Kenyon, M. Wojdak, I. Ahmad, W. H. Loh, and C. J. Oton, Phys. Rev. B **77**, 035318 (2008).

[25] H.-S. Han, S.-Y. Seo, and J. H. Shin, Appl. Phys. Lett. **79**, 4568 (2001).

[26] D. Pacifici, G. Franzò, F. Priolo, F. Iacona, and L. Dal Negro, Phys. Rev. B **67**, 245301 (2003).

[27] D. Navarro-Urrios, A. Pitanti, N. Daldosso, F. Gourbilleau, R. Rizk, B. Garrido, and L. Pavesi, Phys. Rev. B **79**, 193312 (2009).

[28] K. Hijazi, R. Rizk, J. Cardin, L. Khomenkova, and F. Gourbilleau, J. Appl. Phys. **106**, 024311 (2009).

[29] M. Wojdak, M. Klik, M. Forcales, O. B. Gusev, T. Gregorkiewicz, D. Pacifici, G. Franzò, F. Priolo, and F. Iacona, Phys. Rev. B **69**, 233315 (2004).

[30] O. Savchyn, F. R. Ruhge, P. G. Kik, R. M. Todi, K. R. Coffey, H. Nukala, and H. Heinrich, Phys. Rev. B **76**, 195419 (2007).

[31] O. Savchyn, P. G. Kik, R. M. Todi, and K. R. Coffey, Phys. Rev. B **77**, 205438 (2008).

[32] G. Franzò, V. Vinciguerra, and F. Priolo, Appl. Phys. A: Mater. Sci. Process. **69**, 3 (1999).

[33] F. Gourbilleau, M. Levalois, C. Dufour, J. Vicens, and R. Rizk, J. Appl. Phys. **95**, 3717 (2004).

[34] A. J. Kenyon, C. E. Chryssou, C. W. Pitt, T. Shimizu-Iwayama, D. E. Hole, N. Sharma, and C. J. Humphreys, J. Appl. Phys. 91, 367 (2002).

[35] J. Lee, J. H. Shin, and N. Park, J. Light. Tech. **23**, 19 (2005).

[36] N. Daldosso, D. Navarro-Urrios, M. Melchiorri, L. Pavesi, F. Gourbilleau, M. Carrada, R. Rizk, C. García, P. Pellegrino, B. Garrido, and L. Cognolato, Appl. Phys. Lett. **86**, 261103 (2005).

[37] R. D. Kekatpure and M. L. Brongersma, Nano Lett. **8**, 3787 (2008).

[38] D. Navarro-Urrios, A. Pitanti, N. Daldosso, F. Gourbilleau, R. Rizk, G. Pucker, and L. Pavesi, Appl. Phys. Lett. **92**, 051101 (2008).

[39] R. D. Kekatpure and M. L. Brongersma, Phys. Rev. A **78**, 023829 (2008).

[40] O. Savchyn, R. M. Todi, K. R. Coffey, L. K. Ono, B. Roldan Cuenya, and P. G. Kik, Appl. Phys. Lett. 95, 231109 (2009).

[41] O. Savchyn, R. M. Todi, K. R. Coffey, and P. G. Kik, Appl. Phys. Lett. **93**, 233120 (2008).

[42] O. Savchyn, R. M. Todi, K. R. Coffey, and P. G. Kik, Appl. Phys. Lett. **94**, 241115 (2009).

[43] K. Imakita, M. Fujii, and S. Hayashi, Phys. Rev. B **71**, 193301 (2005).

[44] S. Godefroo, M. Hayne, M. Jivanescu, A. Stesmans, M. Zacharias, O. I. Lebedev, G. Van Tendeloo, and V. V. Moshchalkov, Nat. Nanotechnol. **3**, 174 (2008).

[45] W. Miniscalco, J. Light. Tech. **9**, 234 (1991).

[46] D. Pacifici, G. Franzò, F. Priolo, F. Iacona, and L. Dal Negro, Phys. Rev. B **67**, 245301 (2003).

[47] A.J. Kenyon, W.H. Loh, C.J. Oton, and I. Ahmad, J. Lumin. **121**, 193 (2006).

CHAPTER 8. DETERMINTATION OF OPTIMUM Si-EXCESS CONCENTRATION IN Er-DOPED Si-RICH SiO_2 FOR OPTICAL APMLIFICATION AT 1.54 µm

The presence of indirect Er^{3+} excitation in Si-rich SiO_2 is demonstrated for Si excess concentrations in the range 2.5 – 37 at.%. The Si excess concentration providing the highest density of sensitized Er^{3+} ions is demonstrated to be relatively insensitive to the presence of Si nanocrystals and is found to be ~ 14.5 at.% for samples without Si nanocrystals (annealed at 600°C) and ~ 11.5 at.% for samples with Si nanocrystals (annealed at 1100°C). The observed optimum is attributed to an increase in the density of Si-related sensitizers as the Si concentration is increased, with subsequent deactivation and removal of these sensitizers at high Si concentrations. The optimized Si excess concentration is predicted to generate maximum Er-related gain at 1.54 µm in devices based on Er-doped Si-rich SiO_2.

.

8.1 Introduction

The development of on-chip photonic interconnects requires the development of a cost-effective Si-compatible light source.[1-3] One actively investigated approach involves the use of Si-sensitized erbium in Si-rich SiO_2.[4, 5] Erbium in its trivalent Er^{3+} state exhibits sharp optical absorption and emission lines, one of which occurs at a wavelength of 1.54 µm. It is well known that the presence of excess silicon in Er-doped SiO_2 increases the Er^{3+} excitation cross-

section by several orders of magnitude[6, 7] and enables excitation in a wide wavelength range.[4, 8] In Chapter 2 [Ref. 9] and Chapter 3 [Ref. 10] we have demonstrated that Si excess related luminescence centers (LC) are the dominant source of Er^{3+} sensitization in Si-rich SiO_2, as opposed to Si nanocrystals (NC) which were previously thought to be the main sensitizers. As was shown in Chapter 6 [Ref. 8] indirect Er-excitation through Si excess related states occurs even in as-deposited samples. In Chapter 4 [Ref. 11] and Chapter 5 [Ref. 12] it was demonstrated that the excitation is characterized by a fast (< 30 ns) transfer from LC to the Er^{3+} first excited state ($^4I_{13/2}$) as well as higher lying states, the latter resulting in the appearance of an additional slow contribution to the first excited state population. As was shown in Chapter 2 [Ref. 9] low-temperature annealed Er-doped Si-rich SiO_2 exhibits a higher density of sensitized Er^{3+} ions as compared to its Si NC containing counterpart, and is therefore predicted to enable higher gain coefficients. To realize optimized devices based on this material it is essential to determine the Si excess concentration that leads to the maximum concentration of sensitized Er^{3+}. Relatively few studies consider the effect of Si excess concentration on the Er^{3+} emission.[13-15] Furthermore, these studies focus predominantly on Er^{3+} emission intensities, rather than other relevant Er^{3+} characteristics such as lifetime and excitation cross-section, and often only consider high temperature annealed samples. In this study we determine the concentration of Si excess that maximizes the density of sensitized Er^{3+} ions for samples annealed at low temperature (not containing Si NCs) and high temperature (containing Si NCs) by taking into account emission intensities, lifetimes, and excitation cross-sections.

8.2 Experimental Techniques

Er-doped Si-rich SiO_2 films (thicknesses 107 ± 6 nm) containing 0.55 ± 0.05 at. % of Er as well as Si excess concentrations (C_{SiE}) in the range 2.5 – 37 at.% were deposited onto separate silicon wafers by magnetron co-sputtering. For each Si concentration two sets of samples were prepared: samples annealed at 600°C and at 1100°C (labeled LTA and HTA, for 'low temperature anneal' and 'high temperature anneal' respectively) for 30 min in flowing Ar (flow rate 65 SCCM). All samples were subsequently passivated for 30 min. in forming gas (N_2:H_2=95%:5%, flow rate 65 SCCM) at 500°C. Photoluminescence (PL) spectra were taken at room temperature under excitation with the 351 nm emission line of a Kr-ion laser (Spectra-Physics, BeamLok 2060). The irradiance at the sample surface was 2.4 W/cm^2. PL spectra were recorded with a charge-coupled device array (Andor, DU401-BR-DD) and a Ge-detector (Applied Detector Corp., 403S) in the spectral ranges 400 – 1100 nm and 900 – 1750 nm respectively, and were corrected for the system spectral response and sample thickness. Excitation spectra were taken using Xe-lamp emission filtered through a monochromator (Horiba Jobin Yvon MicroHR). All spectral PL measurements were done in the near-linear regime of PL vs. power to minimize the effect of any nonlinear processes (excited state absorption, cooperative upconversion). PL traces were recorded using a photomultiplier tube (Hamamatsu 5509-73) in combination with a multi-channel scaler (Stanford Research Systems, SR430). The spectral resolution in all PL measurements was ~10 nm and the temporal resolution was 0.64 μs and 2.56 μs for LTA and HTA samples respectively. Lifetime measurements of the LTA sample with a Si excess concentration of 2.5 at.% did not provide sufficient signal to noise ratio due to the low Er^{3+}

emission intensity from this sample. More information on the sample preparation and experimental techniques can be found in Chapter 2 [Ref. 9] and Chapter 3 [Ref. 10].

.

8.3 Results and Discussion

Figure 8.1 (a) shows the PL spectra of LTA samples for different Si excess concentrations C_{SiE} on a logarithmic intensity scale.

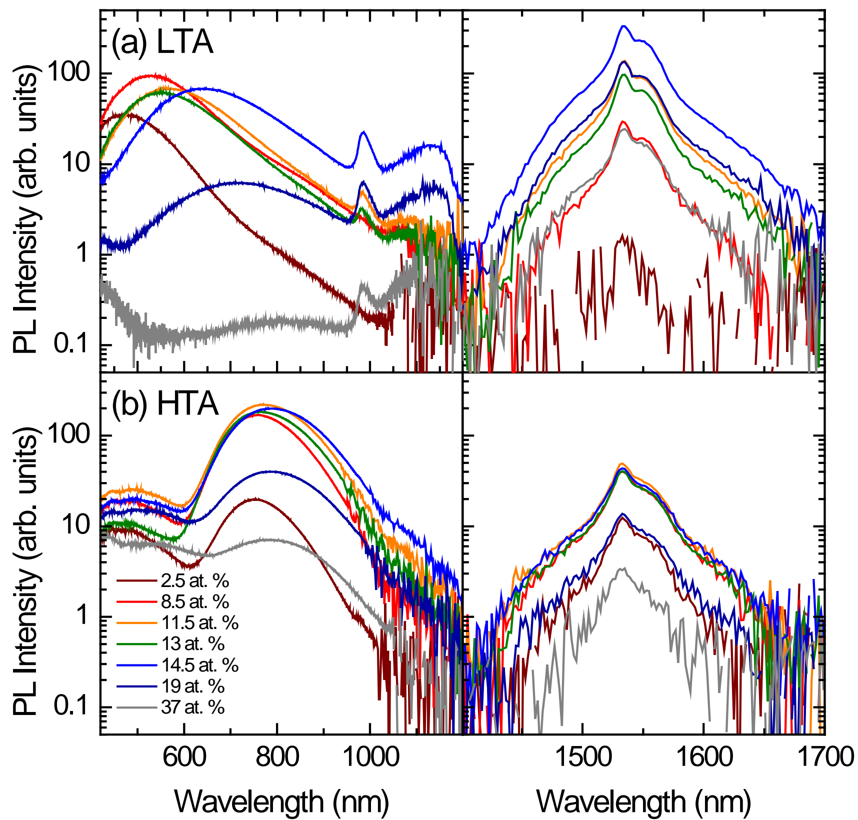

Figure 8.1. (Color) PL spectra of LTA (a) and HTA (b) samples with different silicon excess concentrations.

The spectra show three bands: a broad band peaking in the range 450 – 800 nm ascribed to the Si-excess-related luminescence centers (LC), and two narrow bands at 981 nm and 1535 nm corresponding to the Er^{3+} transitions $^4I_{11/2} \rightarrow {}^4I_{15/2}$ and $^4I_{13/2} \rightarrow {}^4I_{15/2}$ respectively. A fourth broad band peaking around 1130 nm is observed in LTA samples with $C_{SiE} > 13$ at.%. As C_{SiE} is increased, the LC PL spectra exhibit a significant redshift, suggesting that either interactions between adjacent LCs or possibly lattice strain can affect the LC energy levels. In addition, the full width at half maximum (FWHM) of the Er^{3+} PL spectrum at 1535 nm increases by ~ 12 % as C_{SiE} is increased from 8.5 to 37 at.%, suggesting that the excess Si significantly affects the local Er^{3+} surroundings in low temperature processed samples. Figure 8.1 (b) shows the PL spectra of the corresponding HTA samples, exhibiting three bands: a weak broad band peaking at ~ 450 nm corresponding to PL from LCs, a broad band at ~ 750 – 800 nm related to PL from Si NCs, and Er^{3+} PL at 1535 nm. The Si NC PL spectrum shows a redshift with increasing C_{SiE}, which is commonly attributed to an increase of the NC diameter and a resulting reduced quantum confinement. No significant changes in the Er^{3+} PL FWHM are observed in these samples, suggesting that the Er^{3+} local environment is similar in all HTA samples. This could indicate that lattice relaxation occurs during the high temperature anneal, or that the growth of Si nanocrystals leaves behind a significant number of sensitized Er^{3+} ions regions with a reduced local concentration of excess Si. Note that the Er^{3+} PL intensity at 1535 nm varies significantly, indicating a possible change in (a) the density of sensitized Er^{3+} ions, (b) the effective Er^{3+} excitation cross-section, and (c) the emission efficiency.

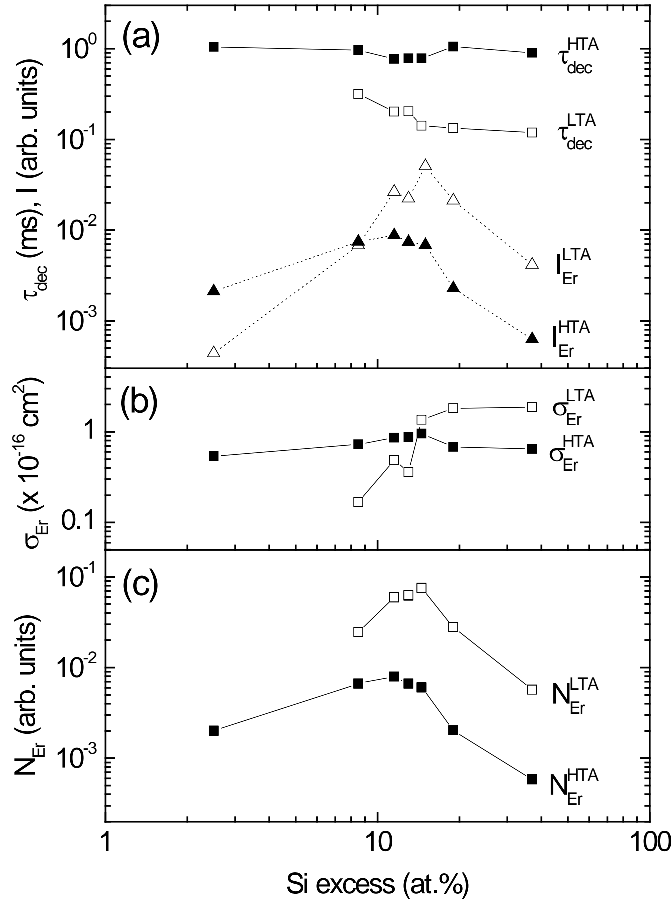

Figure 8.2 (a) PL intensity of Er^{3+} transition $^4I_{13/2} \rightarrow {^4I_{15/2}}$ integrated in the region 1350 – 1700 nm I and the decay time of Er^{3+} PL at 1535 nm τ_{dec}, (b) excitation cross-section of the first excited state of Er^{3+} σ_{Er}, and (c) density of sensitized Er^{3+} ions N_{Er} of LTA and HTA samples as a function of Si excess concentration.

Figure 8.2 (a) shows the dependence of the Er^{3+} PL intensity, integrated in the region 1350 – 1700 nm (I, triangles) for LTA (open symbols) and HTA (solid symbols) samples. In both sample types the Er^{3+} PL intensity initially rises as a function of C_{SiE} until a concentration of ~ 14.5 at.% and ~ 11.5 at.% for LTA and HTA samples respectively, after which the Er^{3+} PL intensity starts to decrease rapidly. In order to determine the origin of the intensity variation,

decay times τ_{dec} of the Er^{3+} PL at 1535 nm were determined by fitting the experimentally acquired decay traces with a stretched exponential function of the form $I(t)=I(0)\times\exp(-(t/\tau_{dec})^{\beta})$, where β is the multiexponentiality factor. The value of β was found to be 0.72 ± 0.06 for all samples. The corresponding decay times are shown in Fig. 8.2 (a) (τ_{dec}, squares) for LTA (open symbols) and HTA (solid symbols). In LTA samples the decay time decreases by a factor ~ 3 as C_{SiE} is increased from 8.5 at.% to 37 at.%. The corresponding increase of the total decay rate by more than 5000 s^{-1} is too large to be attributed to changes in the Er^{3+} radiative lifetime (typically 50 – 60 s^{-1} in SiO_2 based hosts[16]), and is most likely due to an increased non-radiative decay rate associated with the presence of electronic states introduced in the SiO_2 bandgap by the presence of excess Si. In contrast, for HTA samples the Er^{3+} decay time at 1535 nm shows a relatively constant value of ~ 0.9 ± 0.1 ms for all C_{SiE}. This suggests that the high temperature anneal leads to the removal of a significant fraction of such mid-gap states during the Si NC formation process.

The Er^{3+} first excited state excitation cross-section (σ_{Er}) was determined based on the measured decay time (τ_{dec}) and rise time (τ_{rise}) (not shown) using the equation: $\sigma_{Er}\varphi = \tau_{rise}^{-1} - \tau_{dec}^{-1}$ where φ is the known pump photon flux ($cm^{-2}s^{-1}$). The obtained σ_{Er} values are shown in Fig. 8.2 (b). The values of σ_{Er} in LTA and HTA samples are found to be similar within a factor 5 throughout the entire C_{SiE} range, supporting the presumption of a similar Er^{3+} excitation process in both sample types. For LTA samples σ_{Er} is seen to increase by a factor ~ 8 as C_{SiE} is increased from 8.5 at.% to 37 at.%, whereas HTA samples exhibit a relatively constant σ_{Er} in the same C_{SiE} range. The origin of the rising σ_{Er} values in LTA samples as a function of increasing C_{SiE} is not known, however it should be noted that this change correlates with the

appearance of a significant emission band at ~ 1130 nm, near the Er^{3+} 981 nm emission line (Fig. 8.1 (a)). The increase of the Er^{3+} excitation cross-section in LTA samples with increasing C_{SiE} may be attributed to a combination of (a) the excitation of a single Er^{3+} ion by several LCs, (b) a C_{SiE} dependent variation in the electronic configuration of the LCs as inferred from the observed changes in the LC PL spectrum (Fig. 8.1 (a)), (c) a change in the energy transfer process, or (d) the introduction of additional states at wavelengths > 800 nm through which the sensitization of Er^{3+} can occur directly into $^4I_{11/2}$ (981 nm) or possibly even into the $^4I_{13/2}$ (1535 nm) level of Er^{3+}. The latter interpretation is in good agreement with the results presented in Chapter 4 [Ref. 11] and Chapter 5 [Ref. 12] where it was demonstrated that Er^{3+} can be sensitized directly into the first excited state and into the second excited state. It should be pointed out that at C_{SiE} values between 10 – 15 at.% both sample types exhibit similar excitation cross-sections. This finding is in agreement with prior work described in Chapter 2 [Ref. 9] on samples with a similar C_{SiE} of 12 at.%, in which σ_{Er} was found to be only weakly dependent on annealing temperature.

The values obtained in Figs. 8.2 (a) and 8.2 (b) enable the determination of a parameter proportional to the concentration of sensitized Er^{3+} ions N_{Er}. Modeling the Er^{3+} as a quasi-three level system, the Er^{3+} PL intensity I can be expressed as

$$I \propto \frac{\sigma_{Er}\varphi\ \tau_{dec}}{1+\sigma_{Er}\varphi\ \tau_{dec}}\frac{N_{Er}}{\tau_{rad}} \tag{8.1}$$

where τ_{rad} is the radiative lifetime of the Er^{3+} transition at 1535 nm. N_{Er} can thus be found in relative units, assuming that the Er^{3+} radiative lifetime τ_{rad} does not vary significantly. Figure 8.2 (c) shows the resulting N_{Er} values. The maximum N_{Er} value occurs at C_{SiE}

~ 14.5 at.% and C_{SiE} ~ 11.5 at.% for LTA and HTA samples respectively. Note that N_{Er} in LTA samples is a factor ~ 4 – 14 higher than in HTA samples depending on the Si concentration. Apparently the high temperature anneal reduces the fraction of sensitized Er^{3+} ions by an amount ranging from 75% to 93%. This dramatic reduction in N_{Er} is likely due to the removal of excess Si by the formation of amorphous Si clusters and Si NCs for LTA and HTA samples respectively, and the associated removal of excess-Si-related sensitizers from the SiO_2 matrix. Based on these observations, the presence of an optimum in N_{Er} as a function of Si excess concentration is attributed to an increase of the sensitizer density as C_{SiE} is increased, counteracted by a reduction in the sensitizer density associated with the formation of extended Si aggregates or nanocrystals. It should be noted that the optimum excess silicon concentration in LTA samples leads to the highest value of N_{Er}, optimal for high gain, as well as to an increased magnitude of σ_{Er}, suggesting that relatively low threshold pump powers can be achieved in the material.

8.4 Conclusions

In summary, the indirect excitation of Er in Si-rich SiO_2 films was investigated in the Si excess concentration range of 2.5 – 37 at.%. The Si excess concentration providing the highest density of sensitized Er^{3+} ions was demonstrated to be similar independent of the presence of Si NCs, and is respectively ~ 14.5 at.% and ~ 11.5 at.% in samples without and with Si NCs. The optimized Si excess concentration is anticipated to provide maximum Er-related gain at 1.54 μm in devices based on Er-doped Si-rich SiO_2.

8.5 References

[1] N. Daldosso and L. Pavesi, Laser Photon. Rev. **3**, 508 (2009).

[2] B. Jalali and S. Fathpour, J. Lightwave Technol. **24**, 4600 (2006).

[3] R. Soref, IEEE J. Sel. Top. Quantum Electron **12**, 1678 (2006).

[4] M. Fujii, M. Yoshida, Y. Kanzawa, S. Hayashi, and K. Yamamoto, Appl. Phys. Lett. **71**, 1198 (1997).

[5] P. G. Kik, M. L. Brongersma, and A. Polman, Appl. Phys. Lett. **76**, 2325 (2000).

[6] M. Wojdak, M. Klik, M. Forcales, O. B. Gusev, T. Gregorkiewicz, D. Pacifici, G. Franzò, F. Priolo, and F. Iacona, Phys. Rev. B **69**, 233315 (2004).

[7] A. J. Kenyon, C. E. Chryssou, C. W. Pitt, T. Shimizu-Iwayama, D. E. Hole, N. Sharma, and C. J. Humphreys, J. Appl. Phys. **91**, 367 (2002).

[8] O. Savchyn, R. M. Todi, K. R. Coffey, L. K. Ono, B. R. Cuenya, and P. G. Kik, Appl. Phys. Lett. **95**, 231109 (2009).

[9] O. Savchyn, F. R. Ruhge, P. G. Kik, R. M. Todi, K. R. Coffey, H. Nukala, and H. Heinrich, Phys. Rev. B **76**, 195419 (2007)..

[10] O. Savchyn, P. G. Kik, R. M. Todi, and K. R. Coffey, Phys. Rev. B **77**, 205438 (2008).

[11] O. Savchyn, R. M. Todi, K. R. Coffey, and P. G. Kik, Appl. Phys. Lett. **93**, 233120 (2008).

[12] O. Savchyn, R. M. Todi, K. R. Coffey, and P. G. Kik, Appl. Phys. Lett **94**, 241115 (2009).

[13] G. Franzò, E. Pecora, F. Priolo, and F. Iacona, Appl. Phys. Lett. **90**, 183102 (2007).

[14] H. S. Han, S. Y. Seo, J. H. Shin, and D. S. Kim, J. Appl. Phys. **88**, 2160 (2000).

[15] J. M. Sun, W. Skorupa, T. Dekorsy, M. Helm, and A. N. Nazarov, Opt. Mat. **27**, 1050 (2005).

[16] M. J. A. d. Dood, L. H. Slooff, A. Polman, A. Moroz, and A. v. Blaaderen, Phys. Rev. A **64**, 033807 (2001).

CHAPTER 9. SUMMARY

The work described in this thesis discusses the nature of the excess-Si mediated Er^{3+} sensitization in Si-rich SiO_2. Indirect excitation of Er^{3+} was observed independent of the presence of silicon nanocrystals in the SiO_2 matrix. Si excess related luminescence centers rather than silicon nanocrystals were found to be the dominant source of Er^{3+} sensitization in Si-rich SiO_2. Increasing the annealing temperature above 1000°C – the temperature necessary for nanocrystal formation – was shown to result in a significant reduction of the density of sensitized Er^{3+} ions. These results led to an important conclusion: the fact that the sensitization of Er^{3+} can be acquired without the presence of silicon nanocrystals suggests that significantly lower values of confined carrier absorption and scattering typically introduced by silicon nanocrystals can be achieved. The predicted reduced scattering and confined carrier absorption combined with a higher density of sensitized Er^{3+} ions suggests that higher gain values can be acquired in samples annealed at temperatures below the onset of nanocrystal formation than in samples annealed at higher temperatures.

Hydrogen passivation of nanocrystal doped samples was shown to have only a minor effect on the Er^{3+} emission intensity in Si-rich SiO_2 without silicon nanocrystals. In contrast, a significant increase of the Er^{3+} emission was observed for samples containing silicon nanocrystals. This observation was attributed to an increase in the density of fully passivated optically active nanocrystals, and a reduction of nonradiative Er^{3+} relaxation from levels above

the $^4I_{13/2}$ level related to the presence of silicon dangling bonds. This result suggests that for devices based on low temperature annealed Er-doped Si-rich SiO_2 the passivation step can be omitted, simplifying the device fabrication process. Taking into account that the density of sensitized Er^{3+} ions in the films without silicon nanocrystals is higher than in the films with silicon nanocrystals independent of passivation temperature and taking into account that passivation is not required for the former type of films, devices based on films without silicon nanocrystals are not only expected to have superior gain performance as compared with the films containing silicon nanocrystals but will also be more cost effective in terms of fabrication. In addition it was shown that an initially counterintuitive increase of the nanocrystal decay time upon passivation could be explained by considering the inhomogeneous nature of the nanocrystal-related emission band. While the latter result does not have direct implications for the technical implementation of Si-sensitized Er^{3+} excitation in low temperature processed composites, it resolved a long standing issue that had been present in the literature for several years.

In time resolved measurements under pulsed excitation done at a sample temperature of 15K the characteristics of the luminescence center mediated Er^{3+} sensitization were studied. It was shown that the sensitization is fast and occurs not only into the higher energy states of Er^{3+} but also appears to occur directly into the first excited state. Such a multilevel Er^{3+} sensitization was demonstrated to result in two different excitation mechanisms of the first excited state: a fast excitation process directly into the first excited state and slow excitation process due to the relaxation of Er^{3+} from the second excited state to the first excited state. Fast and slow excitation processes are demonstrated to account for an approximately equal fraction of the excitation

events. The presence of direct Er^{3+} sensitization into the first excited state and the relatively high fraction of Er^{3+} ions excited in this way suggest that high excitation efficiencies of the first excited state of Er^{3+} can be achieved.

Through temperature dependent dynamic photoluminescence studies the internal relaxation efficiency from the second to the first excited state of Er^{3+} in Er-doped Si-rich SiO_2 was demonstrated to be nearly temperature independent and approaching unity in the temperature range 15 – 300K. The relaxation of Er^{3+} from the second to the first excited state was demonstrated to account for 50 - 55% of the excitation events of the first excited state in the considered temperature range. These results clearly suggest that relaxation of Er^{3+} from the second to the first excited state does not significantly affect the quantum efficiency of the excitation of the first excited state. Consequently, the findings suggest that high excitation efficiency and stable temperature performance can be acquired in devices based on Er-doped Si-rich SiO_2 without silicon nanocrystals.

The presence of indirect excitation of Er^{3+} in as-deposited Si-rich SiO_2 further confirmed the relative unimportance of Si nanocrystal mediated Er^{3+} sensitization in these samples. The Er^{3+} excitation cross-section in as-deposited samples was demonstrated to be similar to that of the samples annealed at 600°C under both 355 nm and 532 nm excitation. The density of sensitized Er^{3+} ions was demonstrated to be approximately excitation wavelength independent while the excitation cross-section of Er^{3+} was shown to significantly depend on the excitation wavelength. The results suggest that similar maximum gain values can be acquired using a broad range of excitation wavelengths.

In studies of the optical properties of Er^{3+} doped Si-rich SiO_2 at elevated sample temperatures, the optical properties of Er-doped Si-rich SiO_2 with and without silicon nanocrystals were shown to exhibit a similar temperature dependence in the range 20 – 200°C. It was predicted that an increase of the sample temperature from 20°C to 200°C would result in a decrease of the maximum optical gain at 1535 nm by a factor of ~ 1.8 and ~ 1.6 for samples with and without nanocrystals respectively. The erbium related optical gain at significant inversion levels in samples without silicon nanocrystals was predicted to be a factor ~ 9 higher than for samples containing silicon nanocrystals. These findings demonstrate that relatively thermally stable gain performance of the Er-doped Si-rich SiO_2 up to typical processor operating temperatures is possible and indicate that low-temperature-processed erbium-doped silicon-rich SiO_2 is a technologically viable gain medium for use in silicon photonics.

Finally, studies of the effect of the Si excess concentration on the density of sensitized Er^{3+} ions demonstrated that a Si excess concentration of ~ 14.5 at. % is optimum for achieving the highest density of sensitized Er^{3+} ions in low-temperature annealed Si-rich SiO_2 (without Si nanocrystals). A similar optimum Si excess concentration of ~ 11.5 at. % is found for samples annealed at high temperature (with Si nanocrystals). These findings provide the field with a prediction of the optimal concentration of excess silicon for achieving maximum gain.

The results presented in this thesis reveal the actual sensitization process of Er^{3+} in Si-rich SiO_2 and demonstrate that low temperature annealed Er-doped Si-rich SiO_2 without silicon nanocrystals is a preferable candidate for the realization of on-chip optical devices. The dissertation provides the field with optimum fabrication conditions for achieving maximum gain in this medium. The work also contains detailed information on the values of several key Er^{3+}

sensitization parameters (e.g. transfer efficiency, transfer time, relaxation efficiency, excitation cross-section, relative density of sensitized Er^{3+} ions) and on the processes involved in the excitation of Er^{3+} in Si-rich SiO_2. The parameters presented in this dissertation will be of great importance for the modeling of actual gain media and consequently of devices based on low temperature processed Er-doped Si-rich SiO_2.

Future work in this area should focus on the determination of any potential host-induced optical absorption at 1.54 μm, and on the determination on the absolute fraction of sensitized Er^{3+} ions in this material. Studies of the transmission of the pump wavelength of choice through the material should be done to determine the optimal excitation geometry of the devices. Based on the optimized fabrication conditions of the gain medium found in this dissertation together with subsequent device design optimization, waveguide devices based on this material should be fabricated and their gain performance at 1.54 μm should be tested. If these studies produce favorable results, net optical gain in a Si compatible optical amplifier based on Er-doped Si-rich SiO_2 without silicon nanocrystals could be achieved in a CMOS compatible device operating at 1.54 μm.

APPENDIX: LIST OF PUBLICATIONS

Portions of this thesis have been drawn from the following publications:

1. Oleksandr Savchyn, Kevin R. Coffey, and Pieter G. Kik, *Determintation of optimum Si-excess concentration in Er-doped Si-rich* SiO_2 *for optical amplification at 1.54 μm* (in preparation for submission),

2. Oleksandr Savchyn, Ravi M. Todi, Kevin R. Coffey, and Pieter G. Kik, *High temperature optical properties of Er-doped Si-rich* SiO_2 *– implications for gain performance*, Opt. Mat. **32**, 1274 (2010),

3. Oleksandr Savchyn, Ravi M. Todi, Kevin R. Coffey, Luis K. Ono, Beatriz Roldan Cuenya and Pieter G. Kik, *Excitation wavelength-independent sensitized* Er^{3+} *concentration in as-deposited and low temperature annealed Si-rich* SiO_2 *films*, Appl. Phys. Lett. **95**, 231109 (2009),

4. Oleksandr Savchyn, Ravi M. Todi, Kevin R. Coffey, and Pieter G. Kik, *Observation of temperature independent internal* Er^{3+} *relaxation efficiency in Si-rich* SiO_2 *films*, Appl. Phys. Lett. **94**, 24111 (2009),

5. Oleksandr Savchyn, Ravi M. Todi, Kevin R. Coffey, and Pieter G. Kik, *Multilevel sensitization of* Er^{3+} *in lowtemperature-annealed silicon-rich* SiO_2, Appl. Phys. Lett. **93**, 233120 (2008),

6. Oleksandr Savchyn, Pieter G. Kik, Ravi M. Todi, and Kevin R. Coffey, *Effect of hydrogen passivation on luminescence-center-mediated Er excitation in Si-rich* SiO_2 *with and without Si nanocrystals*, Phys. Rev. B **77**, 205438 (2008),

7. Oleksandr Savchyn, Forrest R. Ruhge, Pieter G. Kik, Ravi M. Todi, Kevin R. Coffey, Haritha Nukala, and Helge Heinrich, *Luminescence-center-mediated excitation as the dominant Er sensitization mechanism in Er-doped silicon-rich* SiO_2 *films*, Phys. Rev. B **76**, 195419 (2007).